

NOAA Technical Memorandum OAR PSD-314



**SUMMARY OF METEOROLOGICAL CONDITIONS DURING THE ARCTIC
MECHANISMS FOR THE INTERACTION OF THE SURFACE AND ATMOSPHERE
(AMISA) INTENSIVE OBSERVATION PERIODS**

P.O.G. Persson

Earth System Research Laboratory
Physical Sciences Division
Boulder, Colorado
February 2010

NOAA Technical Memorandum OAR PSD-314

**SUMMARY OF METEOROLOGICAL CONDITIONS DURING THE ARCTIC
MECHANISMS FOR THE INTERACTION OF THE SURFACE AND ATMOSPHERE
(AMISA) INTENSIVE OBSERVATION PERIODS**

P. Ola G. Persson
Cooperative Institute for Research in the Environmental Sciences (CIRES)
NOAA Earth System Research Laboratory/Physical Sciences Division
325 Broadway, Boulder, CO 80305

Earth System Research Laboratory
Physical Sciences Division
Boulder, Colorado
February 2010



**UNITED STATES
DEPARTMENT OF COMMERCE**

**Gary Locke
Secretary**

**NATIONAL OCEANIC AND
ATMOSPHERIC ADMINISTRATION**

**Dr. Jane Lubchenco
Under Secretary for Oceans
and Atmosphere/Administrator**

**Office of Oceanic and
Atmospheric Research**

**Dr. Richard Spinrad
Assistant Administrator**

NOTICE

Mention of a commercial company or product does not constitute an endorsement by NOAA/Earth System Research Laboratory. Use of information from this publication concerning proprietary products or the test of such products for publicity or advertising purposes is not authorized.

For sale by the National Technical Information Service, 5285 Port Royal Road
Springfield, VA 22061

Contents

1. Introduction.....	1
2. AMISA and ASCOS Instrumentation.....	3
3. General Meteorological Conditions.....	7
4. AMISA Intensive Observation Periods.....	11
4.1 <i>Transit Flight; Aug. 8, 2008 (YD221)</i>	11
4.2 <i>IOP 1; Aug. 12-13, 2008 (YD225-226)</i>	19
4.3 <i>IOP 2; Aug. 15, 2008 (YD228)</i>	27
4.4 <i>IOP 3; Aug. 22, 2008 (YD235)</i>	35
4.5 <i>IOP 4; Aug. 23, 2008 (YD236)</i>	41
4.6 <i>IOP 5; Aug. 25, 2008 (YD238)</i>	47
5. AMISA Summary and Science Issues.....	55
6. References.....	57

AMISA



Arctic Mechanisms of Interaction between the Surface and Atmosphere



Kiruna, Sweden · 2008
CU Boulder · NOAA/ESRL
NASA Dryden-Goddard-Langley
Stockholm University
University of Leeds
NSERC

1. Introduction

The Arctic Mechanisms for the Interaction of the Surface and Atmosphere (AMISA) field program utilized the NASA DC-8 research aircraft, based in Kiruna, Sweden, to obtain data over the Arctic pack ice during August 2008. The program was conducted jointly with the Arctic Summer Cloud-Ocean Study (ASCOS), which consisted of the deployment of the Swedish icebreaker Oden north of Svalbard from Aug. 1 to Sep. 9. The Oden drifted with the pack ice near 87.5°N , 5°W between Aug. 12 (YD225) and Sep. 2 (YD246) (Fig. 1.1). Five research missions and two transit flights were flown with the DC-8 (Table 1.1) between Aug. 8 and Aug. 26. Of the 5 research missions, 4 were focused on collecting data in the vicinity of the Oden and one focused on collecting data near the ice edge in Fram Strait between Svalbard and Greenland. The transit flight from California to Sweden included a flyover of the Oden and some data collection in its vicinity. The transit flight back to the United States went across Greenland and included some radiometric measurements of a glacier on the west side of southern Greenland, and is not discussed further here. The location of the aircraft base and its range allowed approximately 4 hours of on-station time for the aircraft in the immediate vicinity of the Oden (Fig. 1.1). The on-station time in Table 1.1 includes the times for the first and last dropsondes; i.e., the time of mission-objective data collection from the aircraft.

The meteorological conditions of the first transit flight and five research missions are described here. The descriptions include a summary of the model forecasts for the mission, satellite images, some data from the aircraft, and some basic rawinsonde and remote sensing data

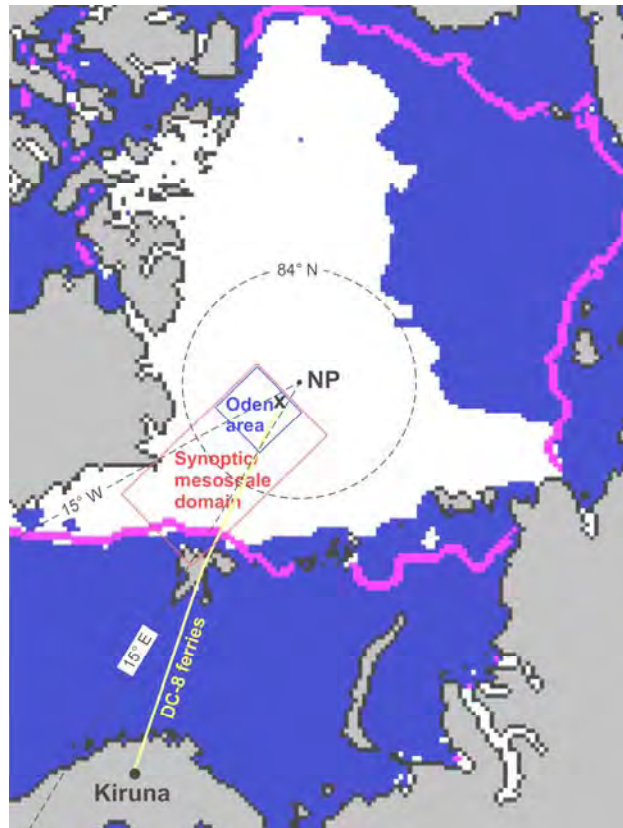


Figure 1.1: ASCOS/AMISA Research Area Aug. 1 - Sep. 12, 2008. The white area shows sea ice extent on Sep. 3, 2007. The magenta line shows median sea ice extent 1979-2000 (National Snow and Ice Data Center).

Table 1.1: List of AMISA DC8 science flight missions

IOP	Type	Date	Time (UTC)	C_p (m/s)	Sondes
Transit	Oden overpass	Aug 8 (YD221)	0003-1215 OS 0700-0840	10.5/ 341°	5
1	mapping, radiation, microphysics near Oden	Aug 12-13 (YD225-226)	1802-0346, OS 2000-0130	14.5/ 81°	7
2	mapping, radiation, microphysics, trajectory near Oden	Aug. 15 (YD228)	0402-1510, OS 0500-1230	13.9/175° (all) 12.4/161° (north)	4
3	ice edge mapping, AMSR-E	Aug. 22 (YD235)	0358-1210, OS 0530-1045	10.3/191°	3
4	mapping, radiation, microphysics, trajectory near Oden	Aug. 23 (YD236)	1204-2045, OS 1400-1830	10.0/165°	10
5	mapping, radiation, microphysics, stratocumulus near Oden	Aug. 25 (YD238)	0851-1923, OS 1100-1730	15.8/254° (upper) 5.0/290° (lower)	9

from the Oden. Satellite-based estimates of system or cloud phase velocities valid during the on-station time are also presented. All times are given in Greenwich Mean Time (UTC), as this was the time used by the Oden.

This report will first present a brief summary of the instrumentation on the DC-8 aircraft during AMISA and of the ASCOS instrumentation, followed by a section describing the general meteorological conditions during the ASCOS/AMISA field program. The fourth section, divided into six sub-sections, describes the meteorological environmental context of each research flight (or intensive observation period – IOP) and provides sample analyses. Data from the NASA DC-8, from the Oden, or from various meteorological services will be used to provide this meteorological context. The last section summarizes the accomplishments of AMISA and provides a synopsis of suggested scientific analyses possible from the various IOPs. Hence, this report provides a meteorological overview of the AMISA field program and the meteorological background of the individual flights necessary for researchers addressing the specific AMISA research objectives. Descriptive flight summaries produced by the NASA flight crew are available at http://www.nasa.gov/centers/dryden/home/AMISA_mission_science_report.html.

2. AMISA and ASCOS Instrumentation

Because this summary of meteorological conditions will utilize data from the various instrument groups on board the DC-8, a brief summary of these instruments will be presented here. An extensive suite of radiometers was installed on the DC-8 aircraft (Fig. 2.1 and Table 2.1). This included a scanning nadir-facing PSR/A imaging radiometer, a C-band radiometer, a

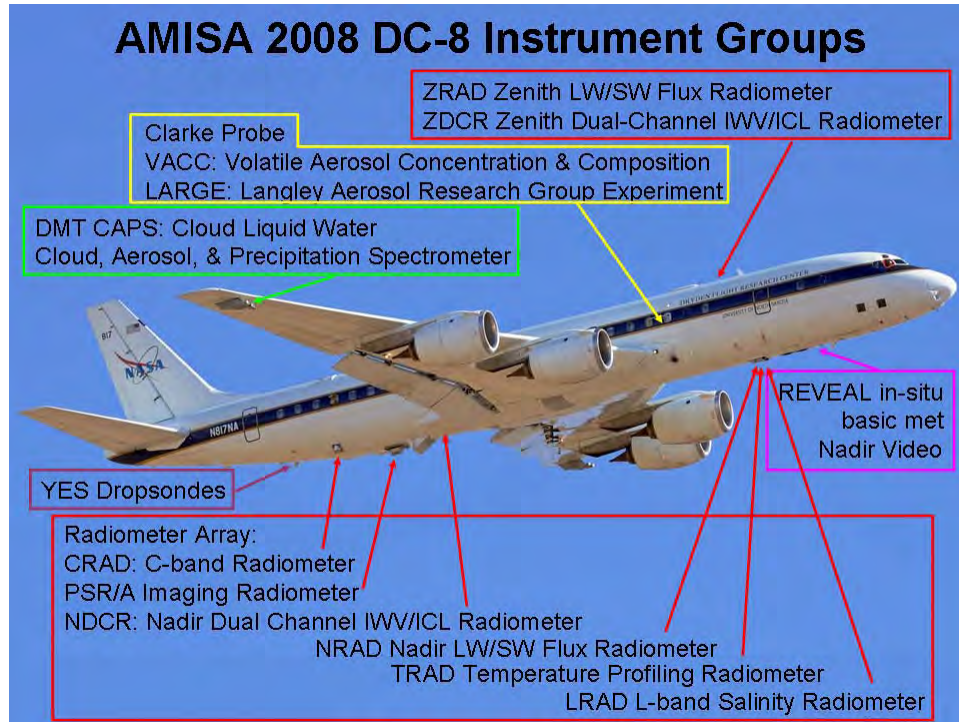


Figure 2.1: The six basic instrument groups on the NASA DC-8 research aircraft during AMISA.

temperature profiling radiometer, and a L-band salinity radiometer. Two radiometers had both a zenith and a nadir facing pair. These were dual-channel integrated water vapor and cloud liquid water radiometers and broadband shortwave and longwave radiometers. Dropsondes developed in conjunction with Yankee Environmental Systems were dropped from a chute in the rear of the aircraft. The Clark probe mounted on the right side of the fuselage allowed direct sampling of aerosol particles by the Volatile Aerosol Concentration and Composition (VACC) system, operated by the University of Leeds, and by the Langley Aerosol Research Group Experiment (LARGE). A Cloud, Aerosol, and Precipitation Spectrometer (CAPS) probe was mounted near the tip of the right wing of the aircraft. This probe also included a hot-wire cloud liquid water probe.

During ASCOS, the atmosphere near and above the Oden was sampled by a suite of surface-based remote sensors and in-situ sensors providing information on the atmospheric thermodynamic, kinematic, and turbulent structure. These sensors included a 5-mm (60 GHz) scanning radiometer providing temperature profiles up to 1 km at time resolutions of 1 s to 10 minutes; a 449 MHz wind profiler providing profiles of wind speed, wind direction, and turbulence intensity to about 6 km every 6-30 minutes; a Doppler S-band cloud and precipitation radar providing cloud macrophysical structure, fall velocity, and spectral width in both clouds

Table 2.1: List of instruments mounted on the NASA DC-8 aircraft during AMISA.

Instrument	Description	Observables
Polarimetric Scanning Radiometer (PSR)	Multiband polarimetric radiometric imaging system; Airborne AMSR-E equivalent; 10, 18, 21, 37, and 89 GHz	high resolution sea ice mapping; cloud cover; integrated water vapor
Dual-channel radiometer (DCR)	21/31 GHz, up/downlooking	integrated water vapor & cloud liquid water above/below aircraft
Temperature profiling radiometer	50-57 GHz, downlooking	Profiles of air temperature
Scanning Low Frequency Microwave Radiometer (SLFMR)	L-band salinity mapping	L-band brightness; mapped salinity with ~5 ppt precision for lead/meltpond discrimination
Cloud, aerosol, and precipitation spectrometer (CAPS)	From Droplet Measurements Technology	Cloud droplet and ice particle spectra, liquid water content, droplet/ice discrimination
Expendable digital dropsondes	Yankee Technology	Sub-aircraft profiles of temperature, pressure, humidity, and wind
OAT Rosemount probe	Outside air temperature adjusted for Mach number	Air temperature
pyranometers and pyrgeometers	Hemispheric integrating thermopile irradiance sensors	Up- and downwelling shortwave and longwave radiative fluxes
DMT Cloud Aerosol and Precipitation Spectrometer (CAPS) – three probes	cloud (optical array) imaging probe (CIP), cloud aerosol spectrometer (CAS), hot-wire sensor (LWC-100)	cloud particle images and sizes (25 μm – 1.55 mm, 25 μm resolution) particle size distribution (0.6 μm – 50 μm) liquid water content (0.01- 3.0 g m^{-3})
Volatile Aerosol Concentration and Composition (VACC)	University of Leeds' system	Aerosol number concentration spectra and aerosol composition

and precipitation to 10 km; a 8 mm (Ka-band) cloud radar providing cloud reflectivity, vertical velocity, and spectral information to 10 km at 45 m resolution, a dual-channel radiometer (23.8 and 31.4 mm), a ceilometer, and a Scintec phased array sodar. The sodar provides turbulence and winds to about 600 m. Other remote sensors deployed during ASCOS included a vertically pointing depolarization mini-lidar providing backscatter and phase-partitioning up to significant cloud water regions, and a scanning Marine-Atmosphere Emitted Radiance Interferometer (M-AERI) providing radiometric spectra from both the surface and the atmosphere. Other than the sodar, the remote sensors were located on the Oden (Fig. 2.2).

In-situ profiling data at ASCOS are provided by 4X daily rawinsondes and 210 hours of basic meteorology parameters, turbulence, and aerosol spectra data (56% of deployment period from 8/17 – 9/1) from a tethered system deployed up to heights of about 700 m. Other than the 4X daily rawinsondes, the profiling observations have a temporal resolution of ~1 min to 1 hour. Time-height data of temperature, wind, cloud outlines, turbulence, and derived parameters (e.g., Richardson number) are combined from the different sensors and examined for basic

boundary-layer structures and transition events. In addition, profiles of surface-layer temperature, humidity, wind, and turbulent fluxes were obtained from two towers (20-m and 30-m) located on the ice near the Oden. Surface measurements of downwelling and upwelling shortwave and longwave radiative fluxes were also made, and solar radiometric flux measurements were also made beneath the ice on the floe near the Oden.

More information on the instrument systems and access to the ASCOS and AMISA data are available from both at <http://www.ascos.se/>. Only basic meteorological parameters from the in-situ aircraft sampling system and the airborne aerosol data are currently available at the ASCOS site. Data from the CAPS microphysics probe, the dropsondes, or the suite of airborne radiation sensors can be requested by contacting Dr. Ola Persson (opersson@cires.colorado.edu) or Prof. Albin Gasiewski (Al.Gasiewski@colorado.edu).

Combining the airborne and ice-breaker based observations allows the examination of many structures and processes associated with the clouds, the Arctic boundary-layer, and the ice surface during ASCOS/AMISA. In this report, the basic in-situ and dropsonde measurements from the NASA DC-8 will be combined with some of the surface-based observations to provide an understanding of the synoptic and mesoscale atmospheric structure sampled by the aircraft during the AMISA IOPs.

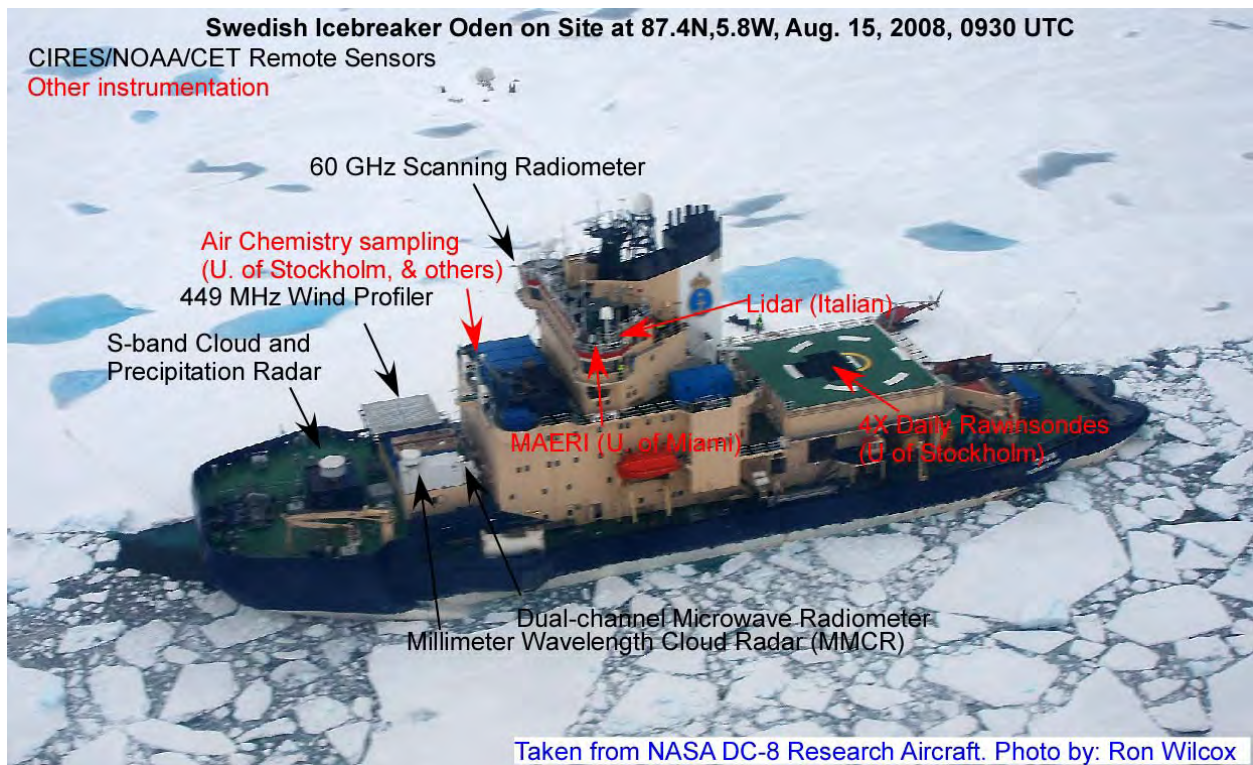


Figure 2.2: Location of many of the remote sensors on the Oden during ASCOS/AMISA.

3. General Meteorological Conditions

During the first two-thirds of the ASCOS field program (Aug. 3-24; YD216-237), synoptic storms were frequent. These storms are typically marked by warm air above the main Arctic inversion near 0.5-2 km, the presence of deep humidity and clouds (Fig. 3.1), and lower surface pressure. The strongest in this series of storms occurred on YD226-228 (Fig. 3.1d), which were sampled by IOPs 1 and 2. From Aug. 25-Sep. 3 (YD238-YD247), the weather at the Oden was marked by drier air above 1 km, colder air and persistent stratocumulus clouds in the lowest 2 kms, and higher surface pressure. Because the AMISA field program ended on Aug. 26 (YD239), the first 5 flights were flown during the period with active synoptic storms. IOP4 sampled the storm ending the cold snap period. Only the last flight, flown on YD238, sampled the drier, colder freeze-up period dominated by stratocumulus clouds, though stratocumulus clouds were sampled in all of the other IOPs over the Oden with the exception of the transit flight.

One of the important goals of AMISA was to sample the atmosphere and surface before and after the onset of freeze-up. This transition can be measured in several ways. One way is to use 7- or 14-day running medians of the near-surface air temperature (T_a) and different threshold temperatures. Using the data from the Oden's meteorological station, the end of the melt season occurred on YD 220 (Aug. 7), YD 229 (Aug. 16), or YD 234 (Aug 21) (Fig. 3.1c). If the criterion of Martin and Munoz (1997) is used ($T_{2, 14d_med} < -0.1^\circ \text{C}$), AMISA failed to sample the end of the melt season and the Oden failed to establish its drifting station before the freezeup. However, with any of the other three criteria [Rigor et al. (2000), $T_{2, 14d_med} < -1^\circ \text{C}$; Andreas and Ackley (1982), $T_{2, 14d_med} < -1.9^\circ \text{C}$; Persson and Solomon (2008), $T_{2, 7d_med} < -1.8^\circ \text{C}$], the transit flight and IOPs 1 and 2 occurred before the onset of the freeze-up, while IOPs 4 and 5 occurred after the onset. In addition, preliminary analysis of on-ice surface energy flux observations was used to characterize ASCOS period into a melt, cold snap, and freeze-up periods. This characterization agrees with the end-of-melt criteria of PS08 and AA82. Hence, AMISA was successful in achieving its sampling goal.

Photographs of the ice surface near the Oden during IOPs 1 & 2 (Fig. 3.2) show clearly discernible melt ponds and leads that have some grease ice. During IOPs 4 and 5, the meltponds are more frozen over and covered by snow, especially during IOP5. For instance, most of the meltponds near the Oden are no longer discernible on Aug. 25. The leads are still discernible, though they have larger areas of grease ice.

The more gradual nature of the freeze-up transition, in contrast to the onset of melt, is evident in the broad temporal scatter of the freeze-up date from the different criteria and the series of photographs in Fig. 3.2. While the AMISA field program may have succeeded in obtaining missions on both sides of the freeze-up date using three of the criteria, more distinct contrasts between the melt season and the freeze-up period would likely have been obtained with an earlier start date and a later end date to the field program.

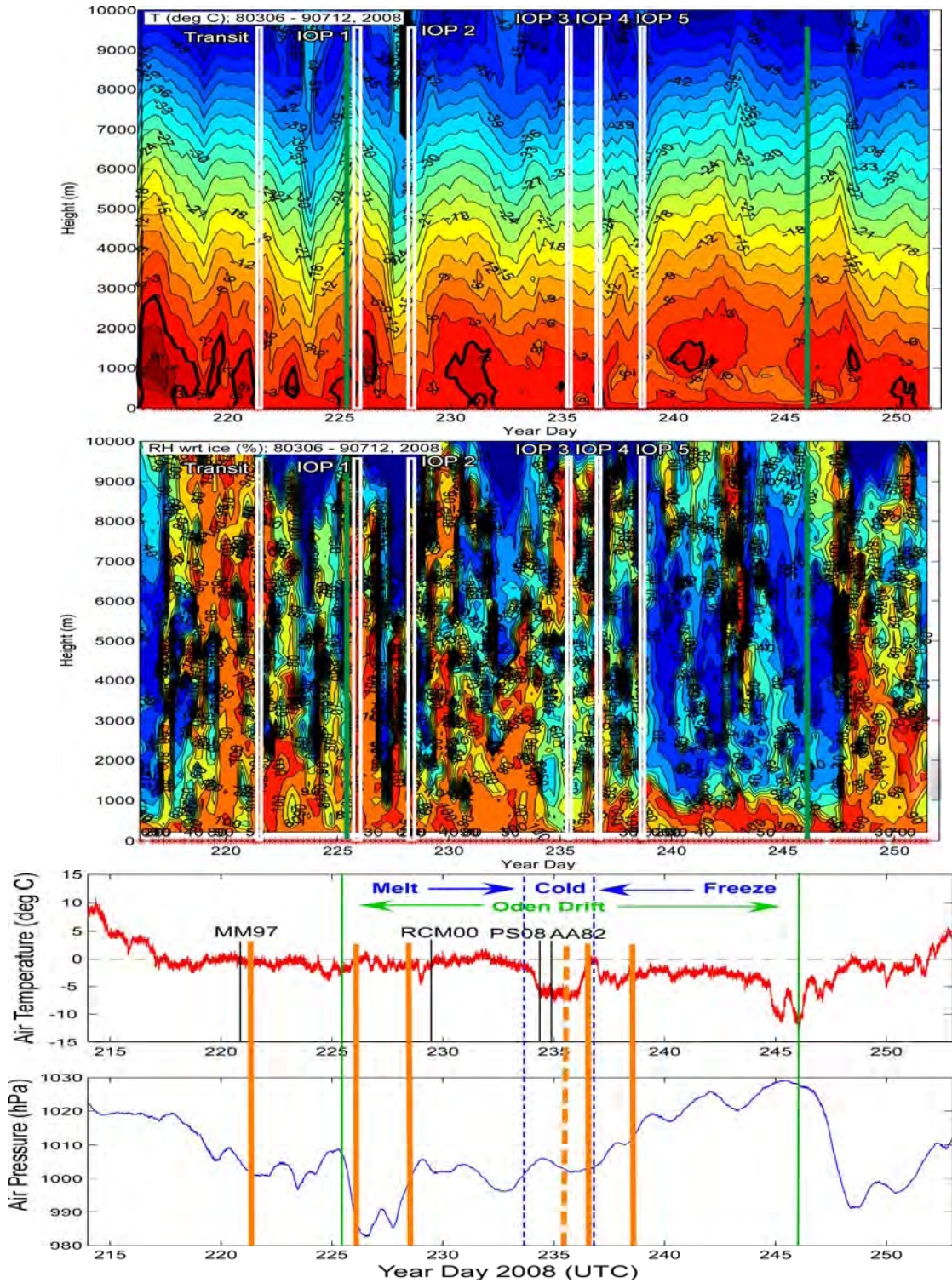


Figure 3.1: Top panels (a,b): Time-height series of temperature and relative humidity wrt ice from the 145 Oden rawinsondes (red stars along abscissa). The white frames show the six DC8 research flights, while the vertical green bars demark the 21-day Oden ice drift period. In a), the 0° C isopleths are bold. Bottom panels(c,d): Surface air temperature and pressure from the meteorological station at 35 m on the Oden. The vertical black lines on the temperature plot show the end of the melt season according to the temperature criteria of Martin and Munoz (1997; MM97), Rigor et al (2000;RCM00), Persson and Solomon (2008;PS08), and Andreas and Ackley (1982; AA82). The melt period, cold snap, and freeze-up periods are delineated by the vertical blue dashed lines.

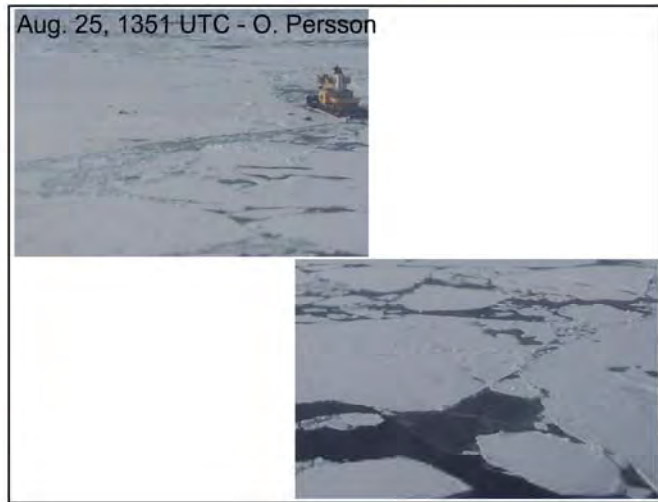


Figure 3.2: Photographs of the ice surface near the Oden during a) IOP1, b) IOP2, c) IOP4, and d) IOP5.

4. AMISA Intensive Observation Periods

4.1 Transit Flight; Aug. 8 (YD221)

Aircraft Takeoff: 00:03:07

Landing:~1215

On Station: 0700-0840

Oden Location when On Station:(82.91, -1.42) - (83.02, -2.04), at 0801 UTC (82.96, -1.76)

Number of dropsondes: 5

Sonde times: 0724 (84.86,-25.82), 0732 (84.51,-17.09), 0801 (82.94,-1.62), 0816 (82.28,+3.51)

Meteorological system phase velocity: 10.5 m/s / 341°

Times of direct overflight: 0806

The forecasts with lead times of 48 h or less (Figs. 4.1.1 and 4.1.2) were able to predict the general surface pressure structure with a primary low located east of Svalbard, and a trough

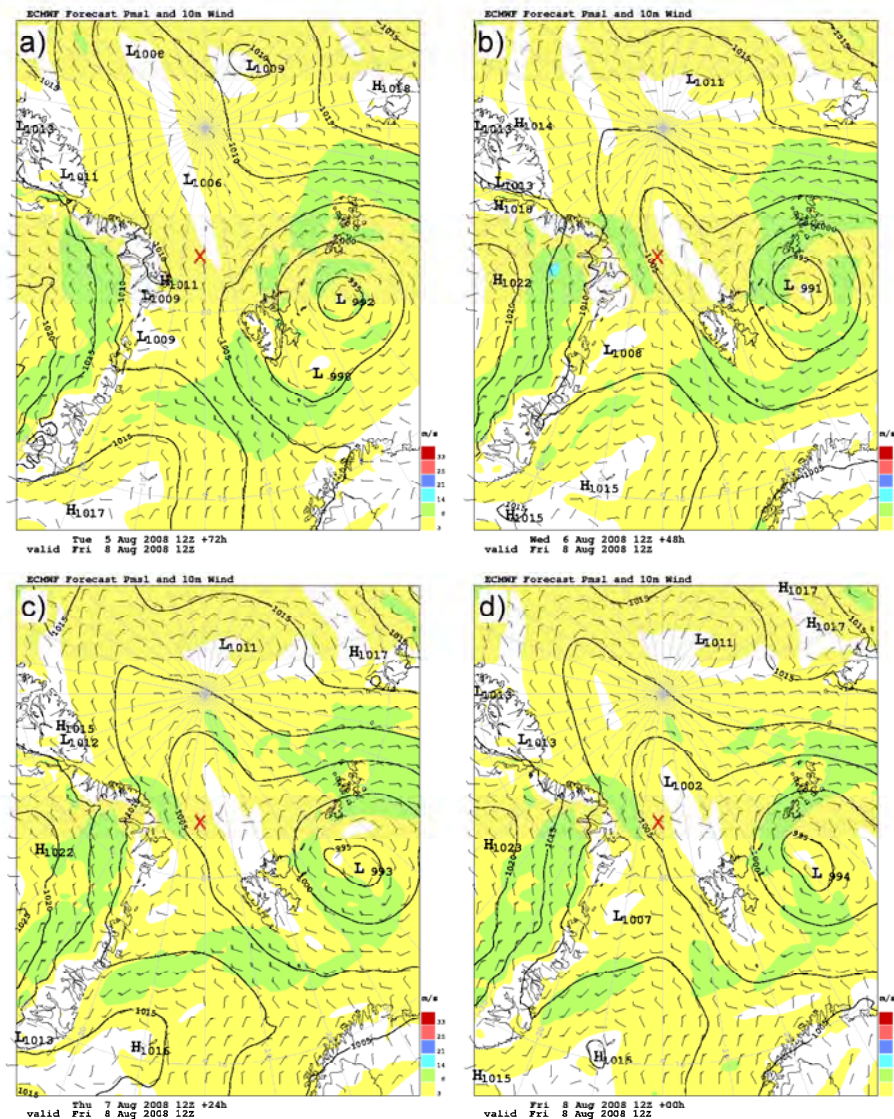
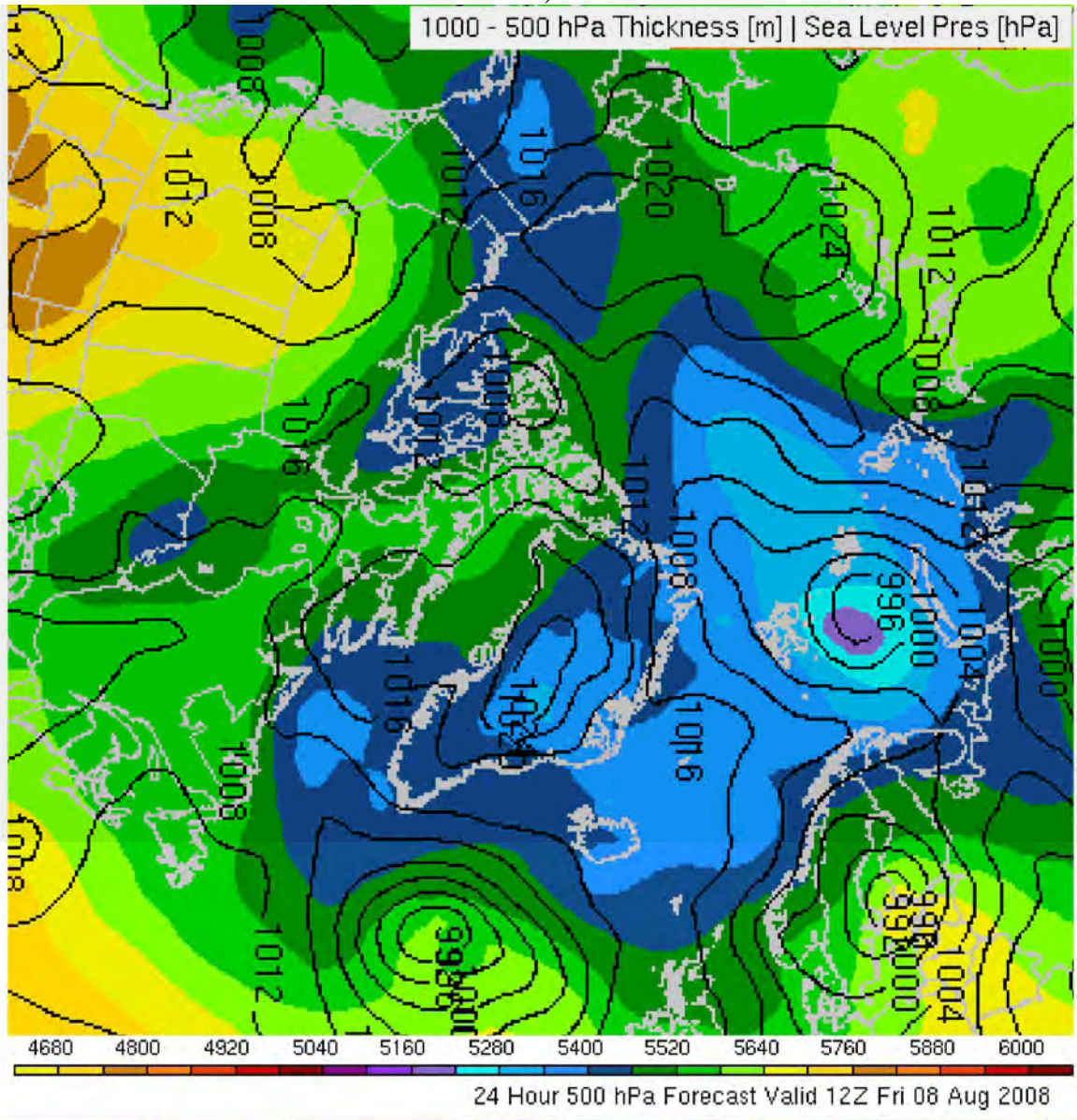


Figure 4.1.1: Sea-level pressure and wind at 12 UTC Aug. 8 (YD221) from ECMWF forecasts of lead time a) 72 h, b) 48 h, and c) 24 h. Frame d) shows the analysis at 12 UTC Aug. 8. Oden is marked by the red "X".

a)



b)

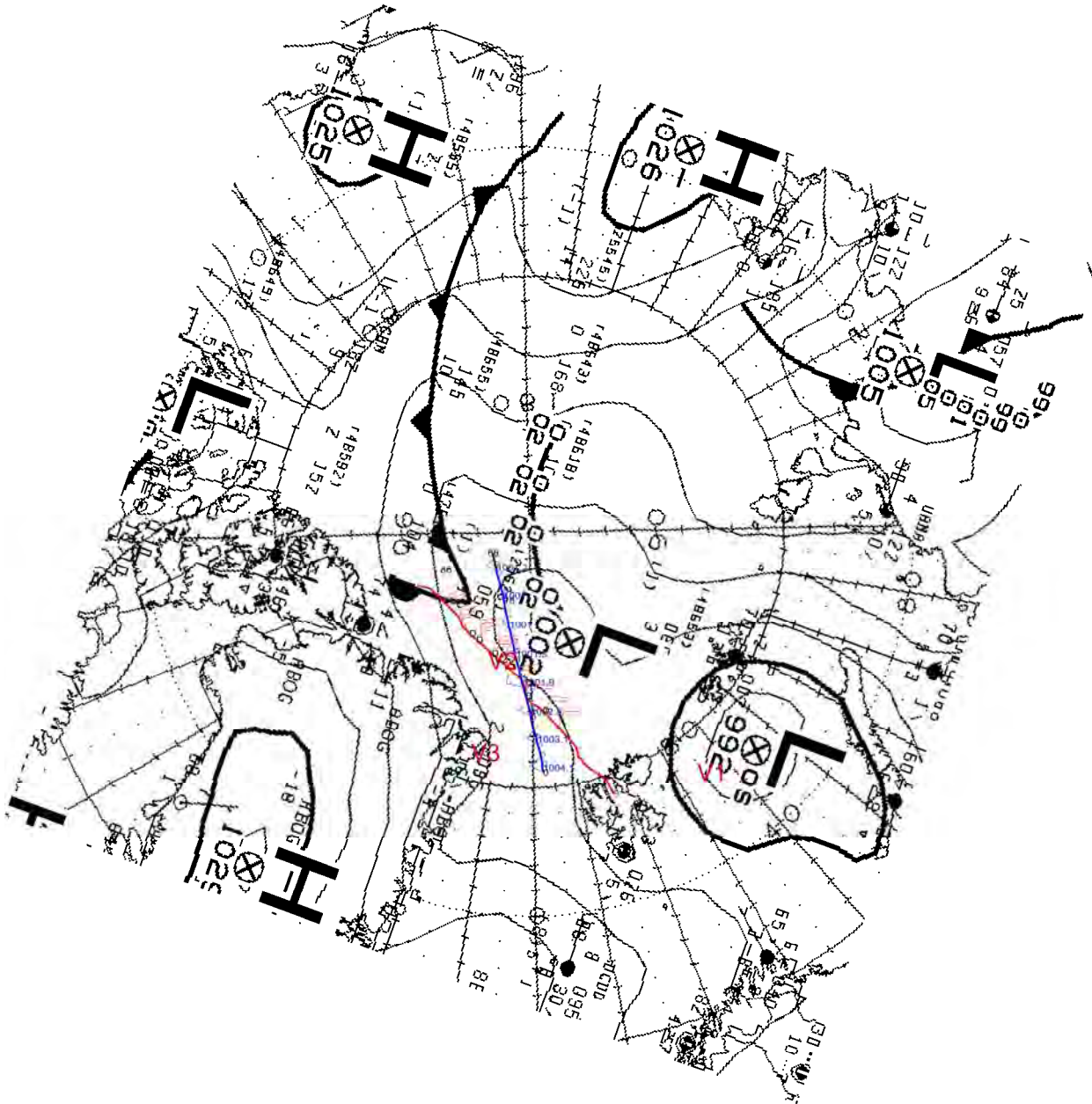


Figure 4.1.2: a) (on previous page) 24-h forecast of sea-level pressure and 1000-500 hPa thickness from the GFS model valid at 12 UTC Aug. 8 (YD221). b) Canadian Weather Service sea-level pressure analysis with frontal interpretation at 06 UTC Aug. 8. The time-space-adjusted tracks for the DC8 (red) and Oden (blue) are seen (see description of Fig. 4.1.3).

line with a secondary low extending northwestward from Svalbard over the region of the Oden, located at about 83°N , 2°W at this time. At the Oden, the near-surface wind was from the northwest. The satellite image sequence (Fig. 4.1.3) shows not only the low-pressure circulation center east of Svalbard (V1), but also two circulation centers NW of Svalbard. Center (V2) is moving southward from the NNW and dissipating, though at 06 UTC the circulation with this system is very clearly defined, and with an apparent frontal cloud band extending eastward north

of the Oden's location. Another circulation center (V3) is present at 06 and 09 UTC along the NE coast of Greenland, with a less distinct cloud band extending NE from its center. All three of these lows are marked on the 12 UTC analysis from ECMWF, though most forecasts did not produce the secondary lows.

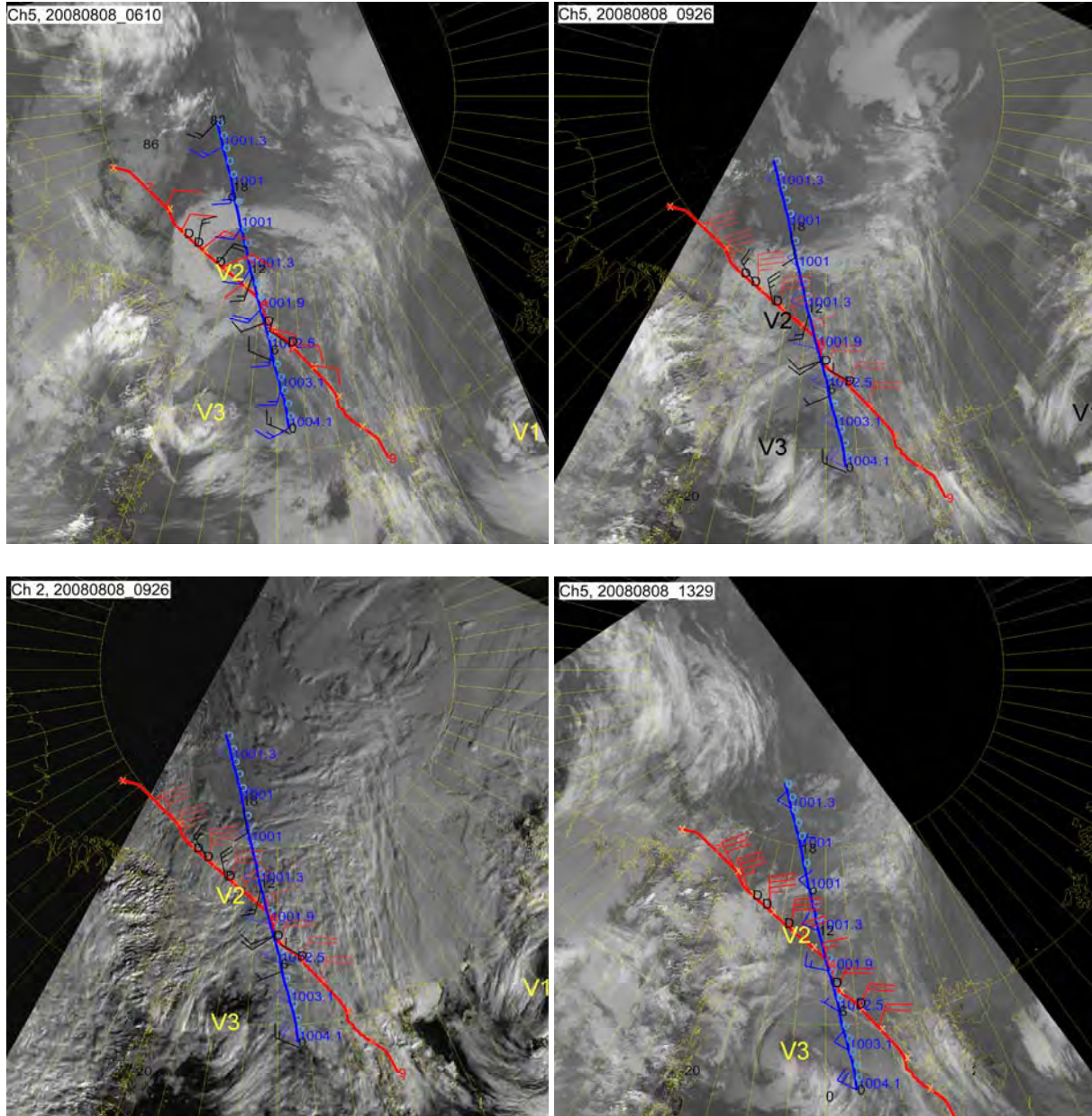


Figure 4.1.3: Satellite images at a) 0610 (IR), b) 0926 (IR), c) 0926 (Vis), and d) 1329 (IR) UTC Aug. 8 (YD 221) near Greenland, Svalbard, and the North Pole. The system-relative track of the DC8 aircraft (red) and the Oden (blue) are shown using a system phase velocity of 10.6 m s^{-1} from 347° . The system-relative locations are shown by the marked hours for the DC8 and the 6-hourly locations for the Oden. The 10-min (hourly) positions are shown by the "x" ("o") for the DC8 (Oden) track. The dropsondes are marked by "D". In , c), and d), the red (blue) wind barbs are those along the DC8 (Oden) track and height. In a), the red (blue) barbs are the system-relative winds along the respective tracks, and the black ones represent system-relative winds at 2 km from the dropsondes and the upsondes. The DC8 flew at 6850 m where wind barbs are marked, and above 11 km outside this area. The vortices V1, V2, and V3 are marked.

Utilizing features evident in the satellite images from 0610, 0926, and 1105 UTC, a system phase velocity of 10.5 m s^{-1} from 341° is estimated. Applying this phase velocity to adjust the locations of the DC8 and the Oden to the times of the respective satellite images, the positions of the two data platforms relative to the main synoptic features can be visualized (Fig. 4.1.3). The aircraft descended to 6850 m shortly after 07 UTC and flew through the circulation center V2, dropping two dropsondes in the main cloud band (one sonde failed) and one dropsonde very close to the circulation center. Sonde 12 in the main cloud band showed the main cloud top to be at 4700 m, with the air being moist to the surface (Fig. 4.1.4). A layer of warm air ($T \sim -1^\circ\text{C}$) existed between 1300-2100 m, presumably through horizontal advection. The winds were between 300° - 355° from 500 m to the surface, with the strongest winds of 18 m s^{-1} occurring between 1300-4000 m from 330 - 340° . Note that no easterly flow, as might be expected by the orientation of the cloud band, occurred in this profile. After the circulation center, the aircraft passed through a cloud enhancement near the intersection of circulation V2 and the cloud band extending from V3. The aircraft passed over the Oden in this region, dropping a sonde right over the Oden at 0806 UTC at the same time as an upsonde was launched from the Oden (Fig. 4.1.5). Compared to sonde 12, sonde 54 showed cooler air aloft, with a

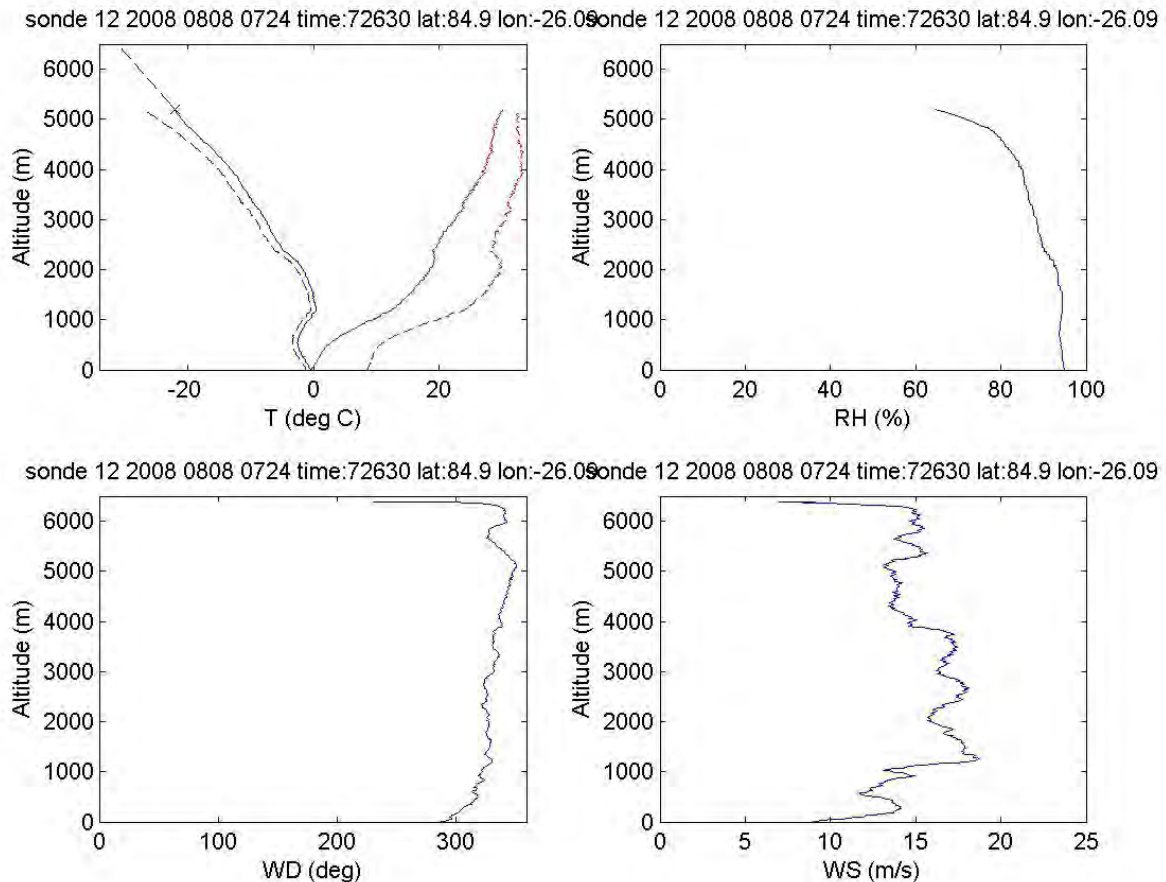


Figure 4.1.4: Dropsonde profiles from sonde 12 (the second sonde). Panel a) shows temperature (solid blue), dew point (dashed blue), potential temperature (solid red), and equivalent potential temperature (dashed red).

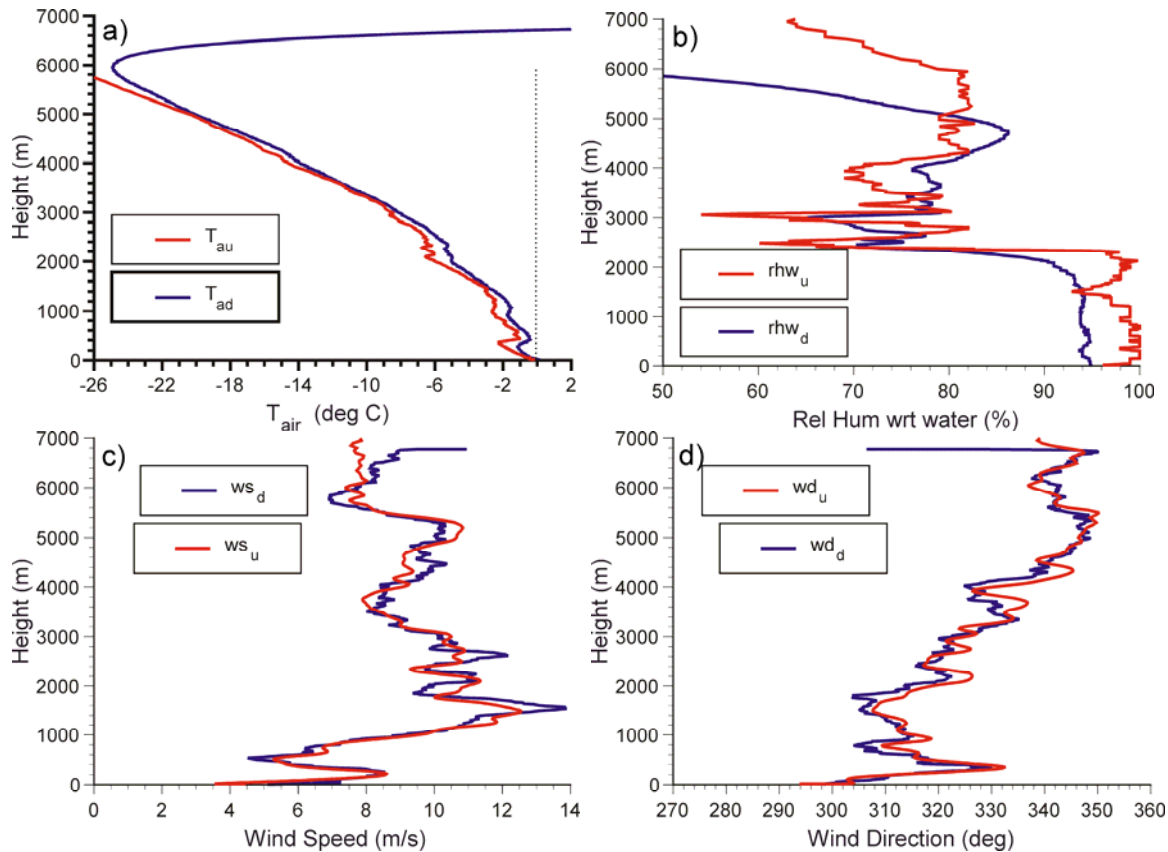


Figure 4.1.5: Comparisons of data from dropsonde 54 (blue) at 0801 UTC Aug. 8 with the collocated upsonde from the Oden (red) showing a) air temperature, b) relative humidity, c) wind speed, and d) wind direction.

primary cloud deck top at 2 km and a secondary moist layer near 5 km. After dropping one more sonde at 0818 UTC, the aircraft ascended at 0840 UTC. Because of a course correction by the aircraft, the DC8 flew along the time-adjusted track of the Oden for nearly 15 minutes (0754-0810 UTC). The Oden sampled this track between 07-10 UTC.

One objective of the simultaneous sondes was to compare the new, Yankee Technology dropsondes with the upsondes from the Oden, as done in Fig. 4.1.5. These particular sondes showed the dropsonde to be about 1°C warmer than the upsonde, the relative humidity to be biased low in the high-humidity region near the surface, and the wind profiles to be in excellent agreement. Future intercomparisons of aircraft, dropsonde, upsonde, tetheredsonde, and remote sensing data will determine whether these differences in this case are representative of other cases. The low humidity bias of the AMISA dropsondes in the moist regions has been noted in other cases.

The track of the Oden crossed the aircraft track near the cloud band from V3 and the cloud enhancement in this region. The track then continued northward, east of the aircraft track, passing through the E-W cloud band from V2 between 15-17 UTC, though the band had weakened by that time (Fig. 4.1.3d). The time-height section from the S-band cloud radar and serial rawinsondes on board the Oden show the vertical structure of the cloud features along the Oden's track (Fig. 4.1.6). The low and upper-level clouds sampled by the DC8 dropsonde are evident, as is the fact that the aircraft was flying along the tops of the mid-level clouds. Note that the spectral width of these clouds was quite low, suggesting that they would contain very little

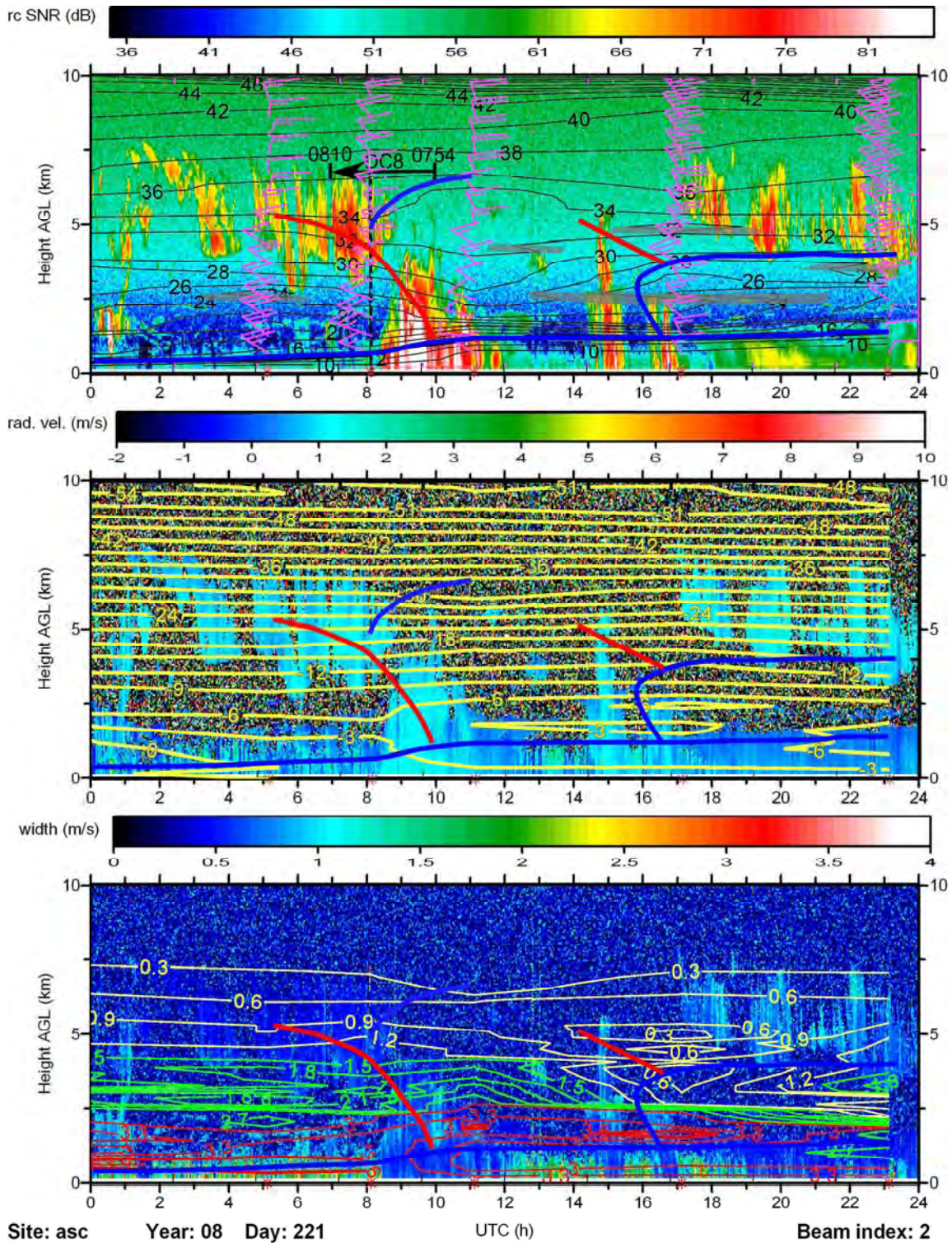


Figure 4.1.6: Time-height sections from the S-band radar and serial rawinsondes of a) SNR (color), θ_e isopleths ($^{\circ}\text{C}$), wind barbs, b) vertical velocity and air temperature ($^{\circ}\text{C}$), and c) spectral width and mixing ratio (g kg^{-1}). The time that the DC8 was over the Oden is marked by a vertical black line. Between 07-10 UTC, the DC8 flew the same line as sampled by the Oden, as seen in the satellite images. Regions of potential instability are shaded in a). The red stars on the abscissa mark the Oden rawinsondes.

turbulence and probably very little liquid water. The time period of coincident ship and aircraft track (07-10 UTC ship sampling time) included a period of low-level boundary-layer clouds with a mid-level cloud deck and a period of more active (perhaps precipitating) clouds extending to 2-3.5 km altitude. The ship's passage through the cloud band from V2 is marked by two active cloud bands near 15 UTC and 17 UTC, with cloud tops reaching up to 5 km, consistent with the earlier aircraft sonde showing high moisture up to 4.7 km in this band further to the west.

The serial rawinsonde ascents show significant layering in the very complex frontal structure. The region of enhanced clouds and precipitation near the intersection of circulation V2 and the cloud band from V3 (0820-1130 in Fig. 4.1.6) appears to mark a cold-frontal feature below 1.5 km, as marked by the 14°C θ_e isotherm (Fig. 4.1.6a). However, the cloud band marked by the enhanced clouds and precipitation extending eastward from V2 has warm, moist air just to its north in an elevated layer between 2.5 - 4.0 km (Fig. 4.1.6b, c). This is in rough agreement with dropsonde 12 which sampled this cloud band 10 h earlier and further to the west. On the other hand, the θ_e analysis suggests that warm/moist air is located in a layer between 2.5-5.0 km between the precipitation band at 1130 and that at 1700, apparently contradicting the conceptual notion that warmer/moister air is located north of the second precipitation band suggested by Figs. 4.1.6b,c). This contradiction may result from temporally interpolating the rawinsonde data which has poor temporal resolution. Other remote sensors on the Oden may resolve this issue. Stratocumulus clouds with a NNE wind are present north of the cloud band extending east from V2, with cloud tops near the top of the strong stable layer. The 60 GHz scanning radiometer data (Fig. 4.1.7) show the strong inversion near the tops of the stratocumulus clouds at 200-400 m before 08 UTC, and the lifting of this stable layer to 700 m and above with the passage of the front at 0830-1130 UTC.

Though many of the airborne measurement systems were not operating during this transit case (e.g., microphysics data), the array of dropsondes and Oden upsondes lends itself to a synoptic analysis of the dynamical structure of a complex Arctic frontal system, and an analysis of the dynamic forcing of the clouds observed by the remote sensing instruments on the Oden.

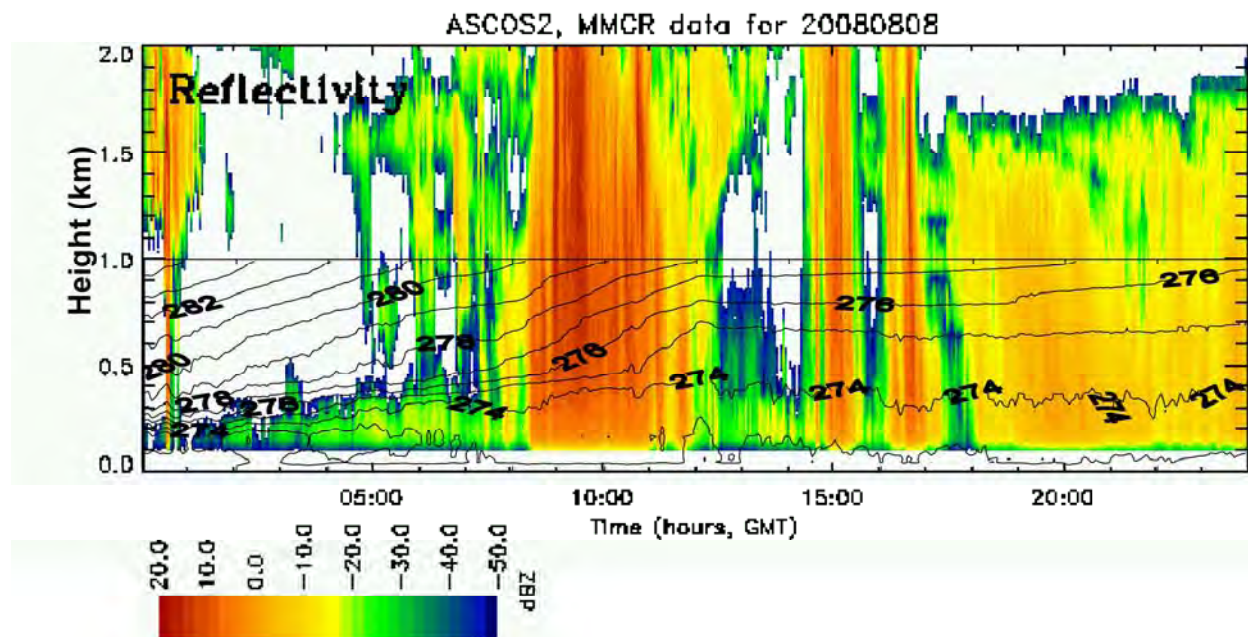


Figure 4.1.7: Time-height series reflectivity from Ka-band radar in lowest 2 km and the retrieved potential temperature (K) from the 60 GHz radiometer in the lowest 1 km on YD221 (Aug. 8, 2008).

4.2 IOP 1; Aug. 12-13 (YD225-226)

Aircraft Takeoff: 18:02:07 Landing:~0346 On Station: 2000-0125
Oden Location when On Station: (87.5, -1.76)
Number of dropsondes: 6 ;
Sonde times(ddhhmmss): 12200519, 12202901, 12204147, 12205703, 13003537, 13010830, 13012017
Meteorological system phase velocity from sat images: 14.5 m/s / 81°
Low-level cloud (~1 km) phase velocity:
Times of direct overflight: 22:17:25 (1614 m), 00:06:00 (114 m), 00:35:50 (2388 m)

After waiting for the Oden to find a solid floe, IOP1 was flown on the evening of Aug. 12 and the morning of Aug. 13, only a few hours after the Oden had moored at 87.5° N, 1.8° W. The objectives of IOP1 were 1) to provide spatial atmospheric sampling near the Oden as a major storm system passed over and 2) to obtain a characterization of the ice conditions near the Oden drift site using the remote sensors before the end of the summer melt. The major low-pressure system moved from northwestern Siberia over the pack ice between Svalbard, passing nearly directly over the Oden and producing a strong low-level flow of warm, moist air from Eurasia over the North Pole (Figs. 4.2.1, 4.2.2, 4.2.3, and 4.2.4). The edge of this plume of

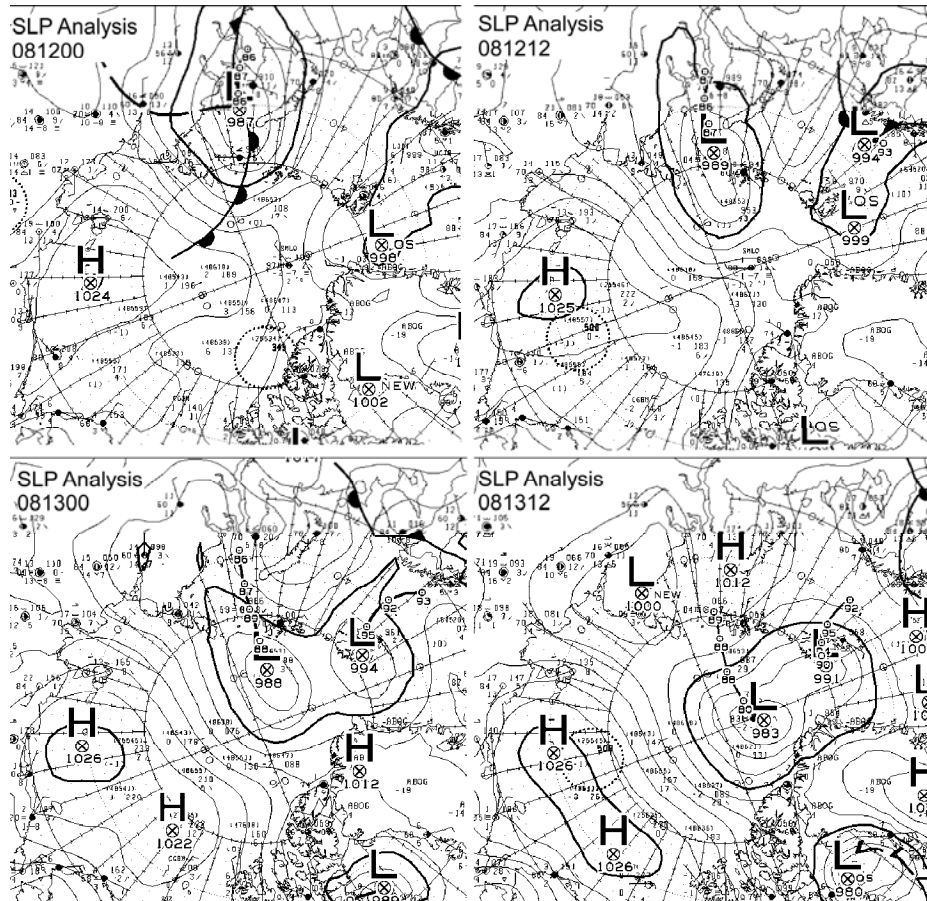


Figure 4.2.1: Canadian Weather Service sea-level pressure analyses at a) 00 UTC Aug. 12, b) 12 UTC Aug. 12, c) 00 UTC Aug. 13, and d) 12 UTC Aug. 13. The Oden is the reporting station at 87.5° N, 2° W.

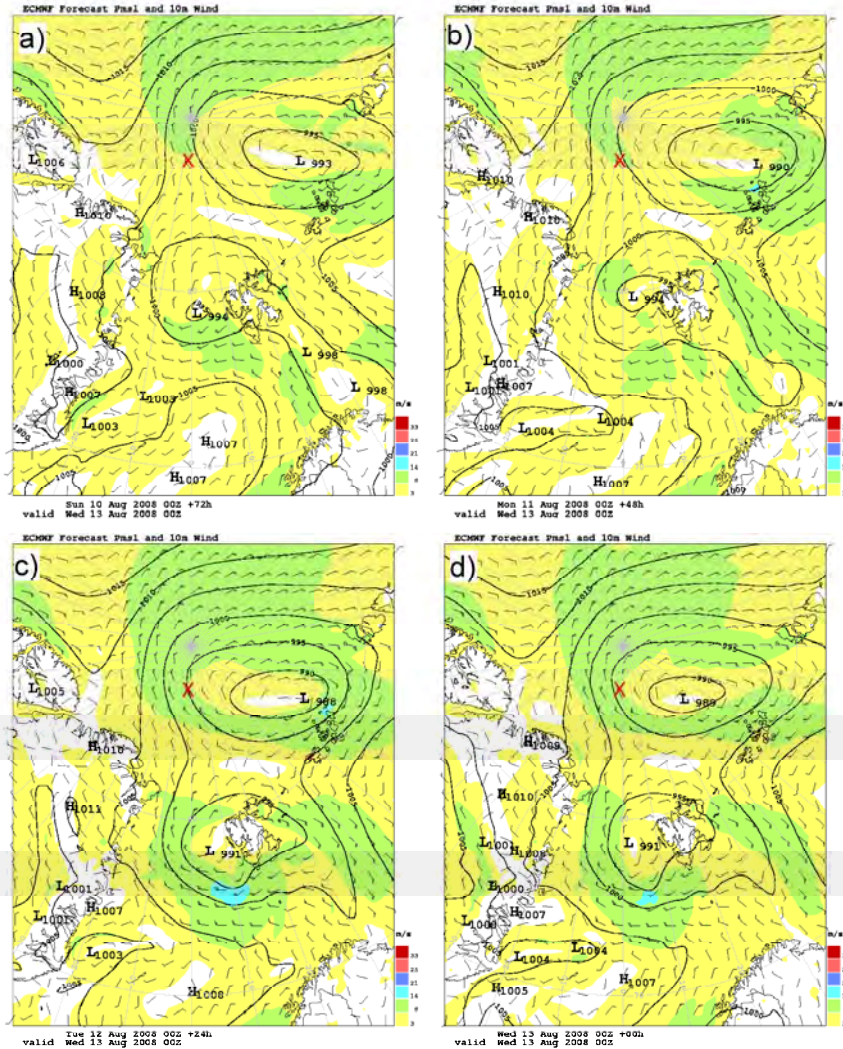


Figure 4.2.2: Forecasts and analysis of sea-level pressure and 10-m winds valid at 00 UTC Aug. 13 from the ECMWF model. Shown are a) 72 forecast, b) 48 h forecast, c) 24 h forecast, and d) analysis.

warm, moist air was forecast to pass over the Oden at about 1.5 km above the surface near 00 UTC Aug. 13 with reasonable accuracy with 24-48 h lead time (Figs. 4.2.3 and 4.2.4), which validations showed to actually happen.

The sequence of satellite images and satellite-derived winds is used to estimate the locations of the surface (or near-surface) fronts (Fig. 4.2.5). In addition, the DC-8 and Oden data are used to refine this analysis. During the afternoon of Aug. 12, warm, moist air flowed from northern Siberia over first open water and then pack ice in the open wave portion of the frontal system. This air was lifted by the warm front and in a diffluent flow, producing clouds in the anticyclonic flow above the warm front over the Siberian and Chukchi Seas as well as in the cyclonic flow over the Oden. The satellite image at 2142 UTC (Fig. 4.2.5c) shows the classical “T-bone” structure (Shapiro and Keyser 1990) of the clouds with this system, which suggests that the system developed in an environment of weak barotropic shear. The Oden was located at the top of the stem of the “T”. Before the low-pressure center arrived near the Oden, the occluded portion of the front passed over the Oden near 2330 UTC Aug. 12 (Fig. 4.2.5c), while

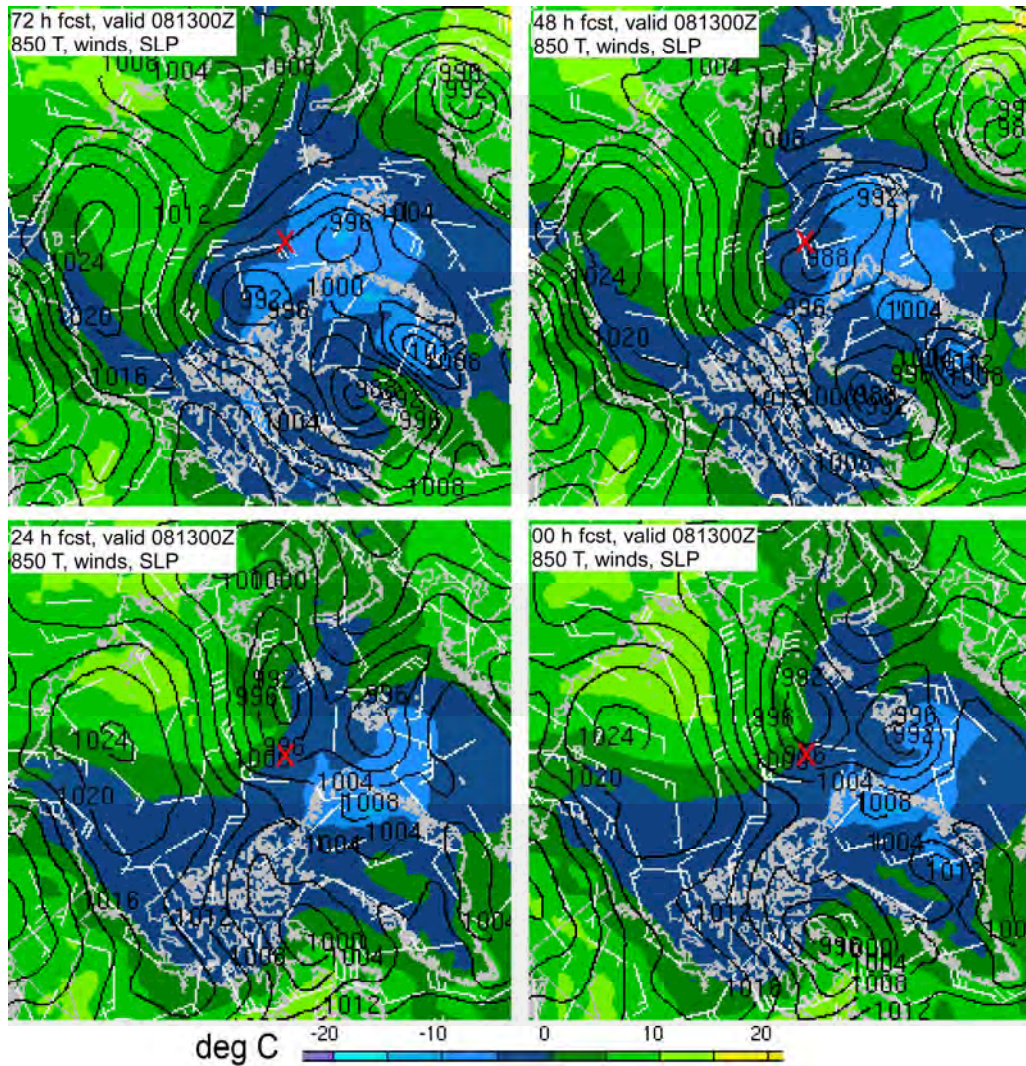


Figure 4.2.3: Forecasts and analysis of 850 hPa temperature (color) and winds, and sea-level pressure (isopleths) valid at 00 UTC Aug. 13 from the GFS model. Shown are a) 72 forecast, b) 48 h forecast, c) 24 h forecast, and d) analysis.

the low passed just south of the Oden near 06 UTC Aug. 13 (Fig. 4.2.5e). The sequence of surface winds at the Oden shows the passage of the low just to its south (Fig. 4.2.5c), and the intensity of this low is revealed by the strong surface winds and the low central pressure (Fig. 3.1d).

The DC-8 collected data in the vicinity of the Oden between ~2000 UTC Aug. 12 and 0130 UTC Aug. 13 during the time of the frontal passage. The track of the DC-8 and its array of dropsondes sampled the “bent-back” portion of the frontal cloud band, the occluded front passing over the Oden, and the low-pressure system (Fig. 4.2.5c). The analysis of the “lawnmower” flight pattern flown at ~1.6 km altitude shows the passage of the warm front aloft, with warmer temperatures and veering winds to the east, along with a significant band of precipitation (Fig. 4.2.6). While the surface temperatures as recorded at the Oden warmed by less than 1 degree during the frontal passage, the temperatures at 1.6 km warmed by 7 degrees. The flow at this altitude is convergent, contributing to the lifting and generation of the clouds and precipitation.

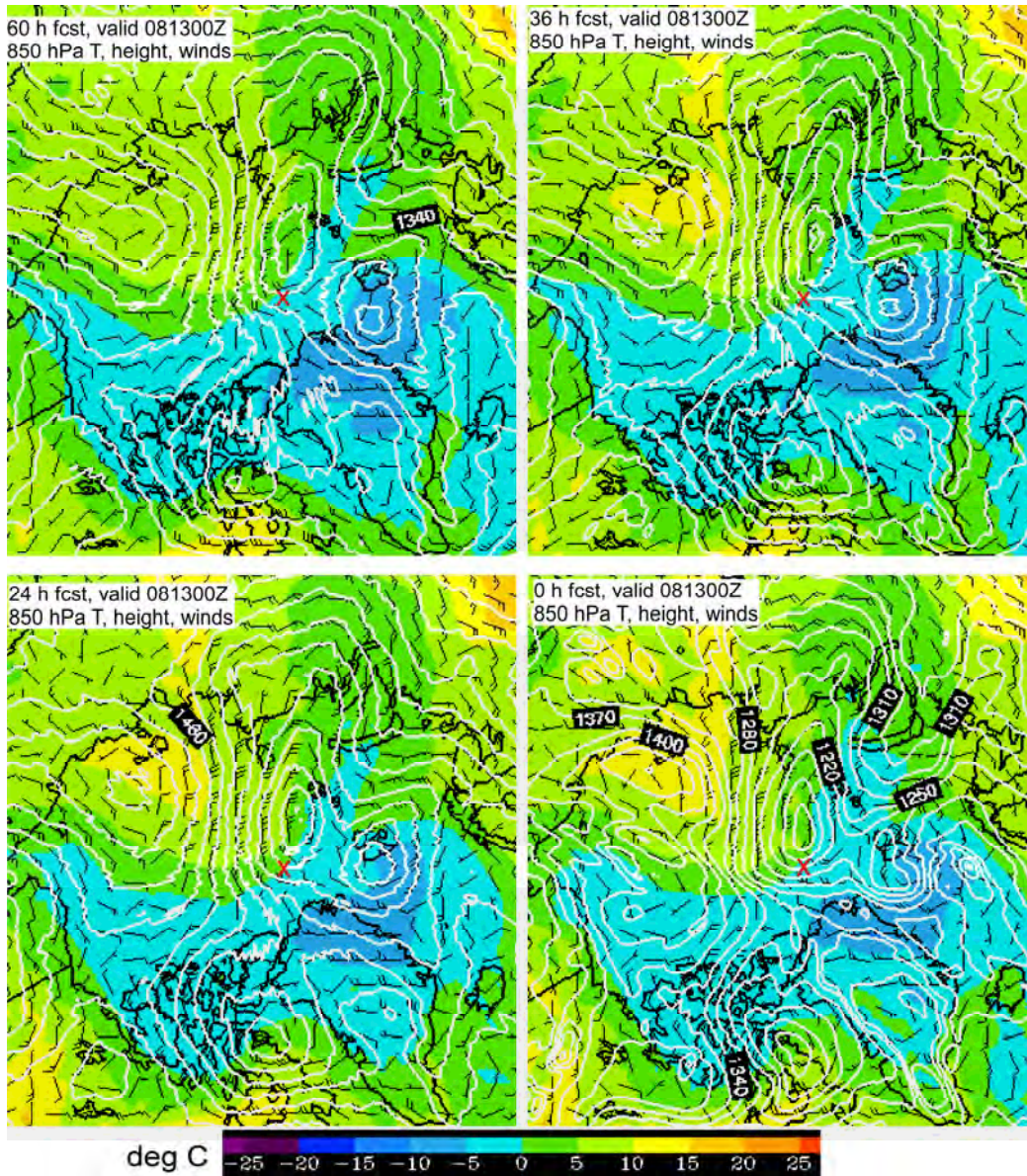


Figure 4.2.4: Forecasts and analysis of temperature (color), winds and height (isopleths) at 850 hPa valid at 00 UTC Aug. 13 from the FIM model. Shown are a) 60 h forecast, b) 36 h forecast, c) 24 h forecast, and d) analysis.

The S-band cloud and precipitation radar images overlaid with thermodynamic analyses from the Oden rawinsondes show that the cloud tops were near 9 km, with the generating cells for the warm frontal clouds aloft located in the low-stability warm air being lifted above the warm front (Fig. 4.2.7). Higher cloud tops and enhanced reflectivity occurs at the leading edge of the lower- θ_e air that comes in after 2330 UTC, or behind the cold front aloft. A very stable layer develops near 1.2 km altitude near 21 UTC Aug. 12, and persists nearly 24 hours. This corresponds to the time that the air between 1-2 km is above freezing behind the warm front. This layer of warm air produces melting of hydrometeors, with freezing rain and sleet at the surface, and shows up as the higher fall velocities in Fig. 4.2.7b. The time-height sections of temperature from the scanning radiometer (Fig. 4.2.8) shows brief periods of less stable air at approximately the time the cold front passes over the Oden above the stable layer, suggesting that frontal passages above the surface influence the stability in the boundary layer.

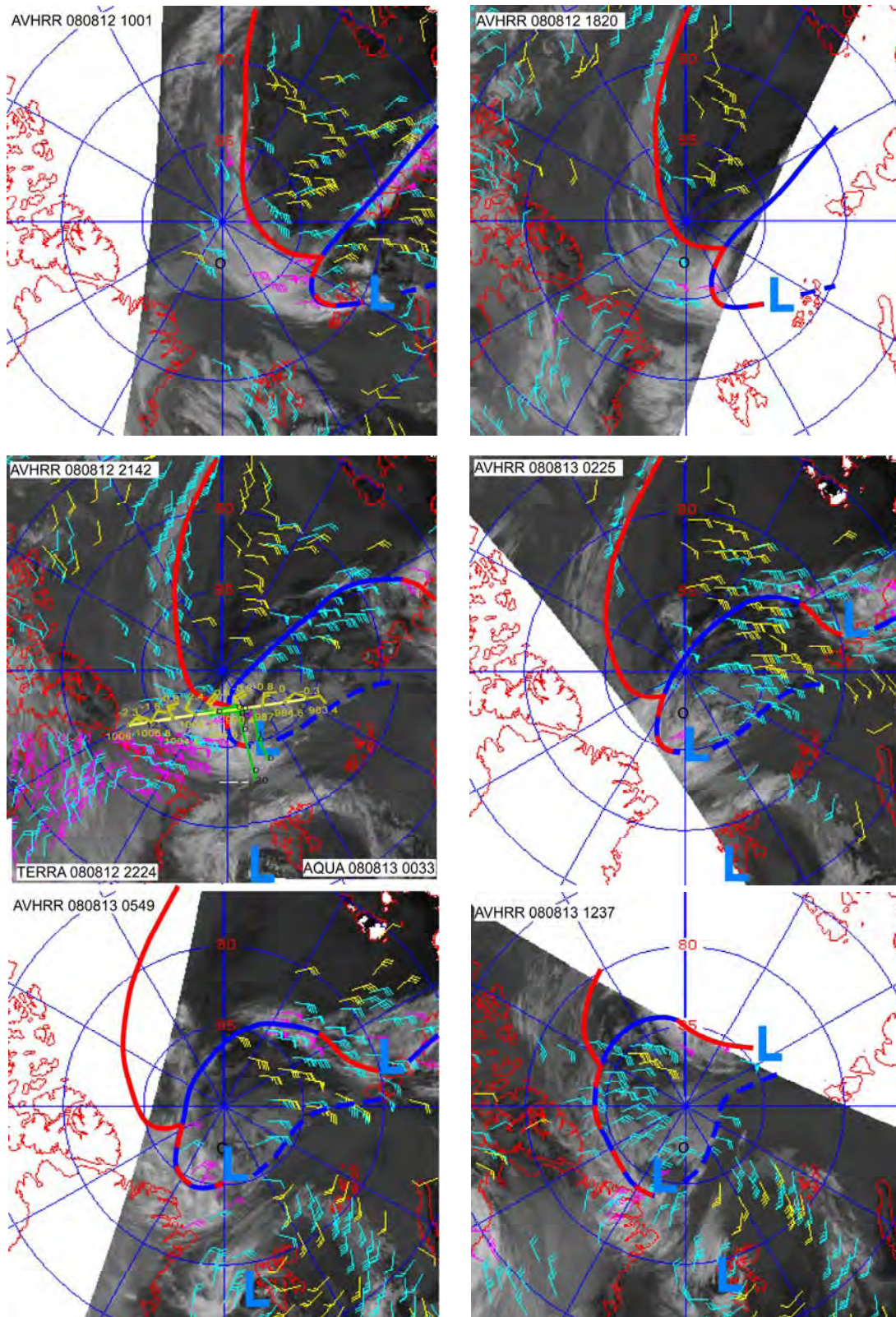


Figure 4.2.5: Sequence of AVHRR satellite images showing the synoptic evolution of IOP1. The satellite-derived winds and the surface frontal features are shown in each image. The tracks of the DC-8 (green) and Oden (yellow) are shown in c) using a phase velocity of 14.5 m s^{-1} from 81° .

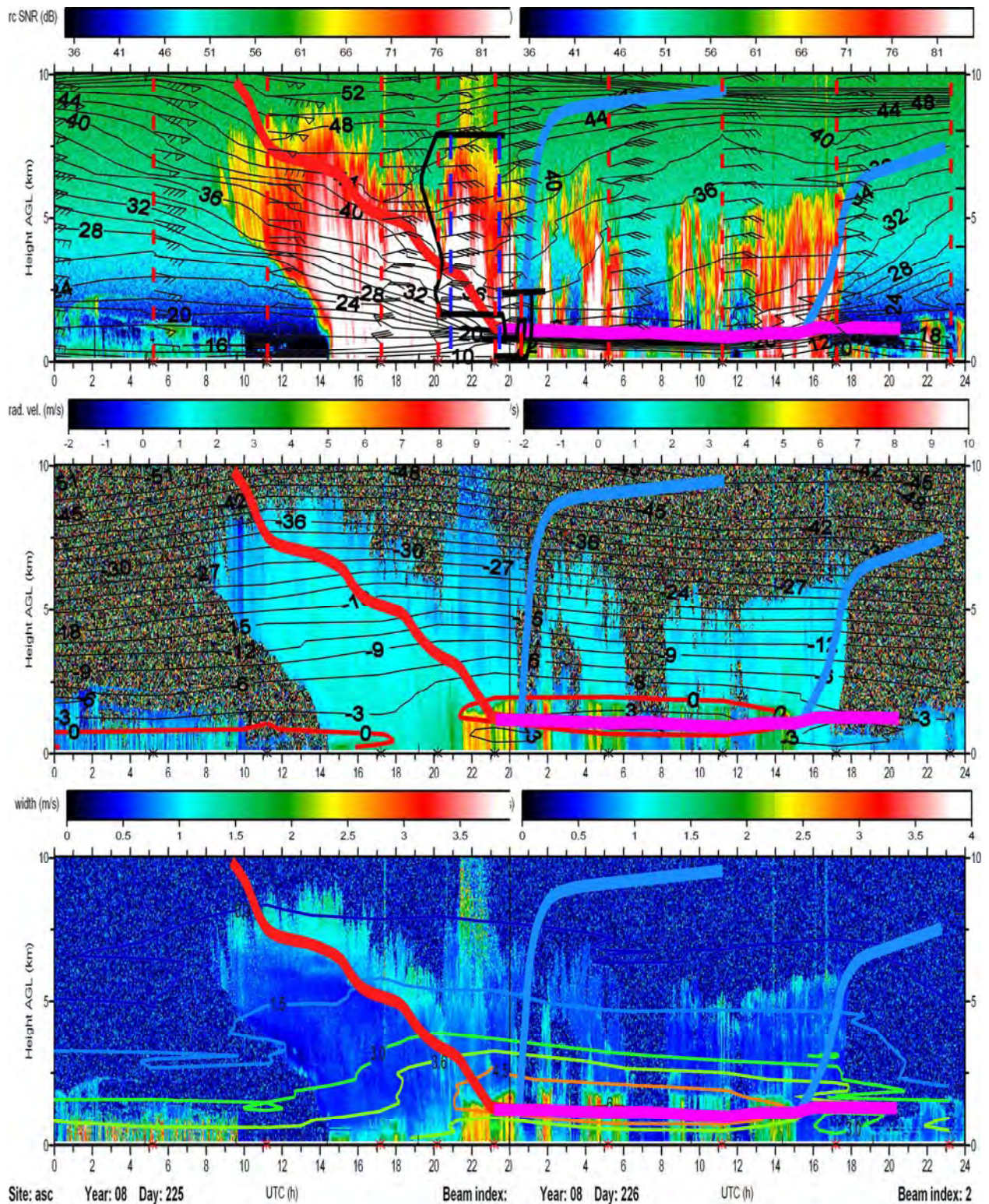


Figure 4.2.7: Time-height cross section of a) θ_e (deg C), wind barbs, and S-band SNR; b) temperature (deg C) and S-band vertical velocity; and c) mixing ratio (g kg^{-1}) and S-band spectral width. Each panel is overlaid with a frontal analysis based primarily on θ_e (heavy red, blue, and purple lines), the DC-8 flight track data (heavy black line), radiosonde times (red stars on abscissa & vertical dashed lines), and dropsonde times and height coverage (vertical dashed blue lines). The heavy red isopleth in b) is the 0°C isotherm.

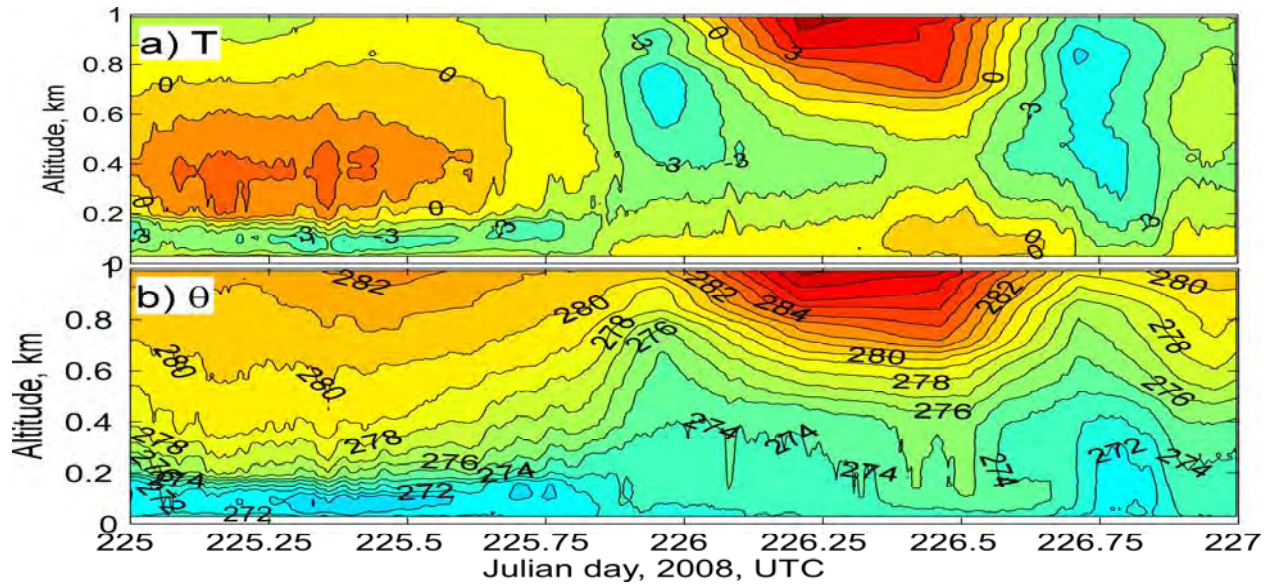


Figure 4.2.8: Time-height sections to 1 km height of the a) temperature and b) potential temperature from the 60 GHz radiometer on YD 225 through YD226.

Table 4.2.1: Times for which the time-space adjusted DC8 and Oden tracks are within ~1.4 km of each other for IOP1. A phase velocity of 14.5 m s^{-1} from 81° was used. The last 3 rows show the times when the proximity of the tracks occurred with the times within 30 s of each other, indicating a direct overflight.

Oden Time	DC8 Time	Altitude (m)	Distance(m)
1930-1945	210720-210900	5300-5842	127-1175
2037-2042	215000-215050	1629-1641	97-1321
2107-2120	215445-215625	1616-1622	107-1178
2121-2127	205510-205540	7768-7771	383-934
2207-2221	221720-221840	1612-1615	171-1336
"	205030-205055	7754-7757	545-1099
2231-2233	232030-232050	760-761	240-1336
2256-2309	223400-223540	1606-1608	171-1216
2311-2313	235520-235535	144-145	153-1255
2330-2333	223820-223830	1601-1604	23-1050
"	002820-002830	2358-2361	545-1034
2348-2352	230445-230455	986-1048	296-1092
"	204030-204035	7768-7769	511-895
2359-0013	233155-233330	742-746	142-1323
"	000600-000640	111-116	522-1213
0026-0122	003440-004100	2384-2388	127-1318
0125-0128	004120-004140	2383-2384	1065-1304
0136	004235	2384	1291
0144-0153	004325-004420	2380-2383	939-1296
Direct Overflight (< 30s difference betw. the two times)			
2217	221725	1614	816
0006	000620	114	643
0036	003550	2388	487

4.3 IOP 2; Aug. 15 (YD228)

Aircraft Takeoff: 04:02:00 Landing:~1510 On Station: 0520-1225
Oden Location when On Station: (87.5, -1.76)
Number of dropsondes: 4 ;
Sonde times (ddhhmmss): 15052249, 15070458, 15084038, 15121925
Meteorological system phase velocity from sat images: 13.9 m/s / 175° (all); 12.4/161° (north)
Times of direct overflight: 0919, 1144

Another objective of AMISA was to obtain air samples in airflow trajectories from the open water south of the Fram Strait to the Oden near the North Pole to assess whether aerosols or cloud condensation nuclei may arrive at the Oden from the marginal ice zone. IOP2 on Aug. 15 was an attempt to sample such a case. The remnant low-pressure system from two days before had filled and positioned itself due north of Greenland (Figs. 4.3.1 and 4.3.2), producing weak southerly surface flow through the Fram Strait. This evolution was forecast reasonably well, though the verification showed the flow to be a little more from Svalbard rather than straight through the Fram Strait (Fig. 4.3.2). The timing suggested that the flow would be more through the Fram Strait before 12 UTC on Aug. 15 (Figs. 4.3.3 and 4.3.4). While the flow would be southerly, the temperatures at 1.5 km were forecast to be much colder than for IOP1 (Figs. 4.3.3 and 4.3.4).

The satellite images (Fig. 4.3.5) show a large vortex in the cloud field north of Greenland corresponding to the main surface low, with a cloud band emanating from the NE corner of Greenland associated with the front, separating flow through the Fram Strait from that circulating north of Greenland. The flight started with two aerosol stacks near the ice edge and another one over the pack ice approximately halfway to the Oden from the ice edge (Fig. 4.3.5). These aerosol stacks were comprised of 3 legs oriented perpendicular to the wind at ~ 250 m, 1100 m, and 1600 m. A third aerosol stack was done over the Oden, and tracks between the stacks consisted of slow ascent/descent profiles to ~8000 m, with a dropsonde released at the apex.

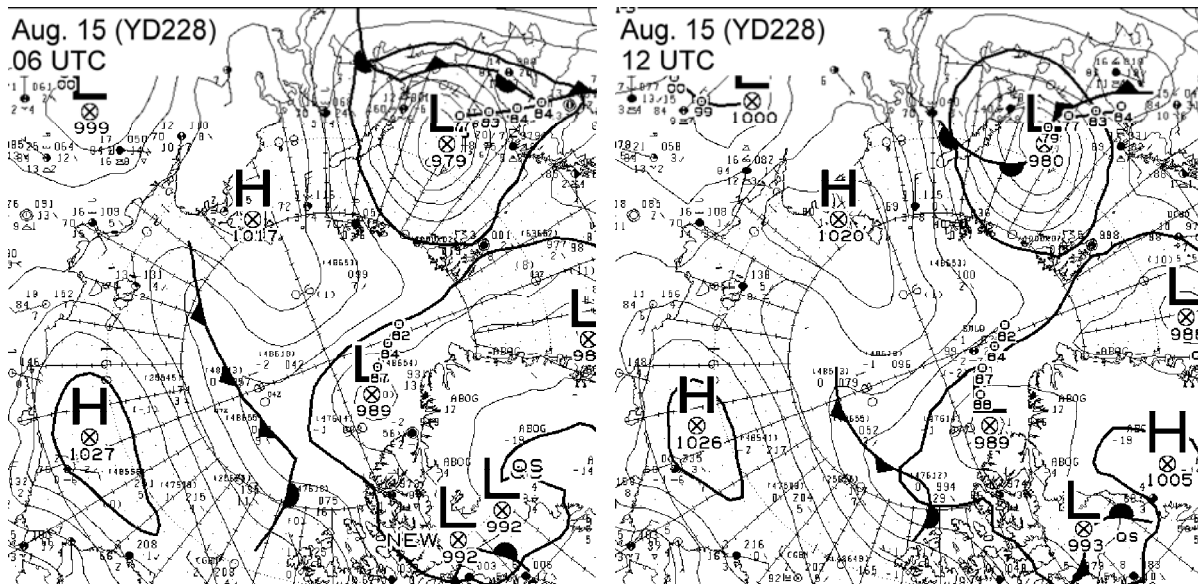


Figure 4.3.1: Sea-level pressure and frontal analysis from Canadian Weather Service at 06 UTC and 12 UTC Aug. 15 (YD228).

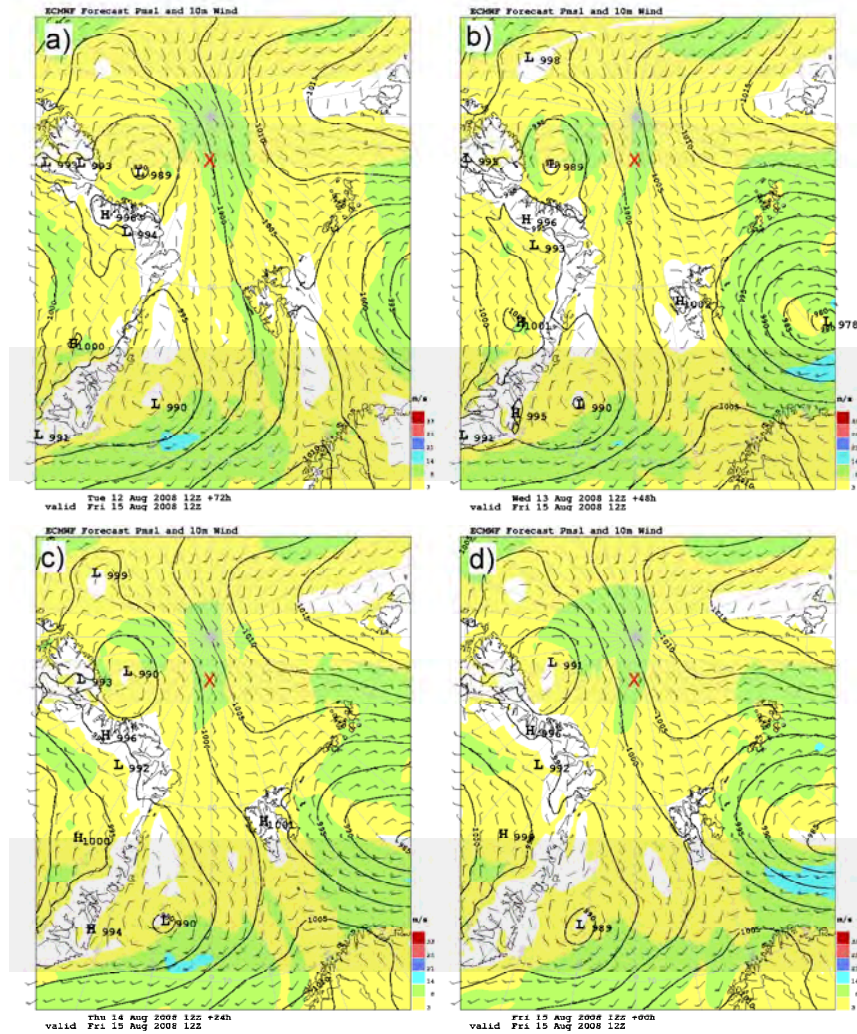


Figure 4.3.2: Forecasts and analysis of sea-level pressure and 10-m winds valid at 12 UTC Aug. 15 from the ECMWF model. Shown are a) 72 forecast, b) 48 h forecast, c) 24 h forecast, and d) analysis.

After the aerosol stack was completed over the Oden, a truncated “lawnmower pattern” was flown to again characterize the sea ice conditions.

Figures 4.3.5 and 4.3.6 show that the flux stacks were performed perpendicular to the southerly flow. The low-level cloudiness near stack #2 suggests that the conditions were perhaps not homogeneous from the ice edge to the Oden. The condensation nuclei (CN) concentrations sampled at the first two stacks show values of $\sim 100\text{-}300\text{ cm}^{-3}$ (Fig. 4.3.6), suggesting that similar air was being sampled. The CN values obtained near the Oden within the frontal cloud band (Fig. 4.3.7b) show similar values on the east side of the front at 1.6 km altitude, while much higher values ($\sim 1500\text{ cm}^{-3}$) were observed on the western side of the cloud band. The temperature field at 1.6 km (Fig. 4.3.7a) shows the air to be warmer on the east side, while the slow westward movement of the band indicates that it is a warm front. The flow is diffluent at 1.6 km (Fig. 4.3.7), indicating that the convergence producing the clouds and lifting must occur at another level.

The track of the Oden is very oblique to the front (Fig. 4.3.7), so the time-height sections provided by the Oden remote sensors and rawinsondes produce a much more gradual transition

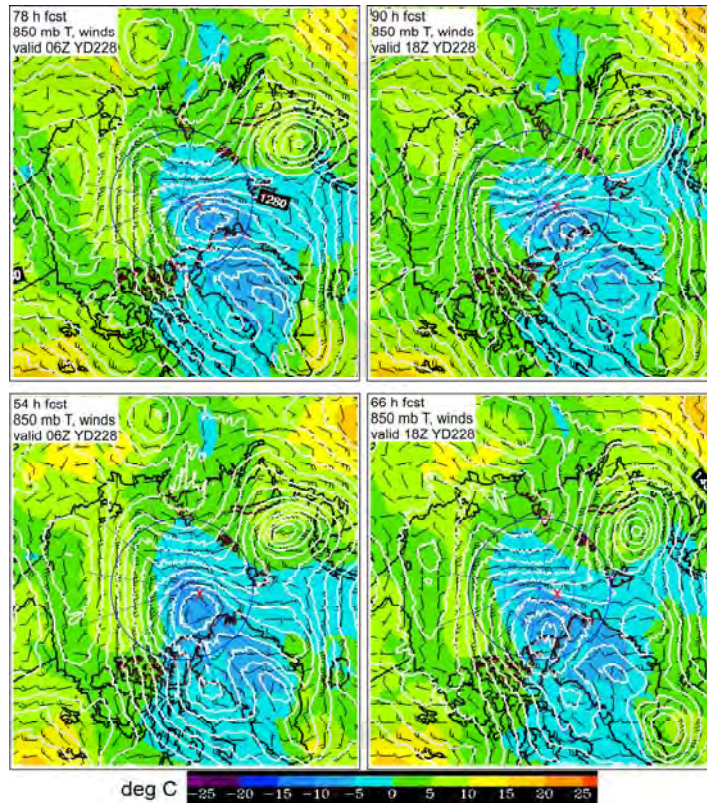


Figure 4.3.3: Forecasts of temperature (color), winds and height (isopleths) at 850 hPa valid at 06 UTC Aug. 15(a,c) (78 h & 54 h forecasts) and 18 UTC Aug. 15 (b,d) (90 h and 66 h forecasts) from the FIM model.

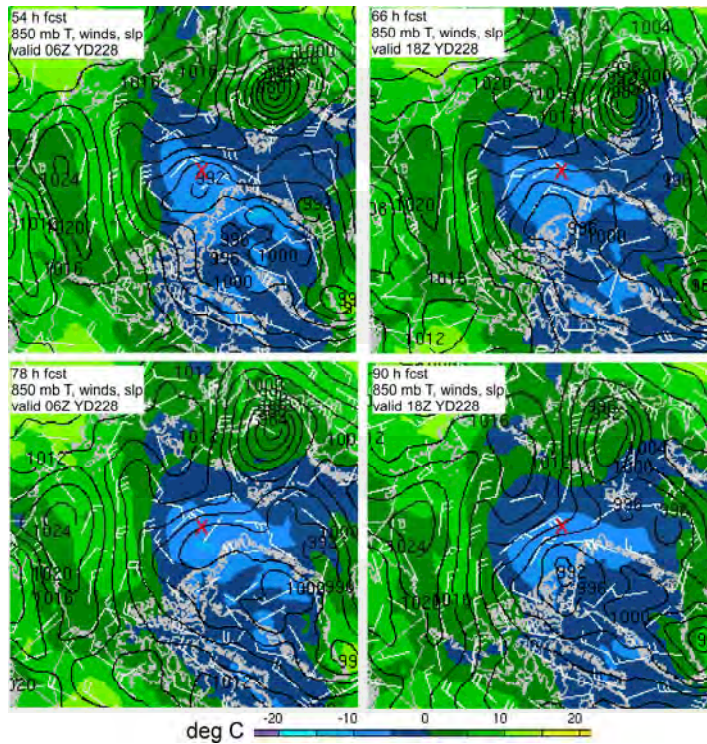


Figure 4.3.4: Forecasts of 850 hPa temperature (color) and winds and sea-level pressure (isopleths) valid at 06 UTC Aug. 15 (a,c) (54 h and 78 h forecasts) and 18 UTC Aug 15 (b,d) (66 h and 90 h forecasts) from the GFS model.

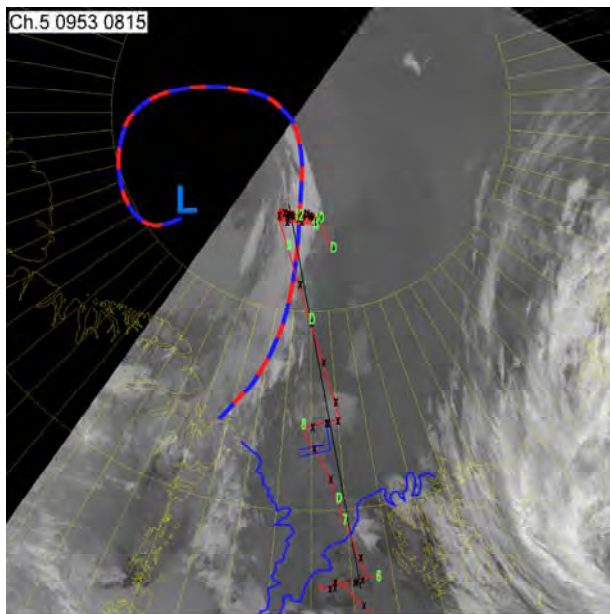
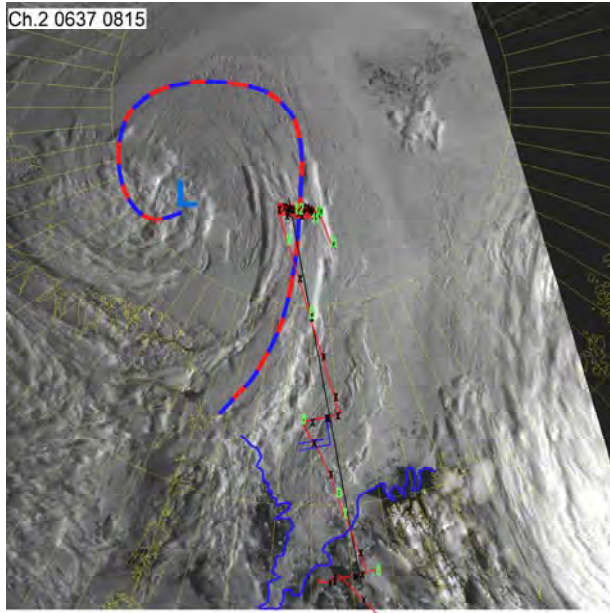


Figure 4.3.5: Visible (a) and infrared (b) satellite images showing the sampled system for IOP2. The complete flight track (red line), hour along flight track (green), 10-min markers ("x"), and ice edge (blue) are shown. A wind barb at 1.6 km at the intermediate aerosol stack is also shown. No time-space adjustment is done to this track (it is geographically correct.)

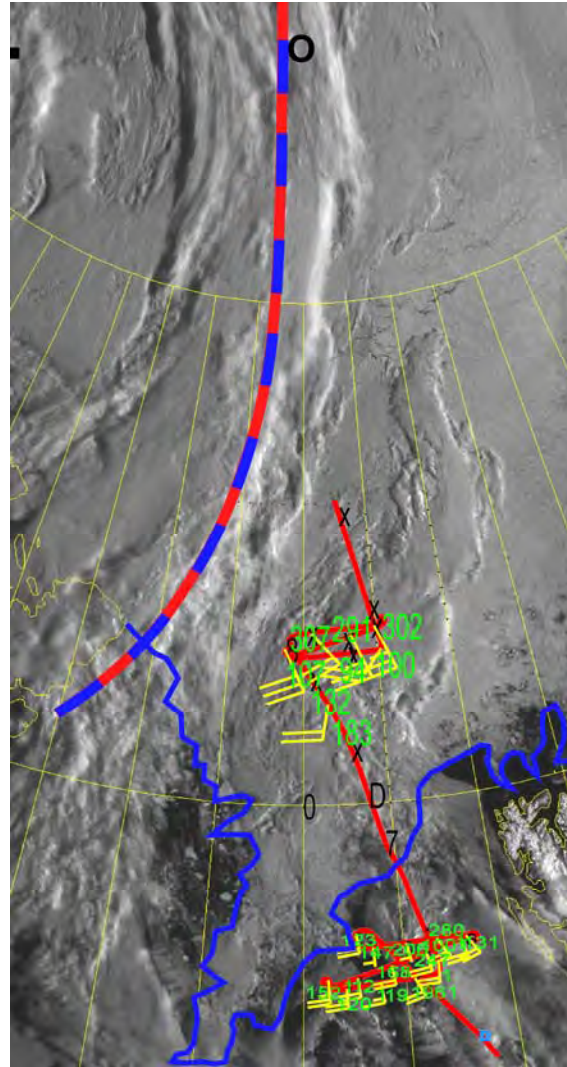


Figure 4.3.6: Flight track time-space adjusted to 0637 UTC overlaid on visible satellite image at 0637 UTC. The green numbers show the cloud condensation nuclei concentration (cm^{-3}). The heavy blue line shows the ice edge.

than would likely be produced with a cross-section perpendicular to the frontal band. Nevertheless, analysis of the serial rawinsondes shows the warm-frontal structure above a few hundred meters above the surface (Fig. 4.3.8). Multiple layers of potential instability and a complex frontal structure in the vertical (as seen on the transit flight case) produces multiple cloud layers. The cloud radar also shows variable reflectivity intensity in the low-level

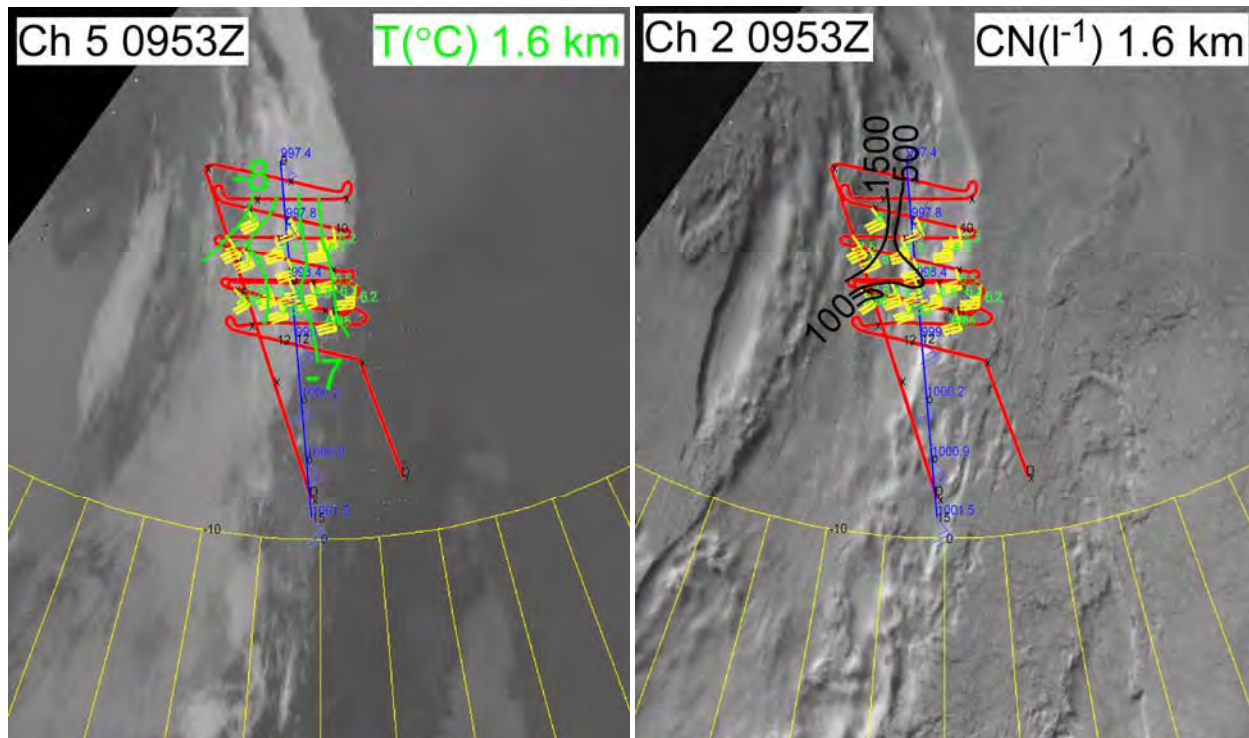


Figure 4.3.7: Infrared (a) and visible (b) satellite images at 0953 UTC on Aug. 15 2008 showing the analysis of temperature (a) and condensation nuclei (CN) (b) at 1.6 km altitude from the aircraft data. The DC8 track (red) and Oden track (blue) are time-space adjusted to 0953 UTC using a phase velocity of 13.9 m s^{-1} from 175° . Wind barbs from the aircraft (yellow) and Oden (blue) and the Oden hourly surface pressure are also shown.

stratocumulus clouds, which seems to be correlated with the variability in the low-level temperature (Fig. 4.3.9). The only precipitation occurs between 0750-1000 UTC, which corresponds to a narrow region of deeper clouds only subtly discernible in the satellite images. However, the aircraft crosses this feature on all of its transverse legs (Fig. 4.3.7).

The DC-8 also flies in various cloud layers, crossing the Oden track at twelve points and heights (Table 4.3.1 and Fig. 4.3.8b). If one assumes that the frontal features seen along the Oden cross-section in Fig. 4.3.8 are quasi-two-dimensional, the aircraft will cross the features from well to the left of the precipitation band to over the low-level stratocumulus on the right at the altitudes marked by a “D” in Fig. 4.3.8b.

The analysis of RH_w at 1.6 km shows the very moist conditions at this level, with water saturation occurring in a cloud layer at this level near the warm edge of the deeper clouds (Fig. 4.3.10a). However, when the aircraft later flies eastward at 900 m below and eventually beyond this upper cloud layer (Fig. 4.3.10c) and in the top of a lower stratocumulus layer, saturation is present in the top of the lower cloud layer at approximately the eastern edge of the upper layer. Furthermore, the aircraft descent through this lower layer at an earlier time showed that it had near-neutral stratification with a very cold cloud top. [Note that this is the stratocumulus cloud for which the 60 GHz scanning radiometer showed strong cooling below 500 m as well (see Fig. 4.3.9).] Furthermore, liquid water contents of $> 15 \text{ cg m}^{-3}$ were observed in the tops of these lower clouds at this location (Fig. 4.3.10b,d). This LWC was more than anywhere else during the flight.

We interpret these measurements as indicating that strong cloud top radiative cooling occurred in the lower stratocumulus cloud layer in the region where it emerged from underneath

the upper cloud layers. When the upper cloud layers are present, radiative effects from this upper layer probably limit the cloud top radiative cooling possible in the lower cloud deck, hence illustrating a mechanism for cloud-layer interactions near frontal systems that can impact the cloud characteristics and the surface energy fluxes. The radiation data from the aircraft and at the surface will be valuable to further explore this hypothesis.

Table 4.3.1: Times for which the time-space adjusted DC8 and Oden tracks are within ~1.4 km of each other for IOP2. A phase velocity of 13.9 m s^{-1} from 175° was used. The last 2 rows show the times when the proximity of the tracks occurred with the times within 30 s of each other, indicating a direct overflight.

<u>Oden Time</u>	<u>DC8 Time</u>	<u>Altitude (m)</u>	<u>Distance(m)</u>
0918-0920	091910-091925	116-117	301-1346
0938-0940	093635-093650	740-741	308-1239
0956-0958	095420-095430	1631-1632	207-1008
1017-1018	100850-100905	1635-1636	415-1083
1039-1041	102515-102525	1640-1642	232-1085
1100-1102	103945-104000	1641-1642	323-1284
1104	111200-111210	1639-1640	566-979
1122-1124	105545-105600	1640	459-1337
1124-1125	112635-112645	1639-1640	720-1220
1143-1145	114410-114420	107-110	76-1111
1205-1207	120210-120225	815-816	89-1217
1427-1438	084020-084105	6988-6994	117-1282
Direct Overflight (<	30s difference betw.	the two times)	
0919	091915	117	301
1144	114415	107	76

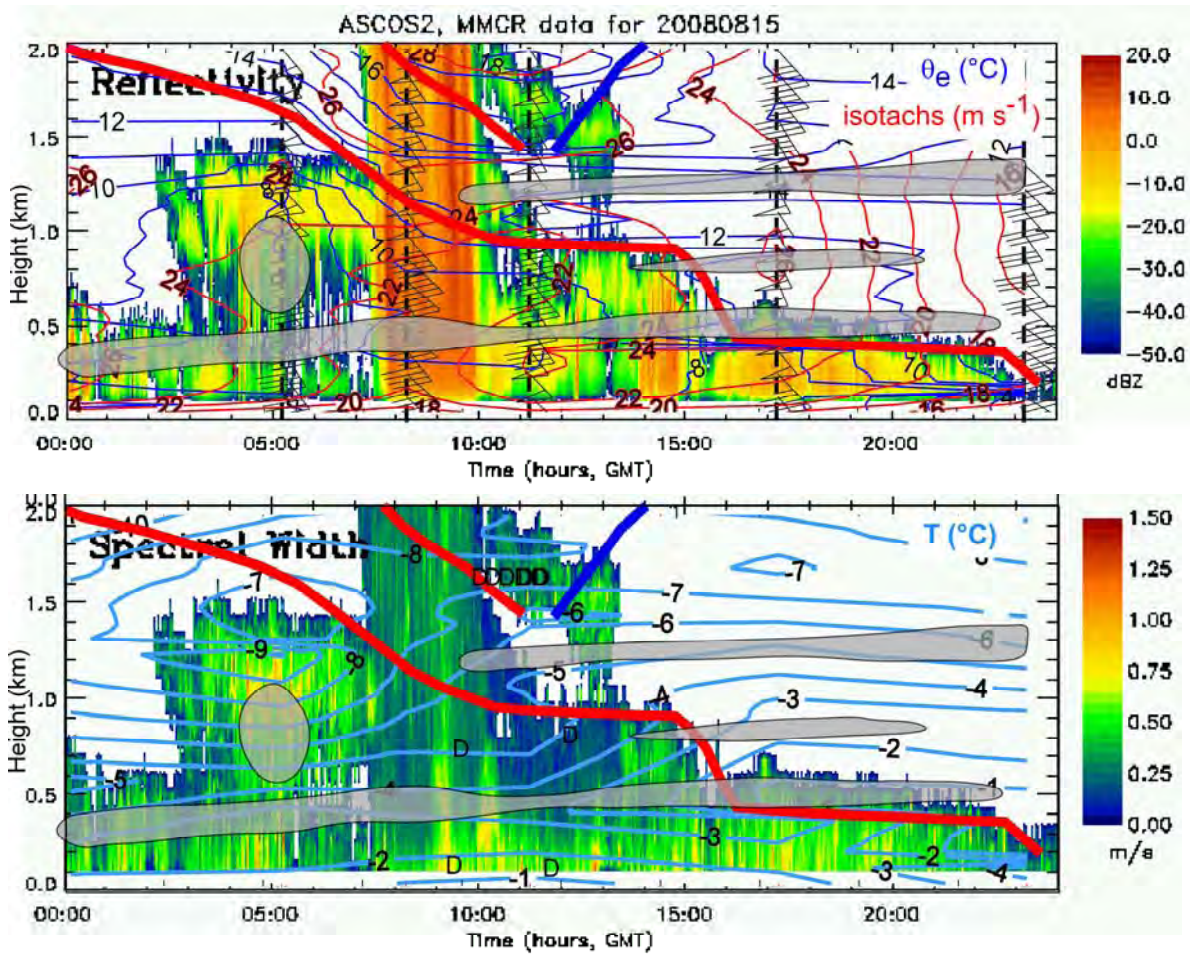


Figure 4.3.8: Time-height series analyses of Ka-band radar and rawinsonde data in the lowest 2 km on Aug. 15 (YD228). Shown are a) reflectivity (color), θ_e (blue), isotachs (red), and wind barbs; b) spectral width (color) and temperature (blue). The times and heights of coincident data from the DC-8 (Table 4.3.1) are shown by a "D" in b). Warm (red) and cold (blue) frontal analysis based on the θ_e field are shown in both panels. Shaded areas depict regions of potential instability and vertical black dashed lines show the rawinsonde ascent times.

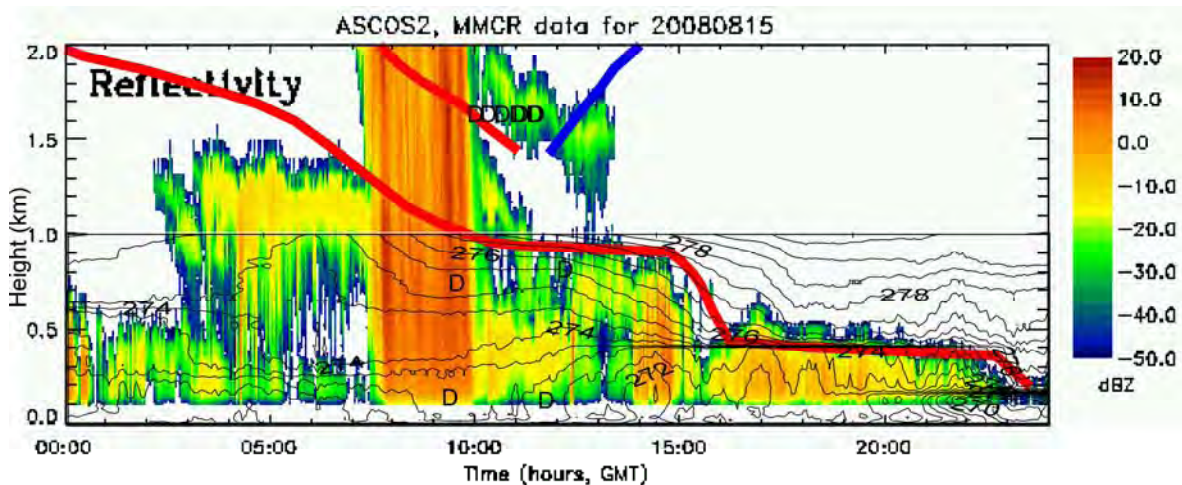


Figure 4.3.9: MMCR radar reflectivity (color) and potential temperature (0.5 K isopleths) from the 60 GHz radiometer for Aug. 15, 2008.

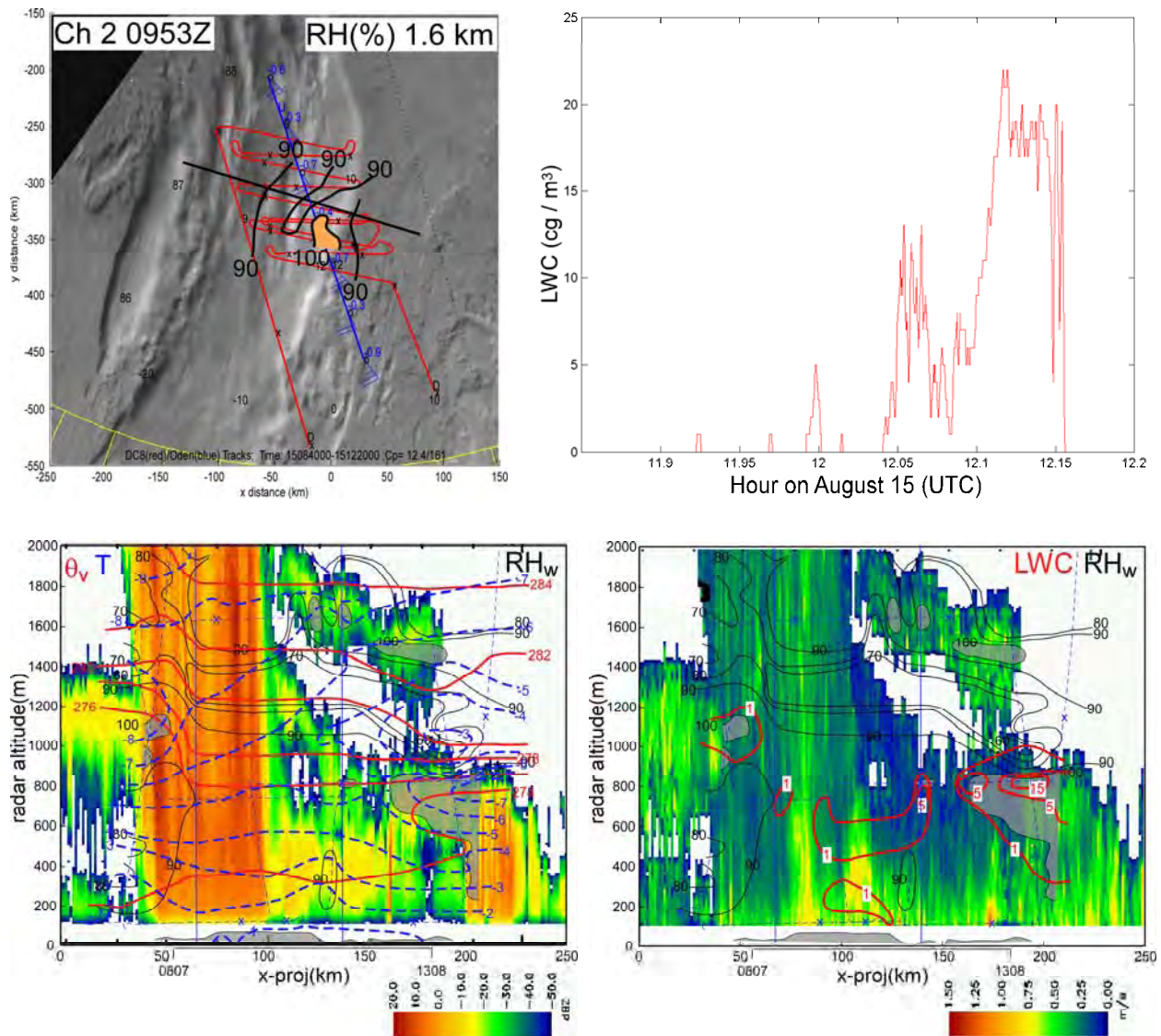


Figure 4.3.10: a) Horizontal plot of the aircraft track and relative humidity analysis at 1.6 km overlaid on the visible (Ch. 2) satellite image, time-space adjusted to 0953 UTC using a phase velocity of $12.4 \text{ m s}^{-1} / 161^\circ$. The Oden track from 08-14 UTC is shown in blue.; b) liquid water content (LWC, cg m^{-3}) measured by the cloud-aerosol spectrometer probe on the DC-8 between 115300 and 121000 UTC Aug. 15; c) analysis of relative humidity wrt water (RH_w , %, thin black solid), virtual potential temperature (solid red, K), and temperature ($^\circ\text{C}$, dashed blue) using data projected to the cross-section along the black line in a) for data within 90 km of the line. Data from the aircraft track (thin blue dashed) and the Oden upsondes (thin blue solid) are used, along with Oden data at 35 m MSL between 0807 and 1308 UTC. The cloud radar reflectivity from the Oden is also projected to the cross-section, though the observations before 0807 and after 1308 are further than 90 km from the line.; d) same as c), but showing cloud liquid water (red, cg m^{-3}), RH_w (black solid, %), and radar spectral width (color background). $\text{RH}_w > 100\%$ is shaded. A 30-sec running mean filter is used on both RH_w and LWC. On the DC-8 track, "x" marks a 10-minute point, while hours are shown by black numbers. "U" and "D" indicate Oden upsondes and DC-8 dropsondes, respectively.

4.4. IOP 3; Aug. 22 (YD235)

Aircraft Takeoff: 03:58:03 Landing:~1210 On Station: 0530-1045
Oden Location when On Station: (87.5, -1.76)
Number of dropsondes: 3
Sonde times (ddhhmmss): 22053137 22060640 22063724
Meteorological system phase velocity from sat images: $10.3 \text{ m s}^{-1} / 191^\circ$
Times of direct overflight: Not in vicinity of Oden

IOP3 was the only observing period not focused on providing data in the vicinity of the Oden. Instead, the purpose was to obtain measurements in a thick and uniform cloud band over both the pack ice and the open water. These measurements are intended to improve the “storm correction” portion of the AMSR-E sea-ice detection algorithm. Because of airspace issues, the only possible area for such measurements was in the Fram Strait, and an opportunity for such a flight occurred on Aug. 22, 2008, when a slow-moving thick band of clouds moved northward through the Fram Strait. A tongue of sea ice extended southward in the center of the Fram Strait (Fig. 4.4.1a), so the flight track was executed along the eastern edge of this ice tongue in the eastern half of the Fram Strait. The thick, nearly uniform cloud shield associated with this system at the time of the flight is shown in Fig. 4.4.1b. This cloud shield, though very coherent and fairly deep, was not associated with any major surface pressure perturbation. While a low pressure system is suggested to be located on the west side of this cloud band by the satellite image (Fig. 4.4.1b), surface analyses only show very weak surface minima along the east and north coasts of Greenland (Fig. 4.4.2).

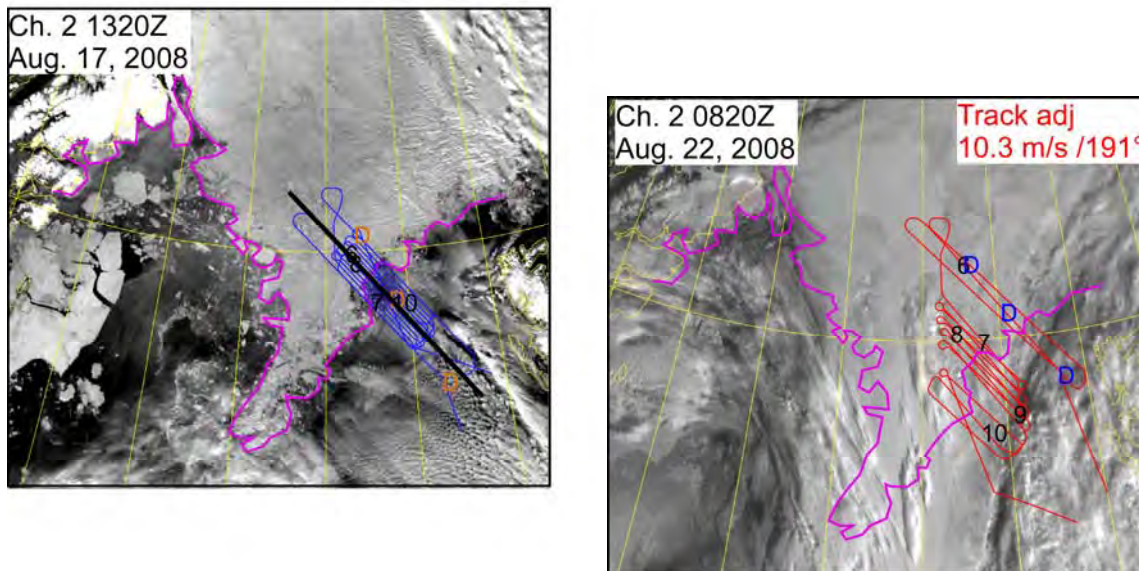


Figure 4.4.1: Images illustrating the location of the IOP3 flight. a) clear-sky visible satellite image from Aug. 17 showing the ice edge (purple) and the geographically located flight track from Aug. 22; b) flight track on Aug. 22 time-space adjusted to the time of the visible satellite image using a phase velocity of 10.3 m s^{-1} from 191° . The dropsonde locations (D) and the hours along the track are shown. The location of the cross-section in Fig. 4.4.3 is shown in a), and the location of the ice edge on Aug. 17 is overlain on the Aug. 22 image in b).

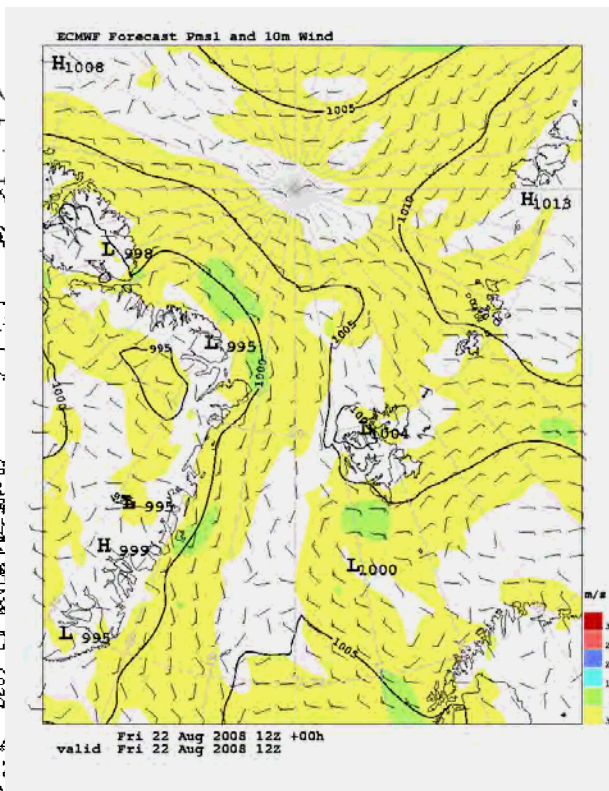
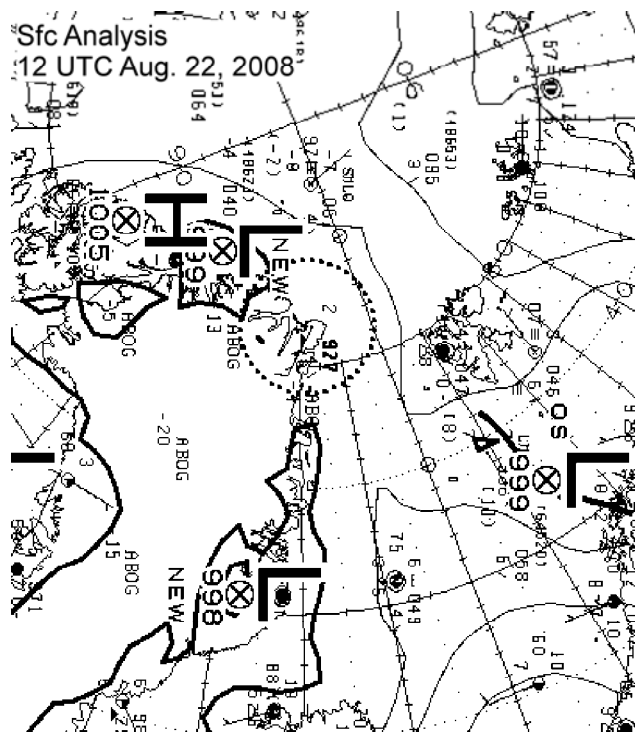


Figure 4.4.2: Surface pressure analyses at 12 UTC Aug. 22, 2008, from a) the Canadian Meteorological Service, and b) the ECMWF.

The system phase velocity estimated from the satellite image sequence was 10.3 m s^{-1} from 191° . The flight track consisted of an upper-level pattern at 8100 m from over the open water to well in over the sea ice with 3 dropsondes placed over the open water, at the ice edge, and over the ice. These are used to characterize the atmospheric cloud structure. These passes were followed by a series of 9 passes in a “lawnmower” type pattern at 1700 m to map out the regional sea ice characteristics. At the end, a series of 3 passes at 150 m were then performed to characterize the details of the surface conditions (Fig. 4.4.3). At the end, an ascent-descent-



Figure 4.4.3: Photos taken from 150 m height at a) 0950 UTC and b) 1007 UTC at the NW and SE ends of the legs, respectively. a) shows pack ice with many meltponds and some leads, while b) shows open water with the edge of the pack ice in the distance. (Photos: R. Wilcox)

ascent leg oriented diagonally across the rectangle defined by the other legs was done to provide some microphysical profiling of the cloud band, with the apex of the first ascent occurring just above cloud top. Note that, because of the movement of the cloud system, the dropsondes, the 1700 m legs, and the 150 m legs with the final ascent/descent/ascent diagonal were done in three different areas of the cloud system (Fig. 4.4.1b). Only if it is assumed that the cloud band was quasi-homogeneous in the along-band direction can we justify overlaying the data from the three different portions of the flight. If we assume that the ice edge is the primary determinant of the cloud structure, then the data was collected in the same cloud region.

The vertical cross-section from the sea ice to over the open water (Fig. 4.4.4) shows that the cloud top was fairly uniform near 3100 m, with slightly deeper clouds at the eastern edge (note that the dropsonde RH was low, with in-cloud values only reaching 90-95%; the aircraft in-situ RH instruments were totally unbelievable during some legs and especially during the last ascent/descent/ascent profiles, and were hence not used in the cross-section analysis). The temperature field and the LWC measurements show indications of cloud top radiative cooling near the ice edge, but none further east. The temperature near 200-300 m is +4° C just east of the ice edge, with slightly cooler temperatures near the surface and further west (Fig. 4.4.4a). The airflow in this cloud band is uniformly from the ENE through its entire depth at the eastern edge, veering to southerly at the western edge of the cross-section and near and above cloud top.

Horizontal fields at 1700 m show slightly greater RH_w in the northwestern half of the measured rectangle (Fig. 4.4.5). The temperature field showed a weak maximum near the ice edge in the middle of the sampled rectangle. The winds show the weak easterly flow to the east and the stronger southerly flow at the western end of the domain. The horizontal temperature field at 150 m, where one would expect stronger impacts from the surface, shows again a slight maximum just SE of the ice edge (Fig. 4.4.6a), with slightly cooler temperatures to the NW over the sea ice. However, the temperatures are above freezing at this altitude even over the sea ice. Again, the wind field shows the weak easterlies at the SE end of the domain and the stronger southerlies over the sea ice. The fields of the main atmospheric parameters showed only very subtle spatial variations (e.g., temperature). However, CN showed large variations (Fig. 4.4.6b). Over open water, CN values were 300-500 cm^{-3} , while over the sea ice values were up to an order of magnitude larger (1000-4500 cm^{-3}). The source of the high CN values over the sea ice is unclear.

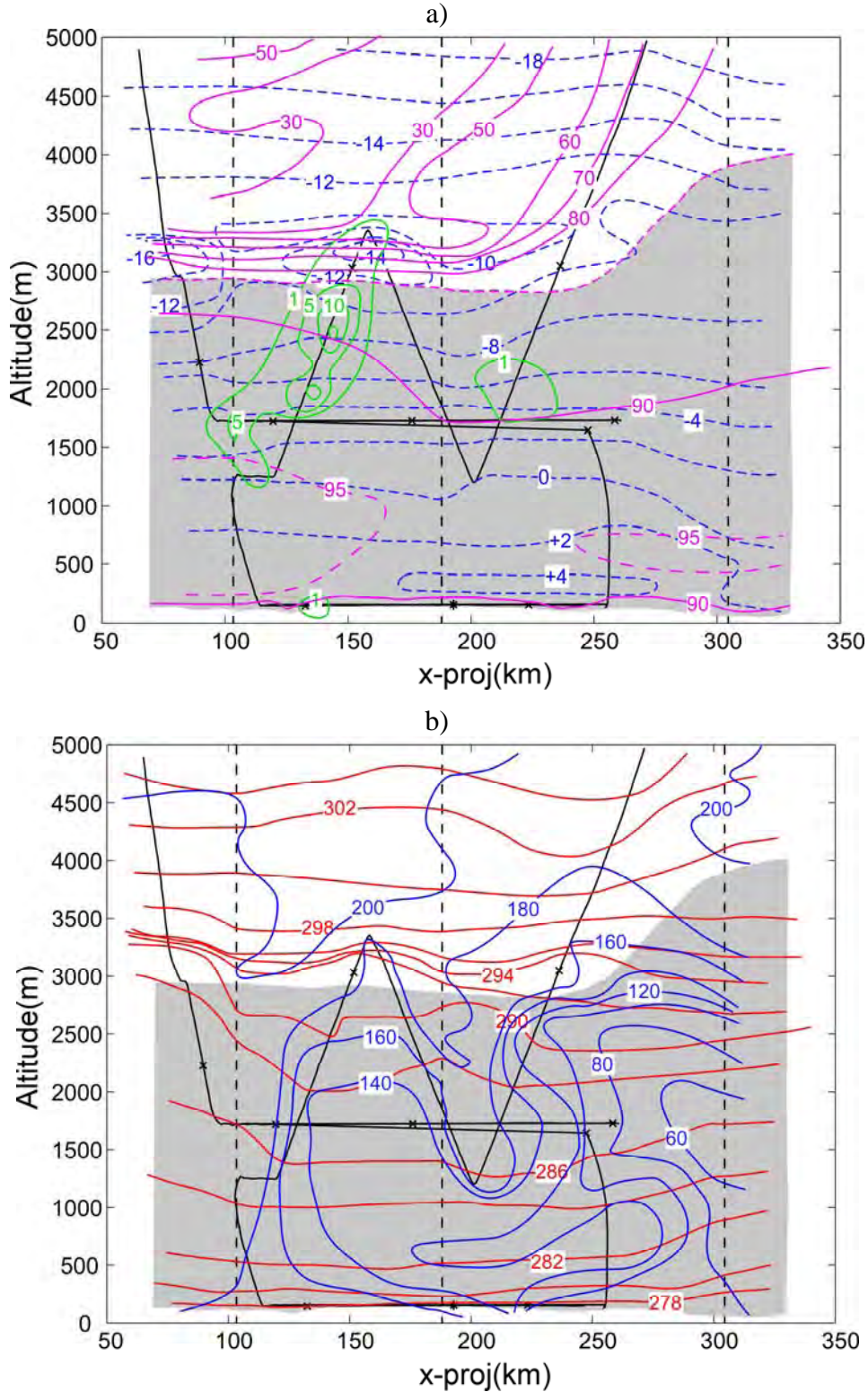


Figure 4.4.4: Cross -sections showing isopleths of a) RH wrt water (magenta), temperature (deg C; dashed blue), and LWC (cg m^{-3} ; green) and b) potential temperature (red; K) and wind direction (deg; blue). The aircraft flight track is shown in black and the dropsonde locations in dashed black. The RH field is determined solely from the dropsonde data and the shaded region shows $\text{RH}_w > 85\%$. The location of the cross-section is shown in Fig. 4.4.1a. The cross-section crosses the ice edge at about 150 km, with the over-ice region to the left.

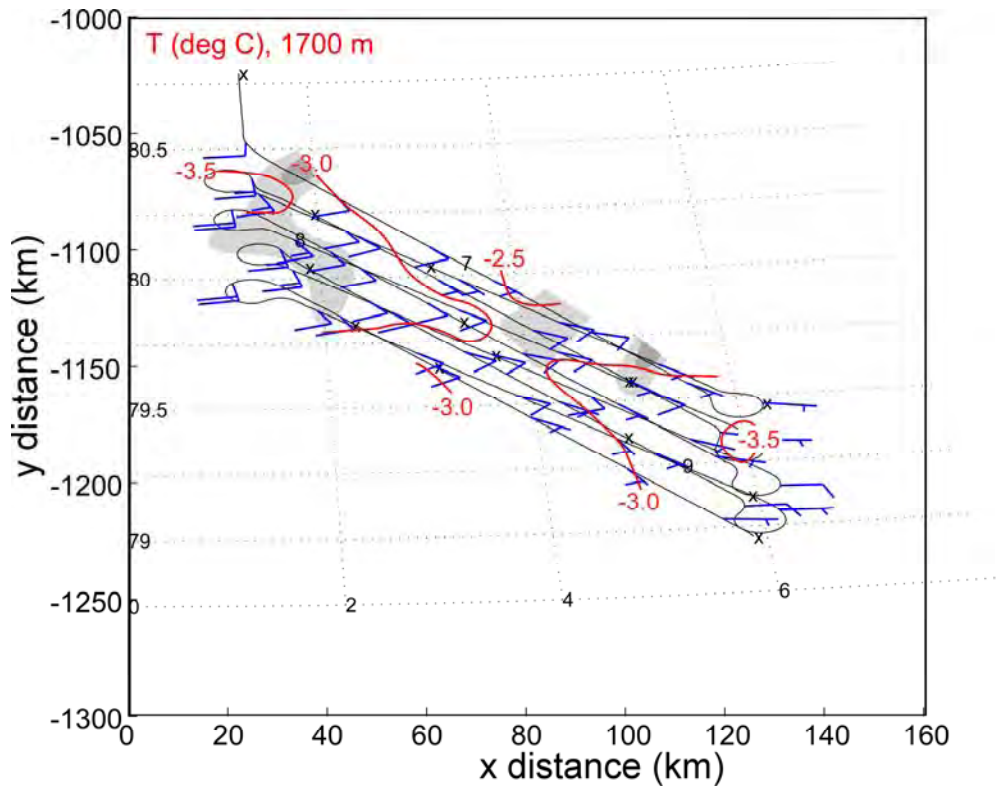


Figure 4.4.5: Analysis of temperature (red isopleths) and wind barbs (blue) from horizontal legs at 1.7 km (0650-0930 UTC) from DC-8 data on Aug. 22, 2008. The aircraft track (black lines) are shown and $RH_w > 95\%$ are shaded.

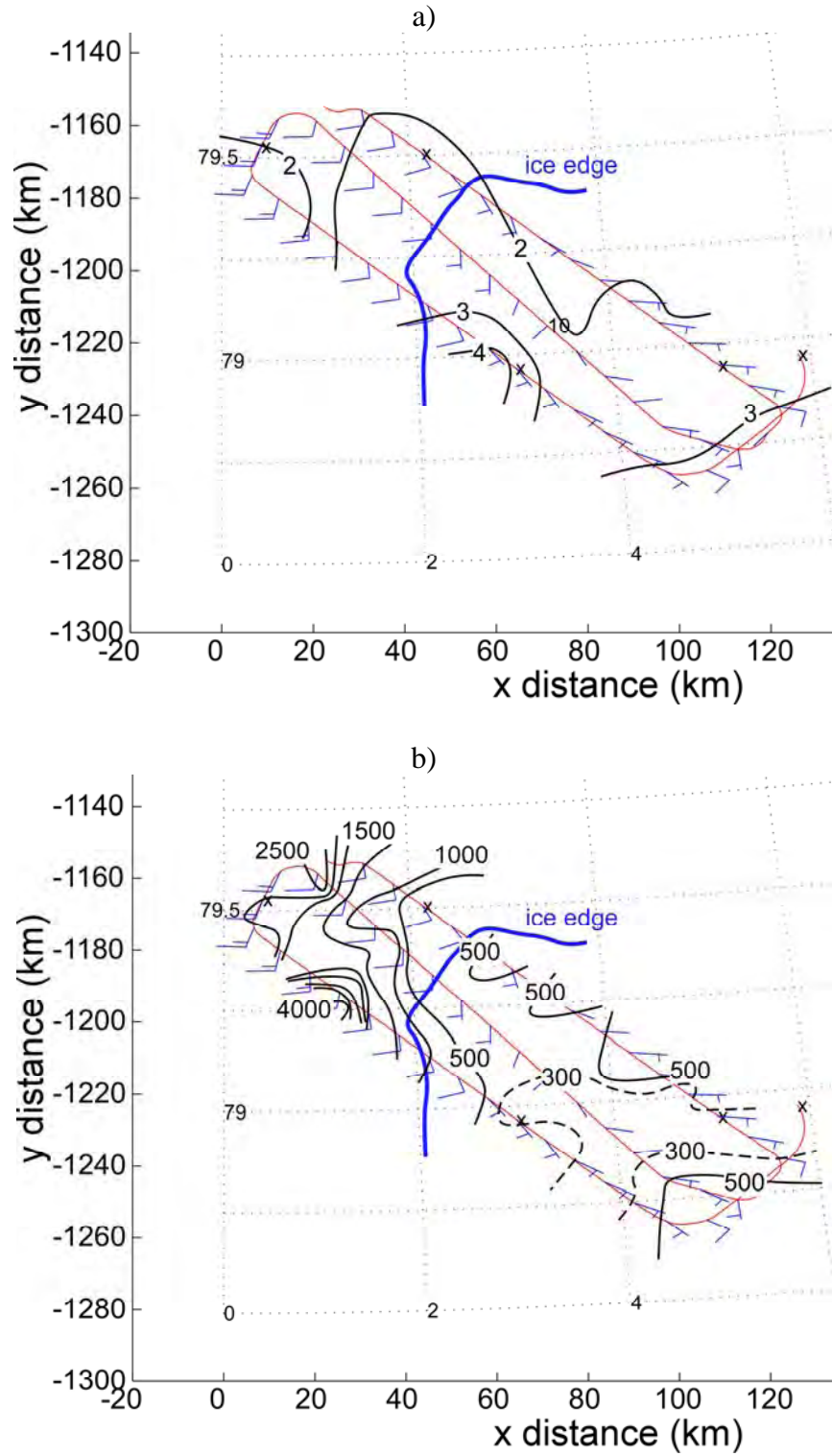


Figure 4.4.6: Flight legs and data analysis at 150 m of a) air temperature (deg C) and b) CN (cm⁻³) between 0930-1023 UTC Aug. 22. The physical position of the ice edge is shown, while the track is adjusted by the system phase velocity (10.3 m s⁻¹/191°). The wind barbs (blue) are also shown in each panel.

4.5 IOP 4; Aug. 23 (YD236):

Aircraft Takeoff: 12:04:27 Landing:~2045 On Station: 1424-1831

Oden Location when On Station: (87.5, -1.76)

Number of dropsondes: 9

Sonde times(ddhhmmss): 23142416, 23144336, 23151042, 23152113, 23153709, 23155219, 23175312, 23181509, 23183031

Meteorological system phase velocity from sat images: $10 \text{ m s}^{-1} / 165^\circ$

Times of direct overflight: 1521, 1701, 1719, 1736

IOP4 occurred the day after IOP3 and sampled the northwestern region of same cloud band as it moved northward over the Oden near 87.5° N (Fig. 4.5.1). A very weak low-pressure system, analyzed to be located just north of Greenland at this time (Fig. 4.5.2), is likely associated with this cloud system. The analysis of the two low-pressure centers in Fig. 4.5.1 is only based on the circulations evident in the cloud images. The θ_e analysis based on the upsondes from the Oden suggests a very complex frontal structure with this system (Fig. 4.5.3). A shallow layer of cold air is capped by a warm front, which gradually brings in much warmer air at the surface, thereby ending the “cold snap” period discussed in the introduction. The leading edge of the northward moving cloud shield marks a weak cold front that is riding up over the warm front (i.e., a warm occlusion). The tethersonde provided extensive sampling of the low-level clouds (up to 400 m -- see Fig. 4.5.4) capped by the warm front between 08 and 14

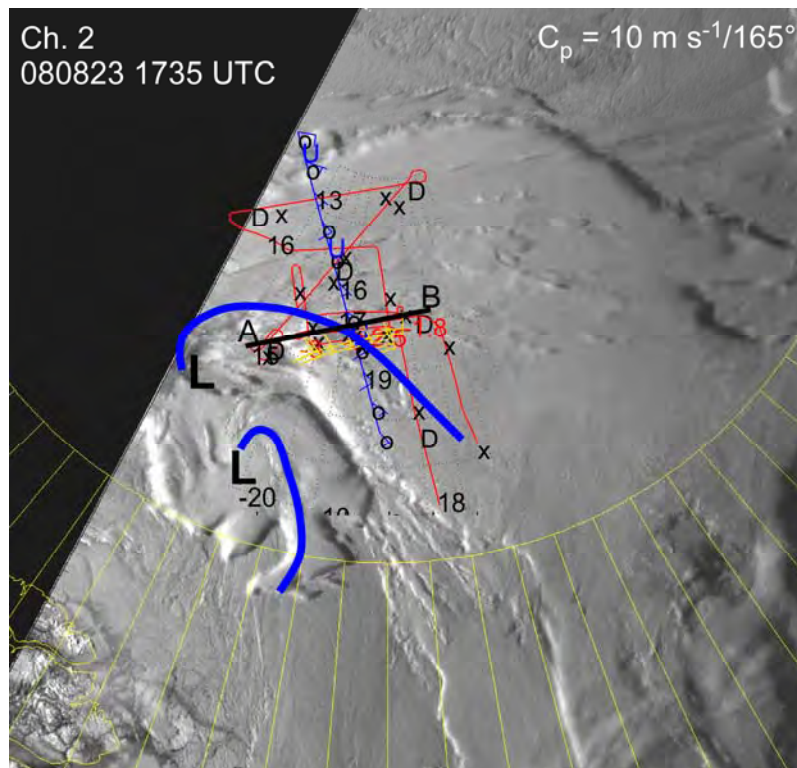


Figure 4.5.1: Visible satellite image at 1735 UTC Aug. 23 with the DC-8 flight track overlaid (red). A time-space adjustment was applied using a phase velocity of 10 m s^{-1} from 165° . The time-space adjusted Oden track is shown (thin blue, and preliminary frontal analyses at $\sim 0.7 \text{ km}$ altitude are also shown (heavy blue). The heavy black line A-B denotes the location of the vertical cross-sections shown in Fig. 4.5.5.

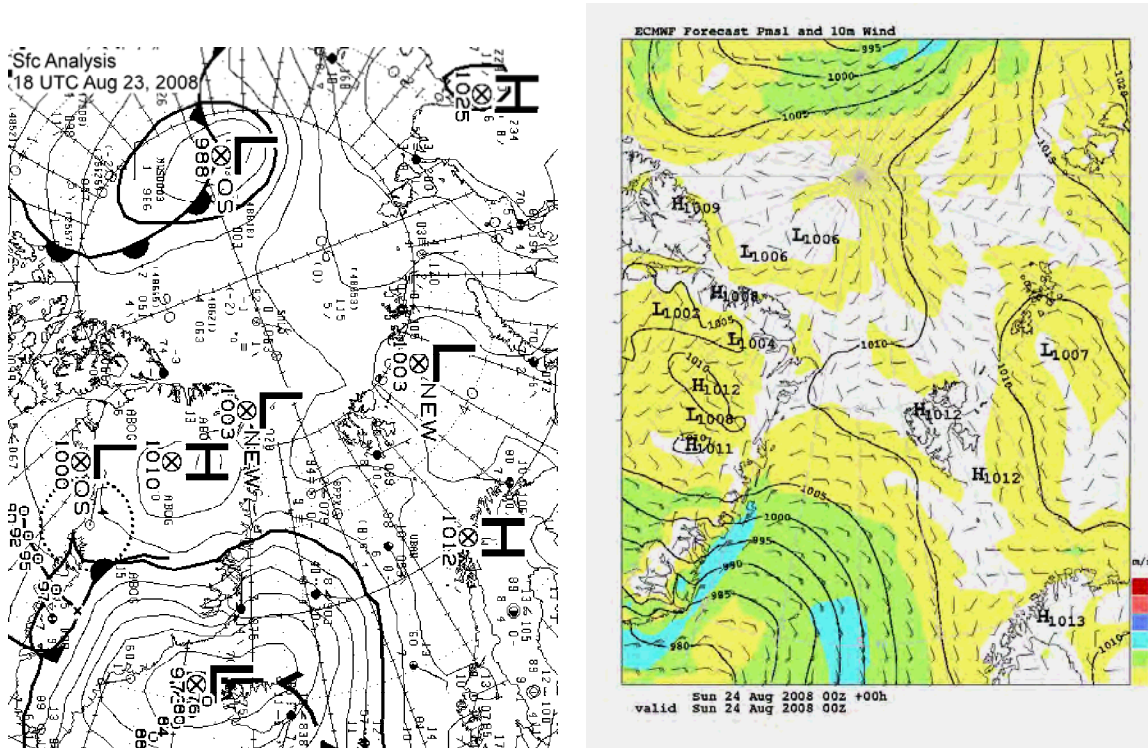


Figure 4.5.2: Surface pressure analyses at a) 18 UTC Aug. 23 from the Canadian Meteorological Service and b) 00 UTC Aug. 24, from the ECMWF.

UTC and in the warm sector after the warm front passed. The deeper clouds and precipitation arriving near 1630 UTC at the Oden are associated with a stronger cold front in the layer 1-3 km above the surface. This cold front is preceded by the classical low-level wind speed jet maximum shortly after 15 UTC, as seen in the wind profiler data (Fig. 4.5.5). A third cold front arriving at about 20 UTC brings in even slightly colder air in the lowest 1.5 km.

After dropping a dropsonde from 8 km altitude on approach to the Oden area, the DC-8 aircraft flew a “Z-pattern” at 5.6 km altitude centered on the Oden, deploying dropsondes at the corners and the center of the pattern (Figs. 4.5.1 and 4.5.3). This dropsonde array was primarily located in the warm sector ahead of the second cold front, though the SW portion of it straddled the second cold front. Vertical profiles of dynamically-related parameters (e.g., vorticity, divergence, deformation) can be obtained from this dropsonde data, while radiative flux divergence of the cloud top at 4.5 km can be obtained from the airborne radiometer data. The aircraft then descended to about 100 m, starting a box of sawtooth patterns (slow ascent/descent on each side of the box) from 100 m to 3 km. This sawtooth box pattern was done after the warm front had passed the Oden and again encompassed primarily the air directly preceding the second cold front (Figs. 4.5.1 and 4.5.3). After the sawtooth box pattern, the aircraft performed two horizontal legs passing over the Oden and perpendicular to the airflow (and perpendicular to the Oden track), one at 100 m and the other at 1200 m (Figs. 4.5.1 and 4.5.4). Both of these were done as the clouds thickened and the precipitation began in association with the second cold front. Among other objectives, aerosol sampling with the VACC was done during these legs. A final pass of the aircraft over the Oden occurred with a slow descent to 100 m from 1200 m, followed by a slow ascent continuing to 5.6 km as the aircraft turned back towards the south.

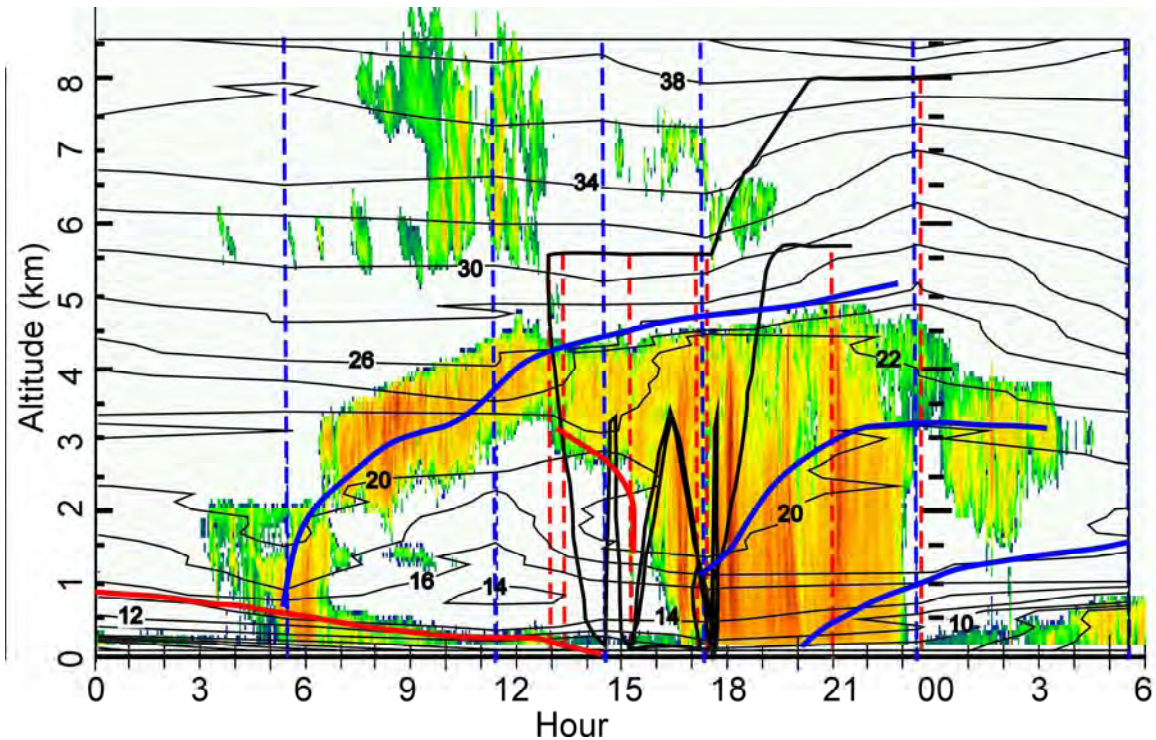


Figure 4.5.3: Cross-section along the Oden track of θ_e (isopleths) and reflectivity (color) from 00 UTC Aug. 23 to 06 UTC Aug. 24, 2008. Shown are the DC-8 track (heavy black), the dropsondes (red dashed), the upsondes (blue dashed), and the cold and warm frontal analysis (blue and red solid, respectively). The aircraft track was calculated using the system phase velocity in Fig. 4.5.1. The θ_e field is determined from the upsonde data.

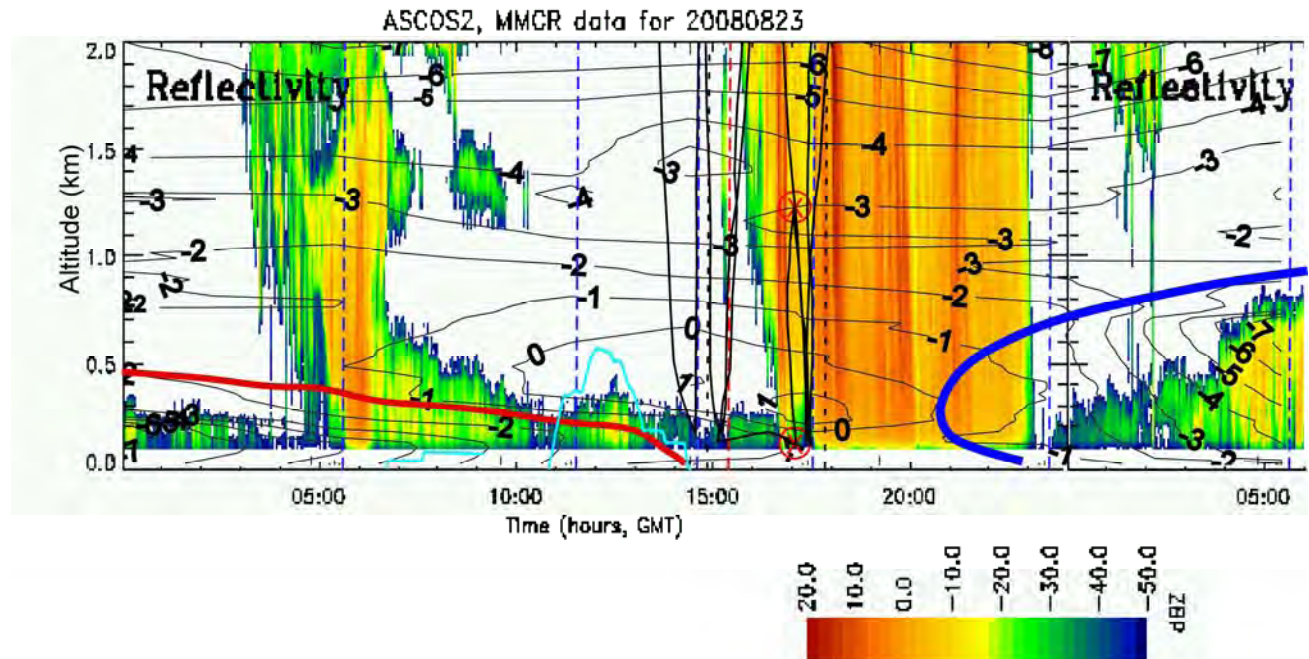


Figure 4.5.4: Time-height section of temperature (thin solid black) from the soundings and the 60 GHz radiometer and Ka-band reflectivity (color) in the lowest 2 km along the Oden track in Fig. 4.5.1. The warm front (red) and the low-level cold front (blue) are marked. Locations of the upsondes (blue dashed) and dropsondes (red dashed) are shown. Also shown are the locations of aircraft ascent/descents (thicker black solid) and two horizontal aircraft legs (circled "X") performed perpendicular to the cross-section. Tether sonde tracks are shown in cyan.

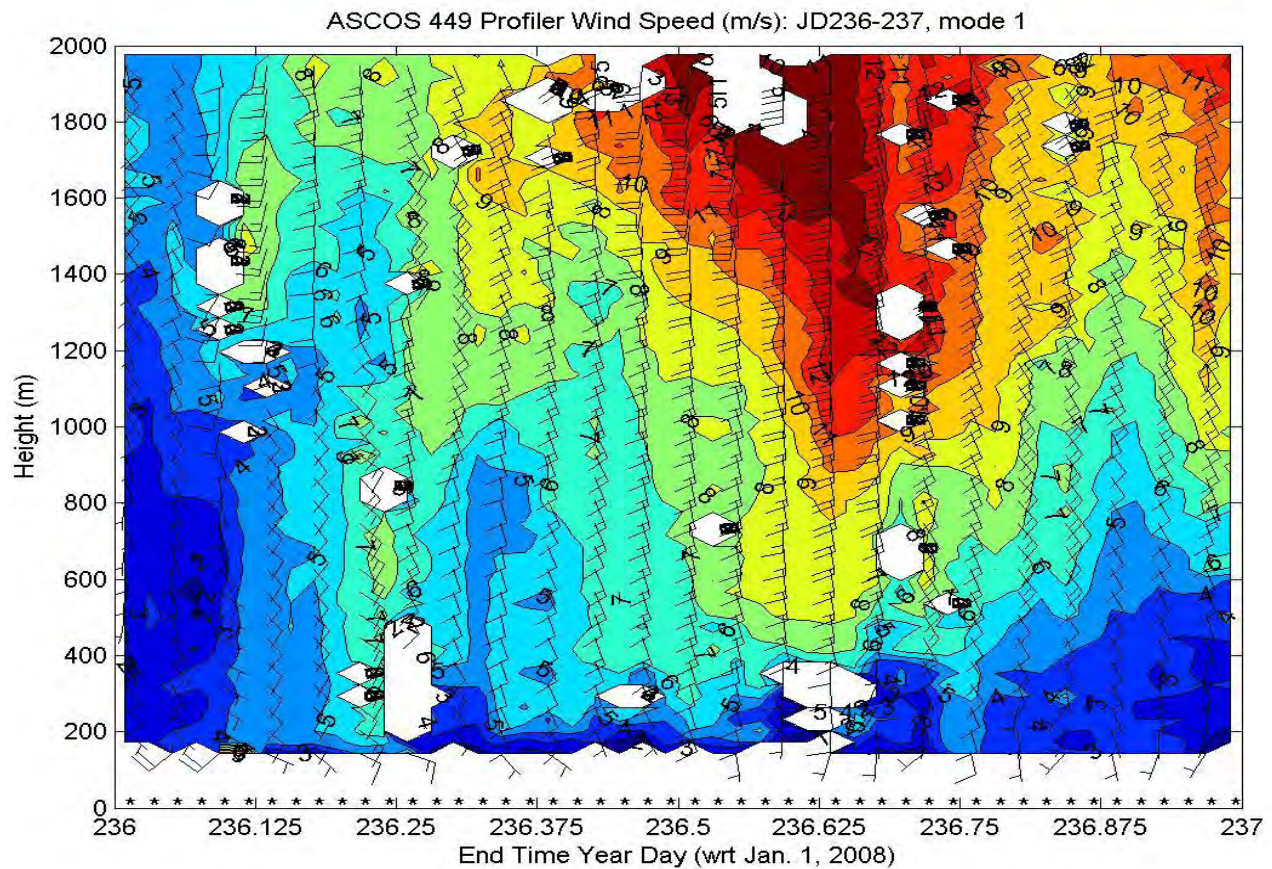


Figure 4.5.5 : Time-height cross section of isotachs in the lowest 2 km obtained from the 449 MHz wind profiler on Aug. 23, 2008 (YD236).

The final ascent may have passed through some of the high reflectivity bands that were reported to have later produced very large snowflakes at the Oden and were generated near cloud top at ~ 4 km (Fig. 4.5.3). This case also featured tether sonde data sampling the same low-level inversion and stratocumulus clouds sampled by the aircraft (Fig. 4.5.4).

The horizontal legs over the Oden, the southern side of the sawtooth box, the final descent/ascent over the Oden, and the 1730 UTC Oden upsonde can be combined into one cross-section oriented nearly west-east (Figs. 4.5.1 and 4.5.6). Analysing the lowest 2 km of this cross-section shows that the second cold front produced clearing to the west and the denser clouds to the east above 600 m. A wedge of above freezing air was located between about 100 m and 500 m above the surface, with slightly warmer air to the east. (The dropsondes at both ends of this cross-sections show temperatures that seem displaced in the vertical by 200 meters or so, so they were not included in the analysis.) Liquid water amounts of up to 12 cg m^{-3} were found in the clouds above the second cold front, while only values to 5 cg m^{-3} were found in the clouds in the lowest 100-200 m (Fig. 4.5.6b).

For IOP4, there were nine 2-4 minute periods when the DC-8 track was within 1.4 km of the Oden track, and there were 4 direct overpasses of the Oden with the DC-8 (Table 4.5.1). The direct overpasses occurred twice at ~ 134 m, once at 1233 m and once at 5582 m.

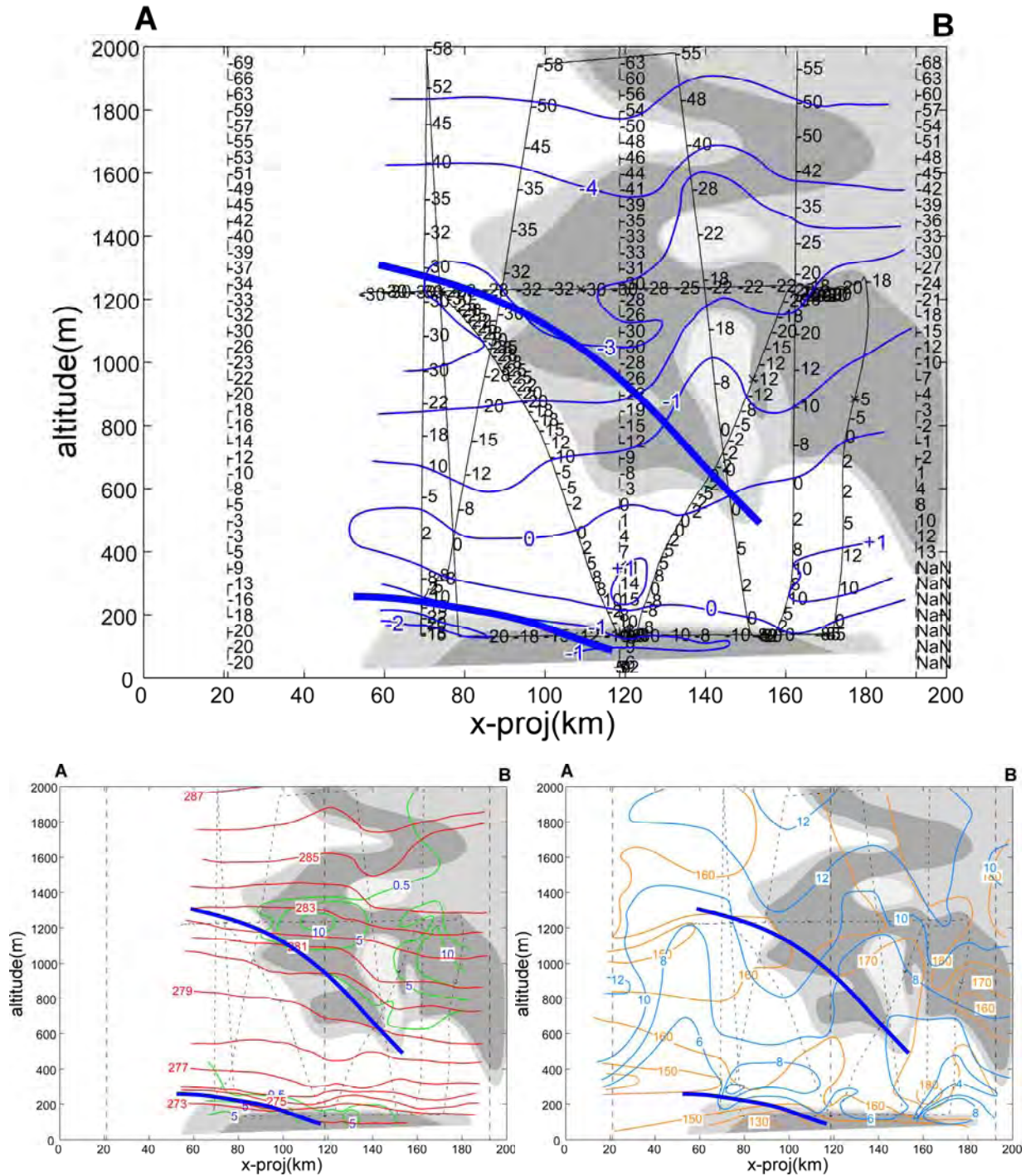


Figure 4.5.6: Cross-sections of a) temperature (blue isopleths, deg C), b) potential temperature (red) and liquid water content (cg m^{-3} ; green), and c) isotachs (blue) and isohyets (brown) along the line A-B shown in Fig. 4.5.1. In each, the regions with $\text{RH}_w > 90\%$ (95%) are lightly (darkly) shaded, and the approximate positions of two cold frontal surfaces are shown (heavy blue). In a), the temperature data used in the analysis are shown in tenths of a degree Celsius, except that the dropsonde data isn't used in the analysis because of potential height offsets. The aircraft tracks are shown as thin grey solid lines in a) and dotted lines in b) and c).

Table 4.5.1: Times for which the time-space adjusted DC8 and Oden tracks are within ~1.4 km of each other for IOP4. A phase velocity of 10 m s^{-1} from 165° was used. The last 4 rows show the times when the proximity of the tracks occurred with the times within 30 s of each other, indicating a direct overflight.

<u>Oden Time</u>	<u>DC8 Time</u>	<u>Altitude (m)</u>	<u>Distance(m)</u>
1312-1315	154605-154610	5578-5579	355-1081
1453-1455	160830-160840	3264-3278	119-1014
1525-1529	152055-152105	5582	367-1225
1658-1700	170115-170125	133-134	496-986
1721-1723	171845-171855	1233-1234	304-1100
1728-1731	144950-144955	5574	632-1194
1731-1734	173540-173555	128-143	421-1079
1751-1754	163010-163020	3141-3229	357-1045
Direct Overflight (<	30s difference betw.	the two times)	
1521	152100	5582	
1701	170115	133	
1719	171855	1233	
1736	173555	134	

4.6 IOP 5; Aug. 25 (YD238)

Aircraft Takeoff: 08:51:03 Landing:~1923 On Station: 1150-1700

Oden Location when On Station: (87.5, -1.76)

Number of dropsondes: 9

Sonde times(ddhhmmss): 25110447, 25113048, 25114447, 25120521, 25122302, 25124021, 25125911, 25165422, 25172139

Meteorological system phase velocity from sat images: 15.8 m/s / 254° (upper clouds),

Low-level cloud (~1 km) phase velocity: 5 m/s / 290° (low clouds)

Times of direct overflight: 1223, 1352, 1433, 1512, 1555, 1632

The purpose of IOP5 was to sample a “pure stratocumulus” cloud case, with no frontal passages complicating the interpretation. The surface pressure analysis showed a weak pressure gradient over the Oden region, though with a surface flow pattern that was fairly complicated (Fig. 4.6.1). Forecasts of high humidity at low levels and weak pressure gradients made Aug. 25 a likely candidate for obtaining a simple stratocumulus cloud field (Fig. 4.6.2). The sequence of infrared satellite images shows the non-descript grey signature of the low-level clouds over the Oden on this day (Fig. 4.6.3). Unfortunately, it also shows a patch of higher clouds, which in further analysis appears to be associated with a jet streak near 500 mb. This patch of higher clouds moves over the Oden between 0930 and 1430 UTC (Fig. 4.6.3c-d and Fig. 4.6.4) between

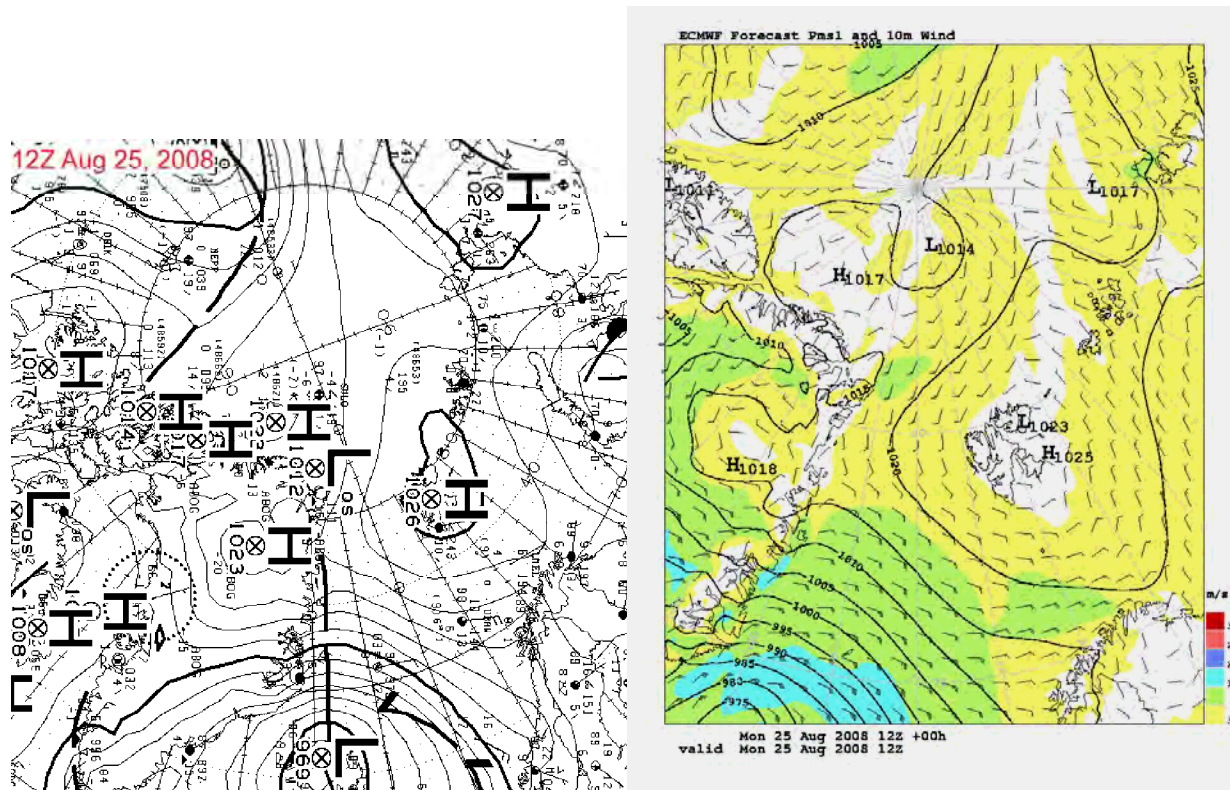


Figure 4.6.1: Analyses of sea-level pressure from a) the Canadian Weather Service and b) the ECMWF at 12 UTC, Aug. 25, 2008.

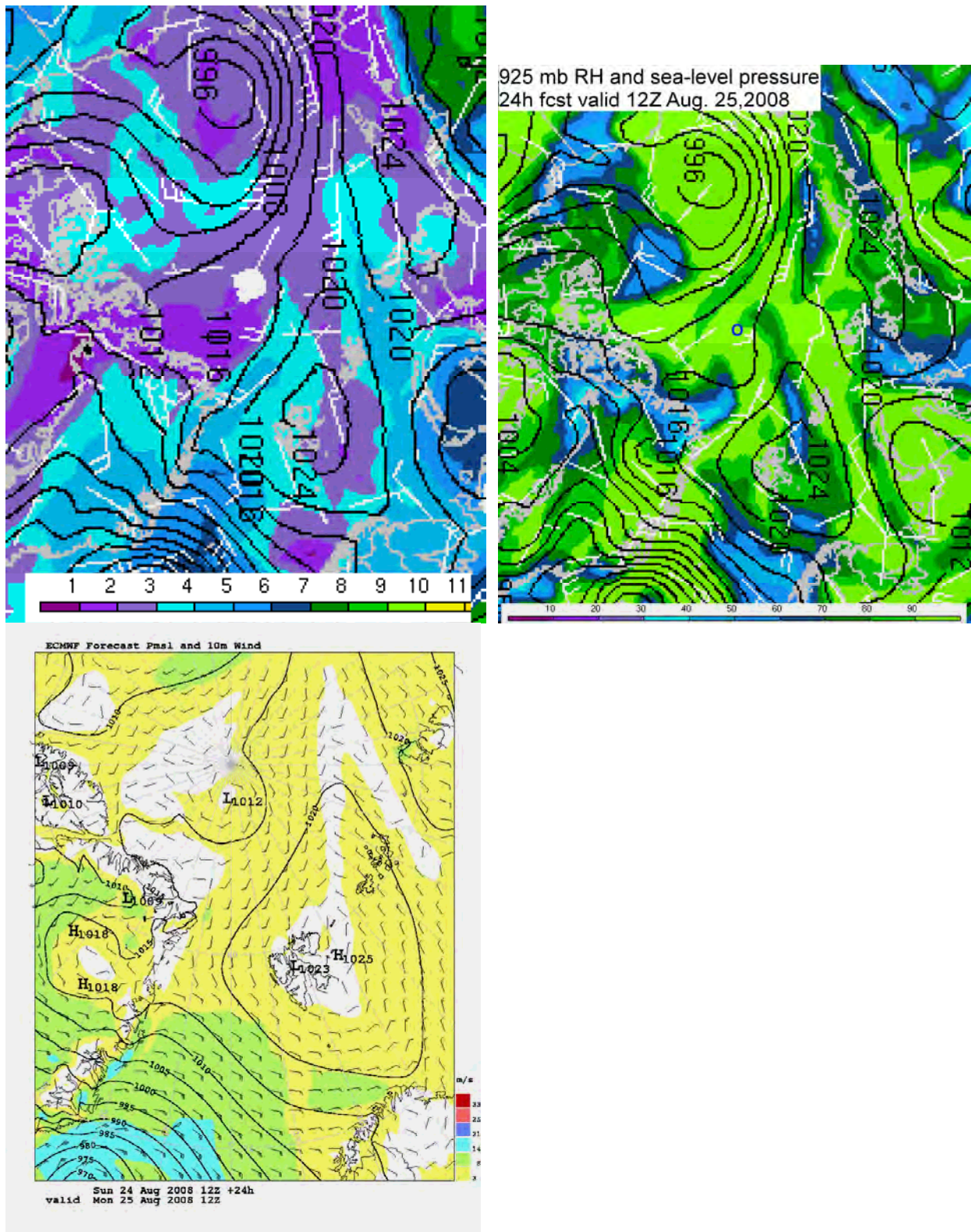


Figure 4.6.2: a) 12h forecast of the sea-level pressure and 850 mb mixing ratio (g kg^{-1}) from the UK Met Office, b) 24 h forecast of sea-level pressure, 925 mb relative humidity (%), and wind barbs from the NCEP GFS model, and c) 24 h forecast of sea-level pressure and 10-m winds from ECMWF. No 24-h forecast from the FIM model was available. All forecasts are valid at 12 Z Aug. 25, 2008.

3 and 6 km altitude. Since the DC-8 arrived in the vicinity of the Oden near 1130 UTC and left near 1630 UTC, the first 3 hours of the mission sampled while a double cloud deck existed, and the last two hours sampled conditions during a pure stratocumulus cloud deck. In addition, the transition from a double-layered cloud deck to a single-layered cloud deck was captured for this case. Because the phase velocity of the mid-level clouds were much different than that in the low-level stratocumulus clouds, two phase velocities are determined for this case. The purpose of the analysis determines which phase velocity is the relevant one.

The first portion of the flight consisted of a “lawnmower” flight pattern at 8 km altitude near the back edge of the mid-level cloud deck. The purpose of this pattern was to document the

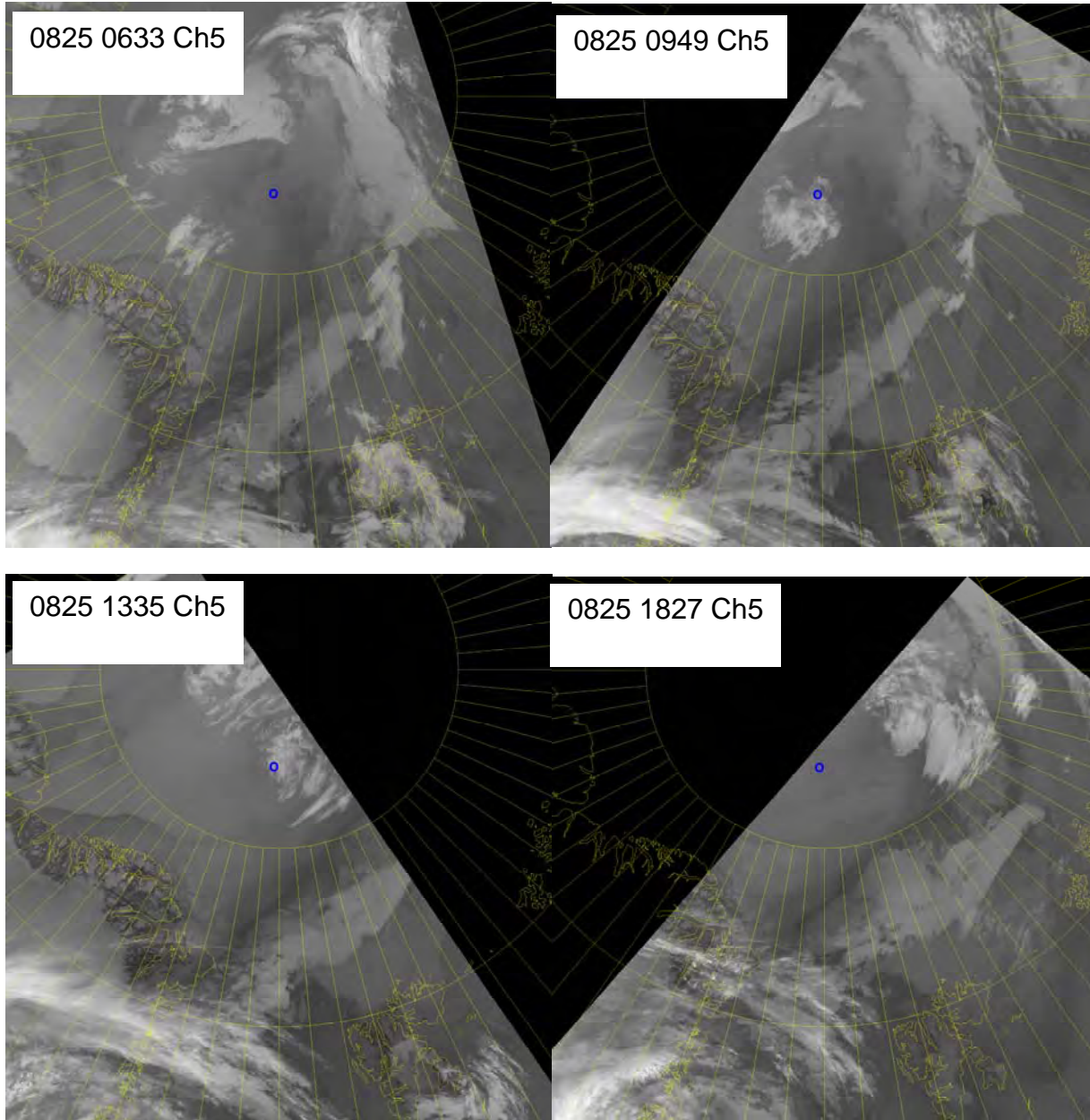


Figure 4.6.3: Sequence of infrared satellite images showing the location of the Oden (blue circle) and the movement of the mid-level cloud patch on Aug. 25, 2008 (YD238).

spatial structure of the sea ice characteristics in the region of the Oden and to obtain a spatial array of dropsondes. Figure 4.6.5c shows the spatial location of this high-level flight pattern and the dropsondes using the phase velocity of the mid-level clouds. Figure 4.6.4 illustrates that many of these dropsondes penetrated both cloud layers. After the high-level pattern, the aircraft descended to ~110 m and began a sawtooth ascent/descent box pattern around the Oden starting at 13:23:53 UTC. With apices at ~1950 m, the top of this box was above the tops of the stratocumulus cloud deck. The north-northeast end of this box was underneath the mid-level cloud deck (Fig. 4.6.5c), while the south-southwest end was in only the stratocumulus deck. After the sawtooth pattern, “racetrack” legs at 110 m, 630 m, and 1000 m were flown. The racetrack leg at 1000 m was only partially completed when icing conditions prevent good sampling from the LARGE and VACC, so a leg was flown at 1680 m. Another lower leg was then flown in the clear air at 1250 m above the stratocumulus clouds, before a final descent/ascent was done over the Oden into the low-level wind. The lower portion of the flight track projected onto the track of the Oden and the Ka-band cloud radar reflectivity field is shown in Fig. 4.6.6. Note that the time that the aircraft spent near the Oden corresponded to a time when the tops of the low-level stratocumulus clouds began an increase from their depth of about 700 m to about 1600 m. At this time, the reflectivity field also shows a low-level clearing from ~1340-1520 UTC. The tetheredsonde sampled many of the same clouds during this day up to a height of ~600 m. The profile centered on 17 UTC may be especially useful for comparison to the aircraft data.

The wind shifted from SE to W in the boundary layer near 09 UTC, and from S to W above the boundary layer near 11 UTC (Fig. 4.6.7). For much of the day, the stratocumulus cloud layer had weak winds. However, the rise in the stratocumulus cloud tops corresponds to a time when a low-level jet of northwesterly flow forms below cloud top, eventually becoming centered between two distinct stratocumulus cloud layers by the end of the day. Hence, while

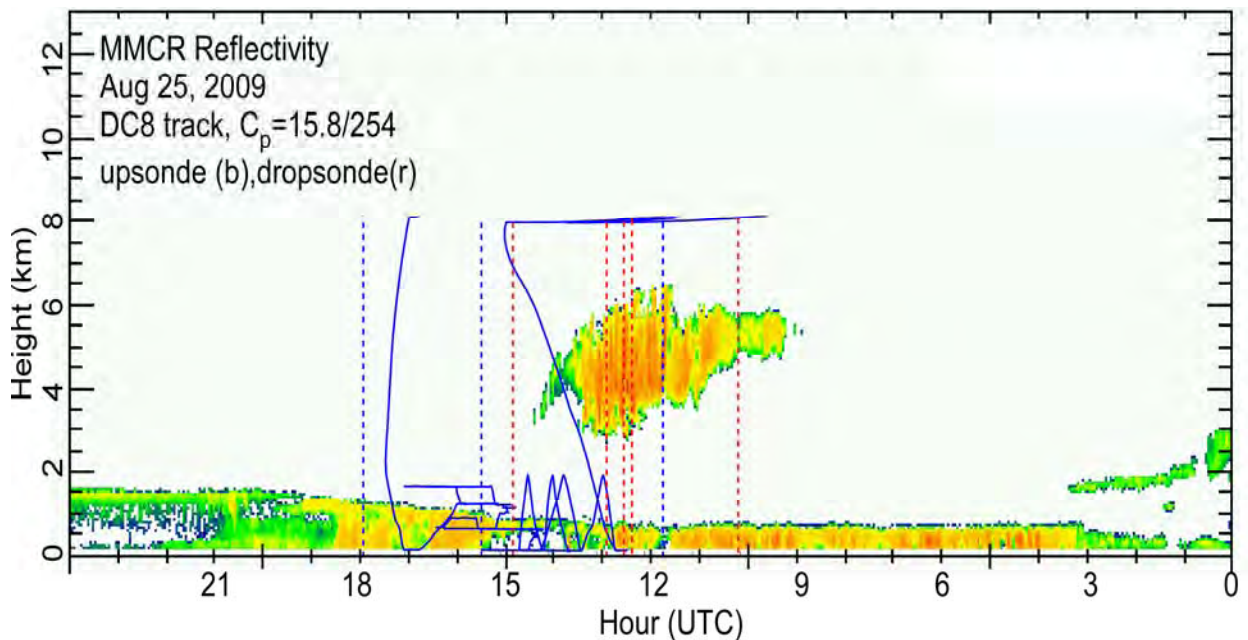


Figure 4.6.4: Cross section along the Oden path of radar reflectivity from the Ka-band cloud radar on Aug. 25, 2008 (IOP5). The aircraft track projected on the cross section is shown (blue solid), and the dropsonde and upsonde locations are shown as red and blue dashed lines, respectively. The track has been adjusted using the phase velocity of the upper-level clouds (15.8 m s^{-1} from 254°)

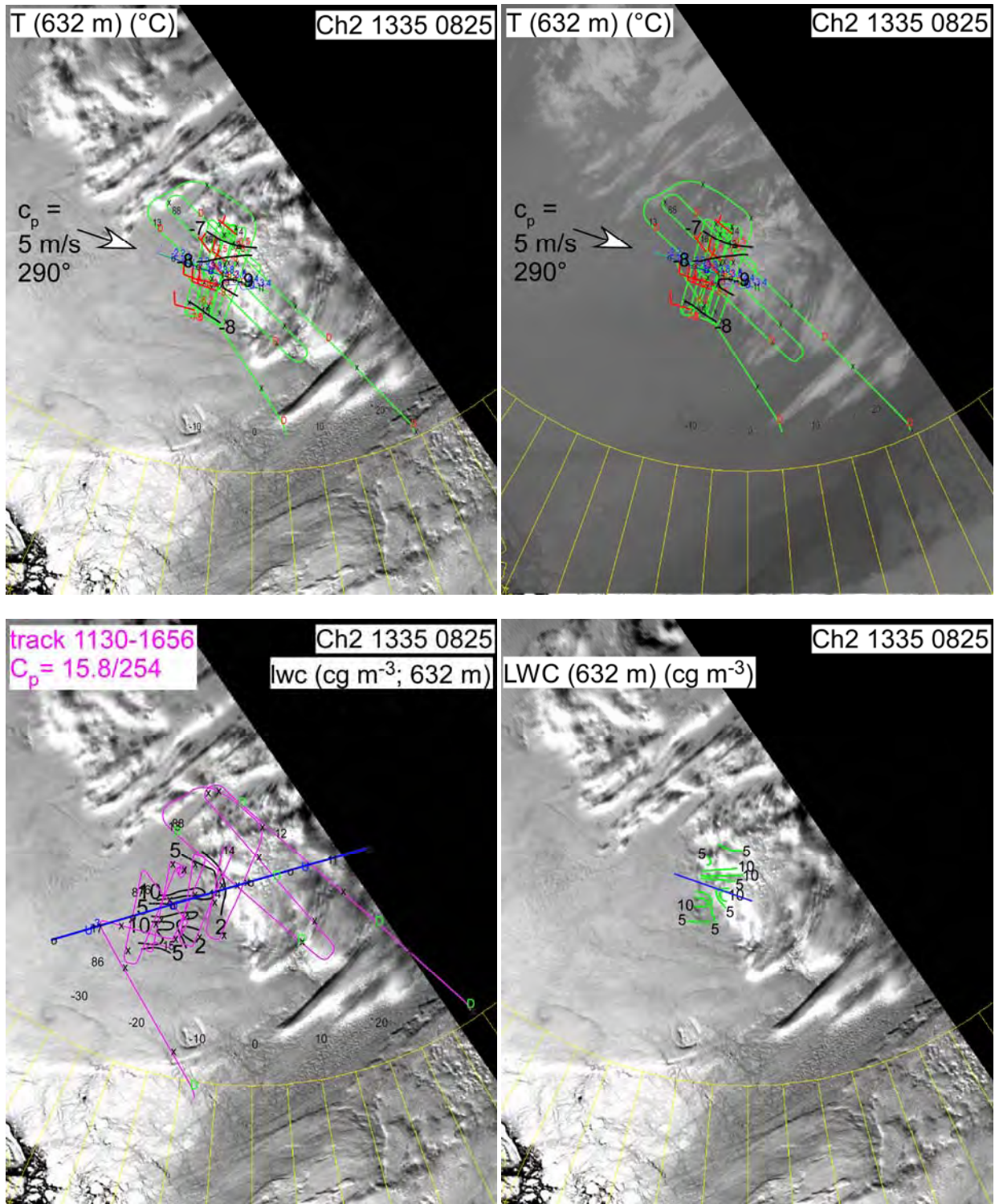


Figure 4.6.5: Zoomed satellite images at 1335 UTC showing the aircraft flight track a) on a visible image using the phase velocity of the low-level clouds, b) infrared image with the low-level phase velocity, c) a visible image with the phase velocity of the upper-level clouds. Panels a) & b) show an analysis of temperature at ~630 m altitude, while panel c) shows LWC at ~630 m (100-300 m below cloud top of lower clouds). Panel d) is the same as c), except showing a LWC analysis using the phase velocity of the lower-level clouds.

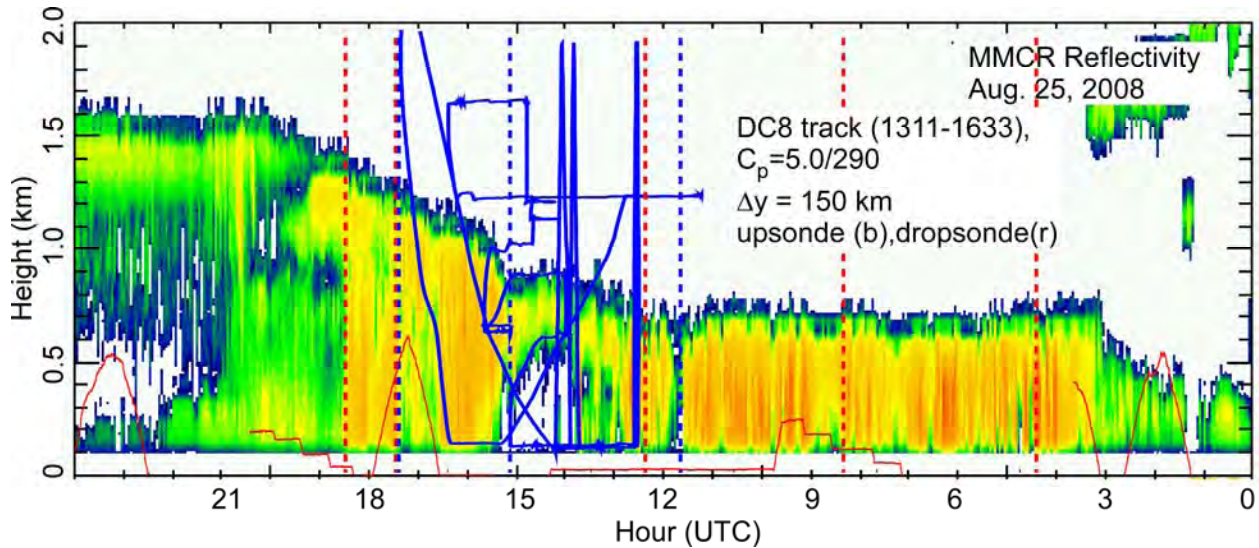


Figure 4.6.6: A 2 km high cross section along the Oden path of radar reflectivity from the Ka-band cloud radar on Aug. 25, 2008 (IOP5). The aircraft track projected on the cross section is shown (blue solid), and the dropsonde and upsonde locations are shown as red and blue dashed lines, respectively. The track has been adjusted using the phase velocity of the lower-level clouds (5.0 m s^{-1} from 290°). The tether sonde track is also shown (thin red solid).

the stratocumulus clouds are the primary cloud structure during IOP5, synoptic or mesoscale changes appear to be linked to changes in the cloud characteristics and the kinematic structure.

The temperature and wind field at the $\sim 630 \text{ m}$ height shows a slightly weaker wind with a more northwesterly component at the northern end of the pattern compared to the southern end (Fig. 4.6.5a,b). A weak temperature gradient existed, with the coldest temperatures at this height occurring in the middle of the pattern. The liquid water content was $\sim 5\text{-}10 \text{ cg m}^{-3}$ at this height (Fig. 4.6.5d), with most of the liquid water occurring in the area not under the upper-level cloud (Fig. 4.6.5c). Vertical cross-sections along the wind direction passing over the Oden (blue line in Fig. 4.6.5d) show that the coldest temperatures occur $\sim 100 \text{ m}$ below cloud top with a

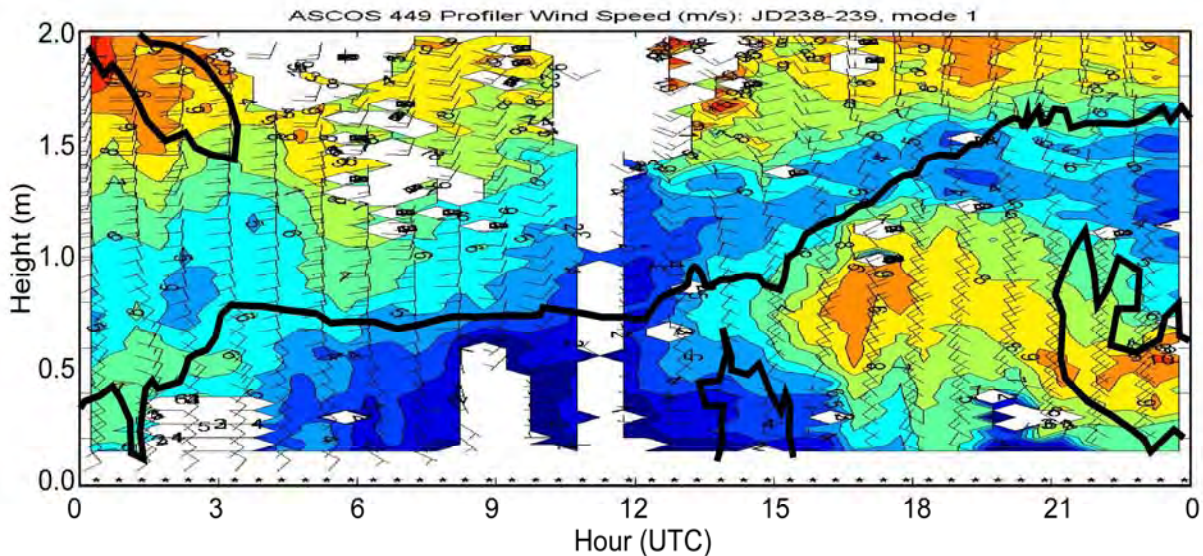


Figure 4.6.7: Isotachs (m s^{-1}) and wind barbs from the low mode of the 449 MHz wind profiler in the lowest 2 km on Aug. 25, 2008. The heavy black lines mark the cloud edges from the MMCR reflectivity in Fig. 4.6.6. Note that the x-axis is reversed from Fig. 4.6.6, with the beginning of the day on the left side rather than the right.

strong inversion right at cloud top (Fig. 4.6.8a). Note that the cold temperatures rise in elevation as the cloud top rises. The θ_v field shows only weak or near-neutral stability below cloud top (Fig. 4.6.8b), but quite strong stratification at and above cloud top. This holds true for the θ_v field derived from the scanning radiometer as well (Fig. 4.6.8c). A liquid water content maximum of 10-15 cg m^{-3} is seen ~ 100 m below cloud top on the aircraft descent profile and one of 5-10 cg m^{-3} on the ascent (Fig. 4.6.8b).

During this flight, the DC-8 passed over the track of the Oden eleven times, with all but one of these passes having a duration of just a few seconds (Table 4.6.1). The aircraft descent/ascent over the Oden between 162045-163310 lasted for ~ 12.5 minutes, however. Direct overflights occurred on 6 occasions.

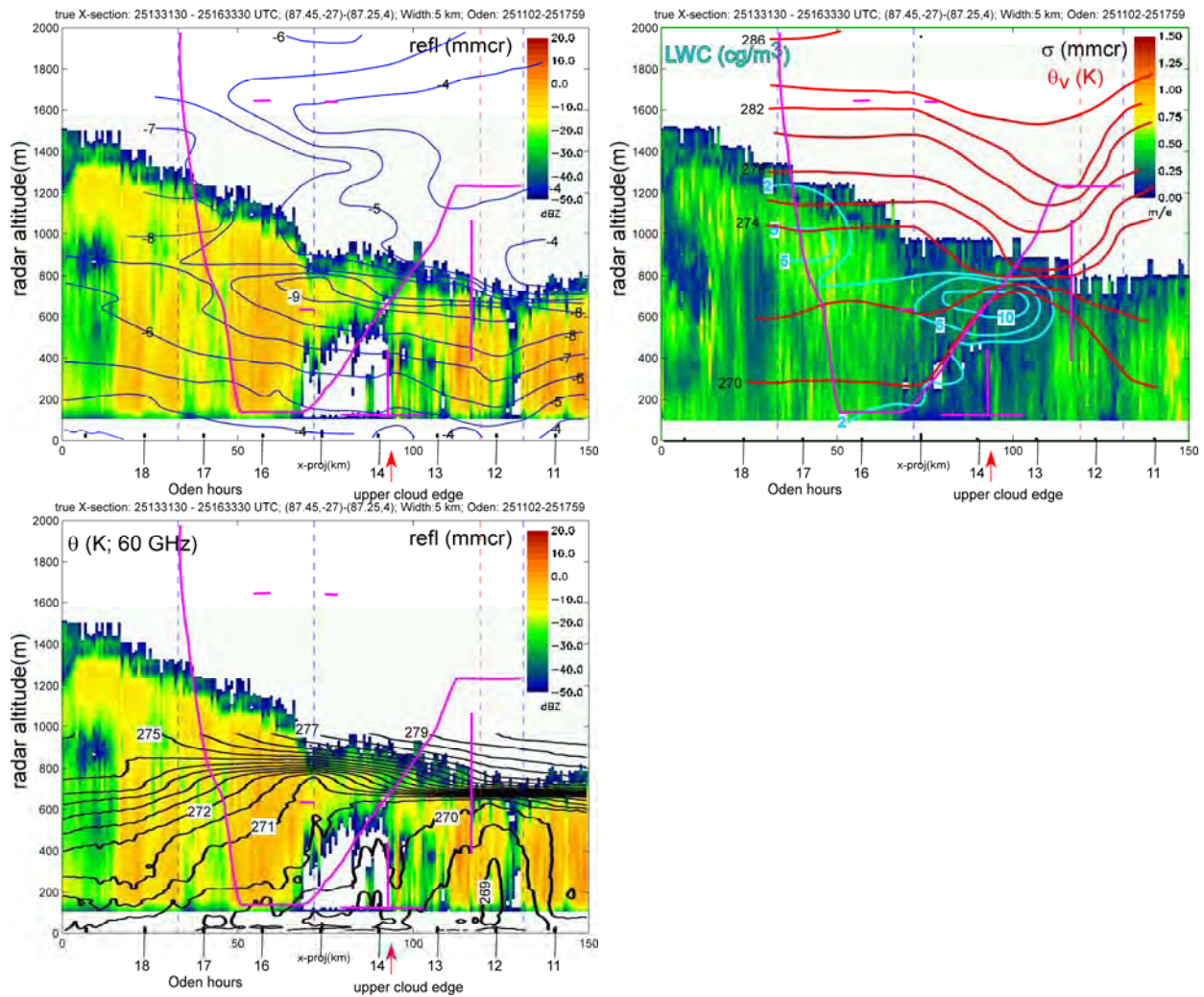


Figure 4.6.8: A 2 km high cross section along the Oden path of radar reflectivity (a,c) and spectral width (b) from the Ka-band cloud radar from ~ 1030 -1920 UTC on Aug. 25, 2008 (IOP5). The aircraft track along and within 5 km of the cross-section is projected on the cross section (magenta), and the dropsonde and upsonde locations are shown as red and blue dashed lines, respectively. The isopleths analyses utilize both the aircraft and the dropsonde/upsonde data and show fields of a) temperature ($^{\circ}\text{C}$) and b) potential temperature (K) and LWC (cg m^{-3}). In c), isopleths of potential temperature from the 60 GHz scanning radiometer are shown. The track has been adjusted using the phase velocity of the lower-level clouds (5.0 m s^{-1} from 290°).

Table 4.6.1: Times for which the time-space adjusted DC8 and Oden tracks are within ~1.4 km of each other for IOP5. A phase velocity of 5 m s^{-1} from 290° was used. The last 6 rows show the times when the proximity of the tracks occurred with the times within 30 s of each other, indicating a direct overflight.

<u>Oden Time</u>	<u>DC8 Time</u>	<u>Altitude (m)</u>	<u>Distance(m)</u>
1203-1709	162045-163310	138-1735	127-1175
1210-1228	122250-122315	7946-7948	225-1180
1225-1231	133200-133210	674-771	331-1168
1310-1317	141300-141315	121-122	325-1084
1345-1352	135145-135200	127-130	171-1336
1351-1357	145215-145225	620-621	82-1347
1429-1436	143235-143250	128-130	85-1305
1436-1443	153850-153900	1641-1642	193-1250
1510-1516	151200-151210	632-633	217-1216
1544-1603	125235-125300	7926-7928	173-1270
1553-1600	155520-155530	1643-1644	308-1160
Direct Overflight (<	30s difference betw.	the two times)	
1223	122300	7946	744
1352	135145	129	1311
1433	143250	128	865
1512	151200	632	573
1555	155520	1643	652
1632	163145	730	1100

5. AMISA Summary and Science Issues

The AMISA field program succeeded in collecting data useful for analyzing the ice surface characteristics, the synoptic/mesoscale atmospheric structure, the cloud microphysical structure, and the aerosol concentrations and types during six flights in August 2008. Five of the flights were directly in the vicinity of the Oden ice breaker and its associated ice camp near 87.5° N, 5° W. and one was over the ice edge in the Fram Strait. This report summarizes the meteorological context of each flight and provides a first look at some of the meteorological data. Integration of the aircraft, ship, and satellite data is a key aspect for understanding the context of the data for each flight. Through the utilization of the phase velocity of the meteorological system obtained from either serial satellite images or from wind speeds at the steering level of the clouds, the system-relative position of the aircraft data and the Oden-based data can be mapped, and represents an illustration of the integration that has been begun. This report illustrates the importance of doing such integration.

It is shown that the AMISA flights succeeded in bracketing the end of the summer melt season, which was a major objective. It has also been shown that the meteorological conditions for all flights, with the possible exception of IOP5, included significant impacts from synoptic weather disturbances.

The first-look at the AMISA/ASCOS integrated data set suggests that observations exist to address the following science issues:

- 1) **Instrument intercomparisons:** Through the use of a system phase velocity, data from all platforms can be placed in meteorological context and be compared to each other. Such an intercomparison is crucial for properly integrating the AMISA and ASCOS data sets and obtaining the most value from the data. Such an intercomparison will also provide useful information regarding the performance of various instrument systems. Data from all IOPs can be used for this purpose.
- 2) **Document the evolution of the surface characteristics during the end of the surface melt and onset of freeze-up:** The flight patterns of IOPs 1, 2, 4, and 5 all contained components from which the ice surface characteristics can be obtained.
- 3) **Determine to which extent synoptic/mesoscale disturbances produce changes in the clouds, thermodynamic structure, and surface energy budget:** Because all cases, except IOP3 and possibly IOP5, had obvious influences from synoptic/mesoscale disturbance, this issue can be examined in four or five of the IOPs, including the transit IOP. In addition, the successful collection of sub-hourly surface energy budget data during ASCOS (Sedlar *et al.* 2010) will allow the assessment of the synoptic/mesoscale impact on the surface energy budget. IOP1 was an especially strongly synoptically forced case.
- 4) **Document quantitative measurements of radiative flux divergence, liquid water content, cloud radar parameters, and the thermal and kinematic atmospheric structure for stratocumulus clouds:** Data from IOPs 2, 4, and 5 are especially well suited for this purpose.
- 5) **Assess the relative importance of dynamic and radiative forcing for cloud microphysical and thermodynamic structure of stratocumulus clouds:** This objective depends on having obtained a well-placed array of dropsondes in a case of significant

amounts of stratocumulus clouds in order to assess the dynamical forcing. IOPs 4, and 5 had such arrays. IOP2 also obtained a good dropsonde array, but the amount of stratocumulus clouds were more limited.

- 6) **Assess the impact of synoptic/mesoscale flow and vertical mixing on aerosol types/concentrations near Oden site:** IOP1 had obvious strong long-range transport to the free troposphere above the Oden. The transport of aerosol from the ice edge to the Oden was documented in IOP2. Flight legs appropriate for aerosol typing with VACC were also obtained in IOPs 4 and 5.
- 7) **Improve NASA AMSR-E algorithm "weather" corrections for satellite sensing of sea ice conditions:** IOP3 was dedicated to this objective.

Acknowledgements

The work of Dr. Albin Gasiewski, project PI, was key for the successful planning and execution of AMISA, with support from co-PIs Don Cavalieri and Michael Tjernström. The extraordinary efforts provided by Eric McIntyre, David Kraft, and Barbara Brooks were a major reason for the success of the data collection. The assistance of Ellen Sukovich, Ankita Chartuvedi, James McQuaid, Andreas Beyersdorf, and Terry Latham during the field program was essential. The enthusiastic and professional support of the crew and staff of the NASA DC-8, especially Chris Jennison, Richard Ewers, William Brockett, Ryan Lubinski, and Rick Shetter, is greatly appreciated. Their willingness to adapt to time and flight patterns helped us achieve the goals of the research missions. The aircraft proved to be a very reliable and capable platform for this research. Expert and enthusiastic ground support was provided by Peter Salomonsson and Kurt Maki. We are grateful for the loan of the CAPS and LARGE probes, facilitated by Bruce Anderson of NASA Langley. Ellen Sukovich processed some of the aircraft microphysical data used in this report. Processing of ASCOS data directly contributing to this report has been done by Matthew Shupe, Paul Johnston, Vladimir Leuski, and David Carter. Special-area, high-resolution satellite data over the area of interest was made available to the AMISA project in real time by the Dundee, UK, Satellite Receiving Facility. Jeff Key at CIMSS, University of Wisconsin-Madison, provided Arctic-basin polar orbiter images and satellite winds. Meteorological surface analyses were graciously made available in real time by Nicole Bois at the Canadian Meteorological Center of Environment Canada. Special product forecast charts were provided in real time by the UK Met Office, Stan Benjamin at NOAA/ESRL (FIM model), and Esbjörn Olsson at the Swedish Meteorological and Hydrological Institute (ECMWF surface forecasts). Funding was provided by a grant from NASA to the University of Colorado.

6. References

- Andreas, Edgar L, and S. Ackley, 1982: On the differences in ablation seasons of Arctic and Antarctic sea ice. *J. Atmos. Sci.*, **39**, 440-447.
- Martin, S., and E. A. Munoz, 1997: Properties of the Arctic 2-m air temperature for 1979-present derived from a new gridded data set, *J. Clim.*, **10**, 1428-1440.
- Persson, P. O. G., and A. Solomon, 2008: "Impact of Synoptic and Mesoscale Disturbances on the Beginning and End of the Summer Melt Season over Sea Ice", *First-year annual progress report to the National Science Foundation, Sep. 2007- July 2008*, NSF Grant ARC 0714053.
- Rigor, I. G., R. L. Colony, and M. Seelye, 2000: Variations in surface air temperature observations in the Arctic, 1979-97. *J. of Climate*, **13** (5), 896-914.
- Sedlar, Joseph, Michael Tjernström, Thorsten Mauritsen, Matthew Shupe, Ian Brooks, Ola Persson, Cathryn Birch, Anders Sirevaag, and Caroline Leck, 2010: A transitioning Arctic surface energy budget: the impacts of solar zenith angle, surface albedo and cloud radiative forcing. In preparation for *Clim. Dynamics*.
- Shapiro, M. A. and D. Keyser, 1990: Fronts, jet streams and the tropopause. *Extratropical Cyclones, The Erik Palmén Memorial Volume*, C. W. Newton and E. O. Holopainen, Eds., Amer. Meteor. Soc., 167-191.

